AMERICAN UNIVERSITY OF BEIRUT

MECHANICS OF LOAD SHARING IN SOFT CLAYS REINFORCED WITH SAND COLUMN GROUPS

by
ABDURRAHMAN AHMAD ALMIKATI

A dissertation
submitted in partial fulfillment of the requirements
for the degree of Doctor of Philosophy
to the Department of Civil and Environmental Engineering
of the Maroun Semaan Faculty of Engineering and Architecture
at the American University of Beirut

Beirut, Lebanon
July 2021

AMERICAN UNIVERSITY OF BEIRUT

MECHANICS OF LOAD SHARING IN SOFT CLAYS REINFORCED WITH SAND COLUMN GROUPS
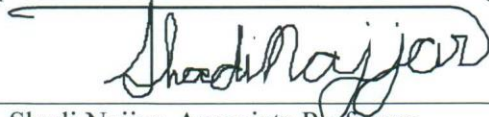
by
ABDURRAHMAN AHMAD ALMIKATI

Approved by:

_____   Advisor
Dr. Salah Sadek, Professor
Department of Civil and Environmental Engineering, AUB

_____   Chair of Committee
Dr. Mounir Mabsout, Professor
Department of Civil and Environmental Engineering, AUB

_____   Member of Committee
Dr. Shadi Najjar, Associate Professor
Department of Civil and Environmental Engineering, AUB

_____   Member of Committee
Dr. Grace Abou-Jaoude, Associate Professor
Department of Civil Engineering, LAU

_____   Member of Committee
Dr. Muhsin Rahhal, Professor
Civil Engineering Department of the Faculty of Engineering, USJ

Date of dissertation defense: July 07, 2021

AMERICAN UNIVERSITY OF BEIRUT

DISSERTATION RELEASE FORM

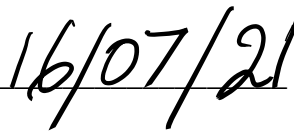Student Name: _____Almikati_____Abdurrahman_____Ahmad_____

                              Last   First   Middle

I authorize the American University of Beirut, to: (a) reproduce hard or electronic copies of my dissertation; (b) include such copies in the archives and digital repositories of the University; and (c) make freely available such copies to third parties for research or educational purposes:

☐ As of the date of submission

☐ One year from the date of submission of my dissertation.

☐ Two years from the date of submission of my dissertation.

☒ Three years from the date of submission of my dissertation.

_____16/07/21_____

Signature   Date

ACKNOWLEDGEMENTS

ABSTRACT
OF THE DISSERTATION OF

Abdurrahman Ahmad Almikati   for   Doctor of Philosophy
                                                  Major: Geotechnical Engineering

Title: Mechanics of Load Sharing in Soft Clays Reinforced with Sand Column Groups

Granular columns are widely used as a soil improvement solution for soft clays. Given that granular columns are seldom designed and constructed as individual elements, there is a clear need to identify and quantify the group effect and load sharing under various drainage conditions. This includes studying the stress distribution between the columns and the surrounding clay under varying area replacement ratios, different columnar configurations, and different drainage conditions (drained and undrained). There is also a need for studying the effect of partial drainage due to radial flow from the clay to the columns on the short-term stability of foundations on reinforced clay systems. To cater for the above needs, a new fully instrumented triaxial test setup was developed and utilized to investigate the overall response of the clay reinforced with single/group sand columns. The instrumented setup allowed for collecting data on volumetric strain during consolidation and shearing, pore water pressure dissipation, contact stress measurement above different soil materials, and global deviatoric stress variation with axial strain. The experimental program revealed the reliability of the miniature pressure sensors that are capable of quantifying the distribution of the stresses in the columns and the surrounding clay at different levels of axial strain. Results indicated that the stress concentration ratios varied significantly with strain, rate of loading, drainage conditions, column configuration and area replacement ratio. Stress concentration ratios in the range of 4 to 6 could be mobilized at very low strains for drained loading conditions. These relatively high ratios decrease to about 1.5 at relatively large strains. For the case of undrained loading, the stress concentration factors are very low (1.5 to 2) at small strains and increase to values as high as 6.5 and 9.5 for cases involving area replacement ratios of 17.1% and 30.4%, respectively. The shear strength and stress concentration factors measured in partially drained tests were bracketed between the fully drained and the fully undrained tests, with average stress concentration factors ranging from 2.0 to 5.0. The presented work included also a geotechnical characterization of Laponite, which is a transparent clay-like material to be used as a replacement to natural/synthetic non-transparent clays. This will facilitate the visualization of internal deformations and assess the mode of failure in a non-intrusive fashion. As such, future works on soft clays reinforced with granular columns could utilize Laponite as the annulus clay to envision internal movements. The insights gained and reported in this work are anticipated to facilitate the development of design methodologies for soft clays reinforced with sand column groups.

TABLE OF CONTENTS

THE EFFECT OF SAND COLUMN CONFIGURATION ON THE RESPONSE OF REINFORCED SOFT CLAYS 135

GEOTECHNICAL CHARACTERIZATION OF LAPONITE 156

ILLUSTRATIONS

Figure

9

TABLES

CHAPTER 1

INTRODUCTION

For structures of relatively light to moderate loads that are distributed over large areas, the costs associated with the use of deep foundations to bypass soft clay layers may be prohibitive. In such cases, granular columnar inclusions have been successfully used to improve the mechanical properties of the soft clay. Columnar inclusions generally include (1) sand drains or sand columns which are used to accelerate the rate of construction of structures or embankments and (2) stone or gravel columns which are associated with vibro-replacement operations that are aimed at replacing a percentage of the soft clay with stiff granular columns.

The use of granular inclusions in the form of sand drains and/or gravel columns has long been adopted as a potential alternative to deep foundation solutions, where it is associated with the replacement of an area/volume of weak soft clay with densified granular columns (Figure 1). This technique results in significant improvements in overall bearing capacity, increased stiffness, decreased settlement and increased hydraulic conductivity.

In current practice, two major installation methods are adopted to install granular columns (whether sand or stone columns). The first method is the vibro-replacement technique under wet or dry conditions. From its name, the method incorporates replacing an existing weak soil with a better material (granular), which is then vibrated using a probe to achieve a certain density. The second technique is ramming the column (mostly gravel/stone) in layers inside the predrilled hole to achieve a high density.

14
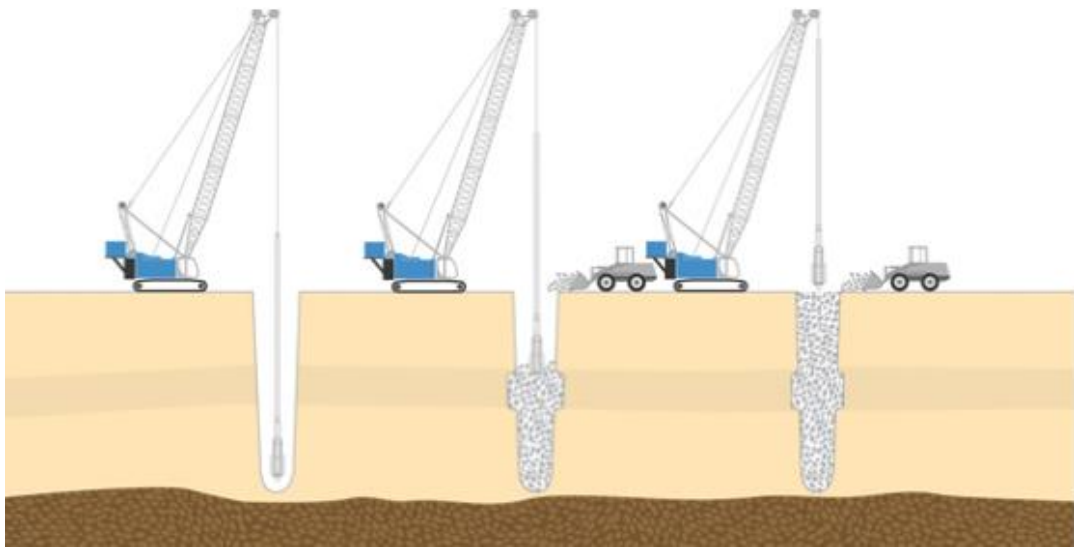
Figure 1: Stone column construction using a crane-suspended downhole vibrator (STA, 2018)

Currently in the Middle East and the region, granular columns is one of the adopted ground improvement techniques by several geotechnical specialty contractors (e.g. KELLER, MENARD, Bauer, Ammico). Ongoing projects includes sites in (1) Port Said, Egypt for building a residential complex; (2) Ruwais, UAE for building a crude oil refinery; (3) Sharjah, UAE, Lulu Hypermarket among many other sites. In Lebanon, stone columns have been used in several projects to improve the soil in place, from which are: (1) Dbayeh Waterfront city, (2) Crystal Tower Project, Antelyas, with the foundation system designed and implemented by Terrasol; and (3) Normandy, Beirut, with GeoPier company responsible for the construction of stone columns and foundations system.

The response of soft clay systems that are reinforced with granular column groups is governed by many factors, including: (1) loading rate and drainage conditions

(whether drained, undrained or partially drained), (2) area replacement ratio (defined as the cross-sectional area of the sand columns to that of the surrounding clay), (3) density of the column, (4) length to diameter ratio of the granular column, (5) and the use of encasements among others.

Granular columns are seldom designed and constructed as single elements, yet most of the studies in the literature focused on the response of soft clays reinforced with single granular columns, with experimental investigations being predominantly based on tests conducted in large one-dimensional (1D) loading chambers (Najjar 2013). Such test setups may be considered to be non-representative of actual field conditions because of limitations related to: (1) inability to control and scale the drainage conditions and the rate of loading to mimic the field loading, and (2) inability to model the correct field stress state which differs significantly from the stress levels encountered in such experiments. As a result, findings from laboratory scale model tests, even if conducted on specimens reinforced with column groups, cannot be generalized or extrapolated to the field scale problem.

To overcome these limitations, there has been significant interest in utilizing triaxial test setups to investigate the response of specimens that are reinforced with sand/stone columns while controlling the stress state, the global drainage conditions, and the rate of shearing. Triaxial testing conditions allow for the control of (1) drainage during testing (drained, undrained, or partially drained) and (2) confining stresses that could be selected to be in the same order of magnitude as those expected in the field. Examples of triaxial-based studies that utilized granular columns with soft clays include the work reported in Juran and Guermazi (1988), Sivakumar et al. (2004), Black et al. (2006), Black et al. (2007), Kim et al. (2007), Andreou et al. (2008), Najjar et al.

(2010), Black et al. (2011), Sivakumar et al. (2011), Almikati et al. (2020), and Najjar et al. (2020). The vast majority of the above-mentioned triaxial studies involve soft clays that are reinforced with single central granular columns rather than column groups.

Contact stress measurement in granular columns and the surrounding clay annulus has proven to be a key element in understanding the stress transfer mechanism between granular columns and the surrounding clay (Aslani et al. 2018). Contact stress measurements allow for determining the stress concentration ratio (defined as the ratio of the stress in the granular column to that in the clay) during loading. The stress concentration ratio is a key variable in the design of soft clay systems that are reinforced with granular columns. The magnitude of the stress concentration factor depends on a number of variables including the relative stiffness of the column and clay material, drainage conditions, column length, area replacement ratio and other construction details (Hu, 1995).

In previous studies that targeted the measurement of the stress concentration ratio (Charles and Watts 1983, Bachus and Barksdale 1984, Muir Wood et al. 2000, McKelvey et al. 2004, Murugesan and Rajagopal 2010, Cimentada et al. 2011, Fattah et al. 2011, Ghazavi et al. 2013, Miranda et al. 2017, and Nazariafshar et al. 2019) continuous measurement of the contact stresses on the column and/or clay using pressure sensors and load cells was done. This allowed for investigating the buildup of stress concentration in the granular column with displacement/strain under laboratory-scale 1-g model setups or large-scale odometers as a basis for testing. Limitations related to such tests were clearly stated in the previous paragraphs. Furthermore, the vast majority of the studies did not quantify the effect of the drainage conditions and rate of loading on the reported stress concentration factors.

Aside from measuring stresses in reinforced soft clays with granular columns and trying to understand the hybrid system, the luxury of visualizing the internal mode of deformation of soils using transparent soil-like material has been the subject of recent studies in the geotechnical world. Such materials that behave like soils are used to visualize the internal structure of soils as well as internal displacements during shearing. Specifically, the transparency of these soils, combined with the use of a laser and seeding particles, have made it possible to track the movement of specific particles within the sample/mass. Transparent soils result from mixing the solid particles with solutions that match their refractive index (RI), thereby decreasing the refraction of light within the medium (Iskander 2010). Different groups of transparent soils have been used, some of which behave like sands, and some behave like clays. Among those behaving like clays and that have been recently utilized in experimental setups to study internal deformation, is Laponite (Wallace & Rutherford, 2015). The characterization of this material is at its initial stages and requires significant additional work and exploration. However, if it is deemed functional as clay material with acceptable hydraulic conductivity, it could be used as a replacement to natural clays in a triaxial system and then reinforced with granular columns. Such setup would allow us a visual/real insight into the behavior/deformations of the granular columns.

The objective of this study is to address the above-mentioned needs. Therefore, a newly developed fully instrumented large-scale triaxial test setup will be utilized to investigate the overall response of the soft clay specimens that are reinforced with column groups with particular emphasis on monitoring pore water pressure and contact stresses over sand columns and the surrounding clay. The metrics for assessing the success in achieving this objective is based on showing that the proposed test setup is

capable of quantifying the evolution/distribution of the stresses between the sand columns and the surrounding clay at different levels of overall axial strain, while controlling drainage and enforcing confining stress levels that are consistent with field applications. In addition, full characterization of the new material, Laponite, will be done in anticipation/preparation of using it as a substitute for matrix clays in experiments designed to document/see actual internal deformations of the granular columns or any other type of reinforcing elements.

A major constraint in designing the test setup is its ability to test soft clay specimens that are reinforced with column groups rather than single columns. This constraint necessitates the utilization of a large-scale triaxial setup that is not commonly adopted in conventional triaxial testing. It is anticipated that the test setup and results presented in this study will facilitate the development/improvement of design methodologies of soft clays that are reinforced with sand column groups.

CHAPTER 2

LITERATURE AND BACKGROUND REVIEW

2.1 Behavior of Reinforced Soft Clays

In this section, a summary of the main findings and conclusions drawn in the past three to four decades with reference to the behavior of reinforced soft clays with granular columns, is presented.

2.1.1 Area Replacement Ratio

The area replacement ratios, a_r, (defined as the c-s area of the sand columns to the area of surrounding clay) could reach up to 40%, with an optimum replacement ratio of 30% to 40%, above which the interaction between the soil matrix and the granular columns may become inefficient (Black et al, 2011). The majority of the studies reported in the literature are based on experiments with a_r between 15% and 30% due to practical consideration/ease in workability (Muir Wood et al. 2000, McKelvey et al. 2004, Ghazavi et al. 2013). Studies show that increasing the area replacement ratio leads to a stiffer response as the load-sharing mechanism/distribution is dominated by the granular columns.

2.1.2 Mode of Failure

The failure mode of columns that are loaded at their top is characterized by bulging at a distance of 0.5–3 column diameters from the top of the column (Watts et al. 2000). Under wide loads, the applied loads add to the lateral passive resistance of

central columns, thus increasing their load carrying capacity and reducing bulging (Greenwood 1970, Brauns 1978). Failure of groups is characterized by bulging, bending or shearing (Muir Wood et al. 2000). Results from 3D FE numerical analyses/models indicate that as one moves away from the center of the group, outward bending of the columns increases, with central columns not showing signs of bending (Shahu and Reddy 2011). In long columns, deformations are generally concentrated in the upper zones while for shorter columns, the columns tend to punch and penetrate into the soft clay (Muir Wood et al. 2000).

In triaxial tests, short columns appeared to bulge and penetrate below the reinforced portion of the clay, while fully penetrating columns bulged relatively uniformly along their length (Sivakumar et al. 2004). Bulging was found to be more predominant in soft clays than in stiffer clays (Narasimha et al. 1992). Limited finite element results from identical rammed and un-rammed granular piers indicate that deeper bulging is expected for un-rammed piers compared to rammed piers (Chen et al. 2009). When loads are applied to columns that are encased with a geofabric, bulging is reduced significantly in comparison to the unreinforced column (Murugesan and Rajagopal 2008). In addition, bulging for encased columns decreases at the surface and is transmitted to greater depths below the top of the column (Gniel and Bouazza 2009). A recent study performed by Nazari Afshar et al. (2019) showed that a granular blanket (gravel or sand) placed over the reinforced soil helps in reducing the bulging to a reasonable degree through stress redistribution for non-encased granular columns.

2.1.3 Improvement in Bearing Capacity and Stiffness

The inclusion of granular columns in soft clays increases the bearing capacity and the stiffness. Results from field, laboratory, and finite element analyses indicate that as the area replacement ratio increases, both stiffness and strength of the reinforced clay system increase. Results from field and laboratory tests involving identical single columns and column groups tested with foundation loading at the same area replacement ratio indicate that the behavior was found to be similar (group efficiency of about 1.0) indicating that a unit cell concept can reasonably simulate the behavior of an interior column in a large group (White et al. 2007). However, results from limited finite element analyses indicate that the ratio of the settlement of the group to the settlement of an equivalent unit cell was found to range from 0.60 to 2.25 depending on the type of soil and width to length ratio of the foundation. Ratios that are greater than 1.0 indicate that the unit cell settlement is not necessarily the upper bound for settlement prediction (Elshazly et al. 2008). These finite element results were confirmed by laboratory tests which showed that for area replacement ratios between 28 and 40 %, the settlement improvement factors measured for the group were about half those measured for the equivalent single columns.

2.1.4 Critical Column Length

For a given area replacement ratio, increasing the length to diameter ratio of the columns results in an increase in the ultimate stress and stiffness. Field, laboratory and finite element results indicate that the column length is significant up to a certain point beyond which increasing the column length will not lead to an increase in strength, although it could still increase the stiffness (Hughes and Withers 1974, Narasimha Rao

22

et al. 1992, Gniel and Bouazza 2009). The stiffer response observed for longer columns could indicate that longer columns may be more efficient for settlement control (McKelvey et al. 2004). It could be concluded that there is consensus that the optimum length of stone columns for effective load transfer lies between 5 and 8 times the diameter of the column. The critical length may increase as the area ratio increases since the failure mechanism could be pushed deeper below the footing (Muir Wood et al. 2000).

2.1.5 Effect of Encasement

The load carrying capacity and the stiffness of the composite increase when the stone columns are encased with geotextiles or geogrids, whereas the generation of pore pressure decreases. The load carrying capacity and the stiffness increase with increases in the stiffness of the geofabric (Murugesan and Rajagopal 2006, Castro and Sagaseta 2011, Pulko et al. 2011). Measurements of lateral stresses next to columns indicated that stresses were higher in encased columns as compared to ordinary columns (Raithel and Kempfert 2000). The improvement due to encasement was found to be smaller for columns of larger diameters and for higher confining pressures (Wu and Hong 2009). With regards to the effect of density, data shows that loose specimens could gain more strength from the confinement than their dense counterparts (Wu and Hong 2009). Results from triaxial tests on sand specimens indicate that the measured friction angle for the encased specimen was equal to or generally smaller than the friction angle of the ordinary sand specimen (Murugesan and Rajagopal 2006). However, the encasement resulted in an apparent cohesion that was reflected in non-zero cohesion intercepts. Most of the proposed design approaches for geosynthetic-encased stone columns model

the effect of the presence of the encasement by an additional confining pressure that is assumed to exist around the column. The magnitude of this additional confining pressure is generally calculated based on the stiffness of the encasement, the thickness of the encasement, the diameter of the column, and the design axial strain or displacement of the column (Lo et al. 2010).

2.1.6 Drained, Undrained and Partially Drained Loading

The field behavior of clays that are reinforced with granular columns could range from undrained to drained behavior depending on the permeability of the clay, the area replacement ratio, and the rate of loading. Gniel and Bouazza (2009) showed through measurements of the water content of the clay before and after loading that drained, or at least partially drained, loading occurred in the clay immediately surrounding the bulge zone of the column. Studies that targeted the effect of partial drainage indicated that measured deviatoric stresses at failure in triaxial tests were the highest for fully drained conditions, the lowest for undrained conditions, and intermediate for partially drained conditions as reported by Juran and Guermazi (1988) and Andreou et al. (2008) and shown in Figure 2. It could be concluded that more research is needed to investigate the effect of partial drainage on the load response of clay-sand/stone column systems using field, laboratory, and FE experiments and analyses.
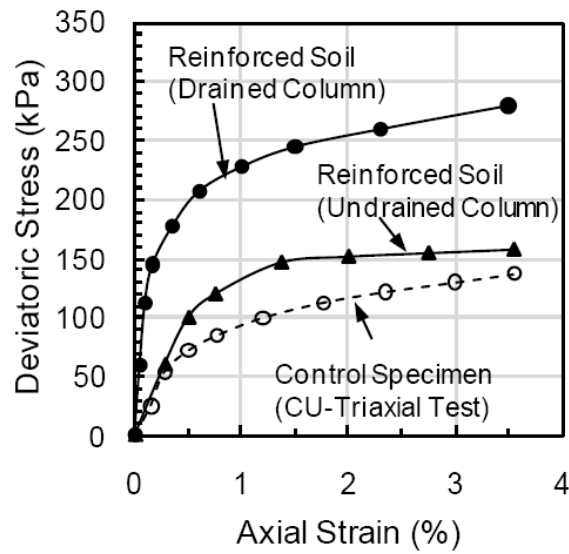
Figure 2: Deviatoric stress variation with axial strain under different drainage conditions (Modified from Juran and Guermazi 1988)

2.1.7 Effect of Arrangement, Installation Method, Type, and Density of Columns

The limited previous work that aimed at studying the effect of stone column configuration/arrangement on the consolidation rate, bearing capacity and load-sharing mechanism between the granular column and the surrounding clay was mainly based on studying the effectiveness of the unit cell concept in representing column groups. Black et al. (2007) conducted triaxial experiments with single and triangular configurations at the same area replacement ratio under drained conditions. Their results showed that the clay specimens that were reinforced with the single column configuration exhibited a stiffer response compared to specimens that were reinforced with the triangular arrangement. Aslani et al. (2018) conducted large direct shear tests to study the effect of single, triangular and square configurations on the peak shear strength of the composite, while measuring contact stresses using load cells. Results indicated that the square

configuration exhibited the stiffest response, followed by the triangular and the single column configurations.

Data on the effect of column installation methods on the loads carried by rammed and un-rammed piers from very limited FEM and field studies show contradicting results, with the data from the 3D FEM study by Chen et al. (2009) indicating that the rammed pier capacity could be more than twice that of the ordinary equivalent aggregate pier capacity, while the results from the field study conducted by Stuedlein and Holtz (2012) showed that vibro-compacted piers exhibited a 15% increase in capacity compared to the tamped piers. With regards to the composition and density of the column material, results from the field study conducted by Bergado and Lam (1987) indicated that the capacity of single rammed aggregate piers that were comprised of sands increased consistently as the density of the sand increased, while the piers in which gravel replaced part or all of the sand exhibited increases in capacity. Along the same lines, the field tests conducted by Stuedlein and Holtz (2012) indicated that columns comprised of uniformly graded gravel exhibited a higher stiffness and load carrying capacity compared to columns comprised of well graded mixture of gravel, silt, and sand. It should be noted however, that the effects of column material and method of installation witnessed above in the tests conducted by Stuedlein and Holtz (2012) on single columns "vanished" for tests conducted in the same test program on column groups with an area replacement ratio of about 30 %. This led the authors to conclude that the role of the matrix soil in a group loading could be more important than the effects of installation and column type and composition.

2.2 Experimental Setups, Instrumentation and Stress Concentration Ratio

2.2.1 Setups in Previous Studies

As mentioned previously, the majority of research experiments were done in laboratory-scale 1-g model setups or large-scale odometers as a basis for testing, with very few utilizing triaxial setups. It is clear that any serious attempt at contributing to the understanding of the mechanisms as work, would require that we develop and build a highly instrumented triaxial setup, equipped with special sensors for contact stresses measurement. As such, it was critical that a thorough review of the available literature and a detailed analysis/assessment of the setups/systems that have been used in similar previous research studies be conducted. Such a review would be used to guide any/all instrumentation and measurement systems adopted.

Charles and Watts (1983) used large scale instrumented laboratory tests to assess the effectiveness of granular columns in reducing the vertical compression of soft clays. The testing program consisted of running five tests on a group of granular columns in a triangular grid under drained conditions. The area replacement ratios used were 21% and 33%. The instrumentation of the testing program consisted of small and large earth pressure cells by Kulite Co. that read total stresses above the gravel columns and above the clay annulus, respectively. The small earth pressure cells had a diameter of 55 mm and a thickness of 10 mm, whereas the regular earth pressure cells had dimensions of L x W x t = 200 x 300 x 10 mm. Figure 3 shows the side cross sectional view of the odometer with the sample inside, with the leads outlet being at the bottom even though the sensors were all mounted at the bottom of the top plate.

The authors did not show the graphs of contact stresses with loading, but reported only the residual stress concentration factor for $a_r = 21\%$ and 33% with values of 2.2 and

4.8, respectively. Errors in all stress measurements on the order of 17% were detected. These errors were reported to occur due to improper calibration, rotation of the cells during the test and temperature variation.
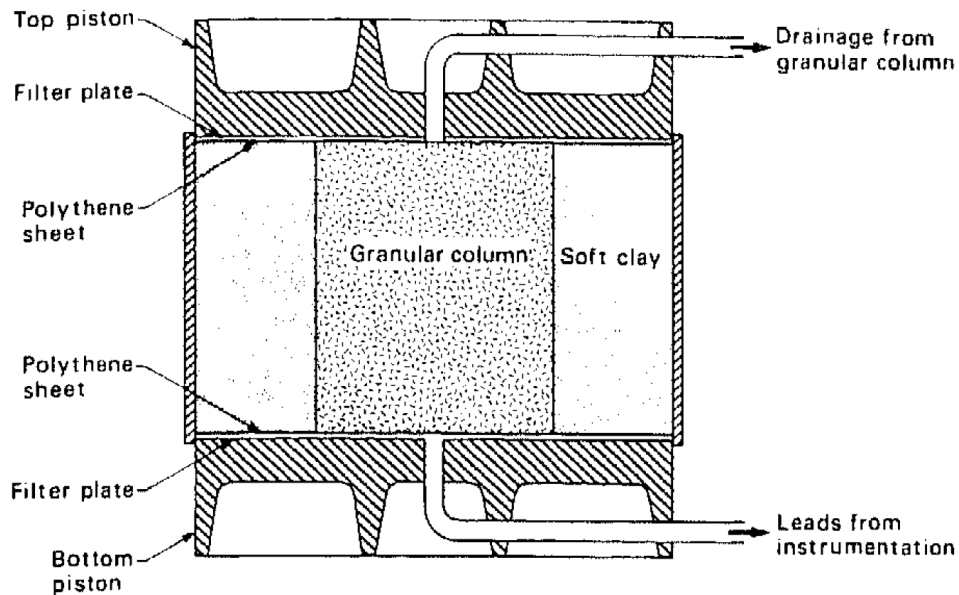
Figure 3: Cross section of large odometer sample (Retrieved from: Charles and Watts 1983)

Bachus and Barksdale (1984) conducted tests on single and group columns using an experimental setup consisting of a Plexiglas unit cell with a diameter of around 11 cm and a height of 30.5 cm for the single tests and a box with dimensions of 17.3 cm x 50.5 cm x 30.5 cm for the group tests. Pressure cells were used and mounted at five elevations in either the center of the end walls or the side faces of the box to measure lateral pressures developed between adjacent columns (Figure 4). The dimensions and capacity of the pressure cells were not mentioned in the study. The 1-D odometers allow for placement of side pressure cells to measure lateral stresses given their rigid outer

boundary. Loading was done using a loading plate instrumented with pressure cells to measure stresses in the clay and sand column. Samples with a_r of 7% and 25% were tested. Stress concentration factors were reported to increase from 1.5 up to a peak of 5.0 at low stress levels, then converging to values of 2.5-4.0 upon loading to failure. These measurements were for tests performed under drained conditions, where for the undrained conditions the stress concentration factor had an increasing trend to reach values around 4.0.
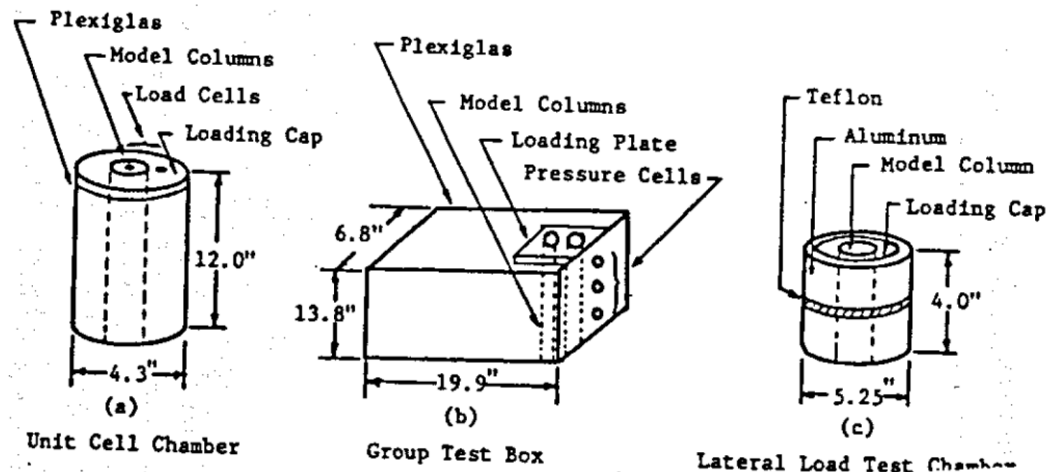
Figure 4: Schematic diagrams of tests chambers used in the model stone column studies (Bachus and Barsdale 1984)

Juran and Guermazi (1988) used a modified triaxial cell to investigate the effect of partial drainage of a soft silty soil reinforced with sand columns at a_r of 4% and 16%. As shown in Figure 5, the testing setup included four porous stones located at the bottom to measure the pore water pressure under the sand and the clay at different locations. Two load cells, with unknown dimensions, capacity and type, were mounted at the top to measure the deviatoric stress as well as the contact stress mobilized on the

clay. The loading plate used was of two parts, a central circular plate with the same

exact dimensions as the column, with the other part of the plate matching exactly the

dimensions of the surrounding clay. This made it possible to connect the second load

cell to the second part of the plate to measure the clay contact stresses, while ensuring a

proper strain compatibility between both plate compartments. The stress in the sand

column was calculated rather than measured in order to calculate the stress

concentration ratio. No details about the sensors used nor the

instrumentation/calibration were reported in the study.

The stress concentration ratio was equal to ~ 6 for samples that were reinforced

with the drained columns compared to ~3 for samples reinforced with undrained

columns. The authors stated that the soil-column interaction depends on several

parameters, including the loading process and the loading rate, the replacement factor,

the group effect, and the partial consolidation of the soft soil due to radial drainage

through the column.
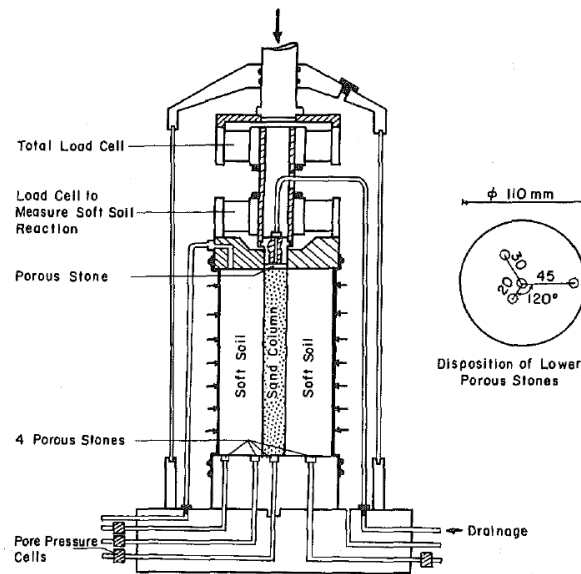
Figure 5: Modified triaxial cell for testing reinforced soil specimens (Retrieved from Juran and Guermazi 1988)

Muir Wood et al. (2000) performed load tests on stone column groups under a footing in a one-dimensional loading tank. The authors varied the spacing, diameter, and length of columns and focused on studying the mode of failure of the columns. The model tests were performed in a loading tank having a diameter of 300 mm using Kaolin clay with quartz sand columns arranged in groups. The area replacement ratio used were between 10% and 30%. Miniature pressure sensors were used, as stated by the author, above the clay and the sand columns without indicating the geometry and their capacities. These sensors were used to determine the stress concentration ratio without presenting the results of the contact stresses measured above sand columns and above the clay. The reported stress concentration ratios were for a_r of 21% and 24% for both a field and model test, respectively, which showed a great correlation, increasing from around 1.0 at low stresses to 5.0 after reaching higher stresses. (Why no picture of setup?)

McKelvey et al. (2004) investigated the load deformation behavior of a small group of sand columns under strip, pad, and circular footings. Two types of material were used in the experimental work, the first being Kaolin clay and the second being a transparent clay-like material that had almost the same properties as Kaolin clay. The internal diameter of the loading chamber was 413 mm and its length was 1200 mm and an area replacement ratio of 24% was used. After constructing the columns, a loading plate was installed at the top of the columns. Three miniature pressure cells, 18 mm in diameter, were located on the base of the pad footing (Figure 6). These were used to measure the vertical pressures at various positions on the footing base. Each pressure cell had a working pressure range of 600 kPa. Two types of columns were tested in kaolin clay at the same area replacement ratio, the partially (P) penetrating and the fully (F) penetrating columns. The results shown in Figure 7 indicate that there is an effect of penetration depth on the stress mobilization in sand columns. The stress concentration ratio for the test with fully penetrating sand columns were in line with previous studies as mentioned by the author; however for the partially penetrating columns, the stress concentration ratios were building up with axial strain rather than going over a peak at low axial strains and softening afterwards. Interestingly and at higher loading stresses, the stress ratio appeared to approach a constant value (approximately 3), regardless of the column length. This observation agrees well with previously reported data, particularly from field studies (Bachus and Barksdale, 1984).
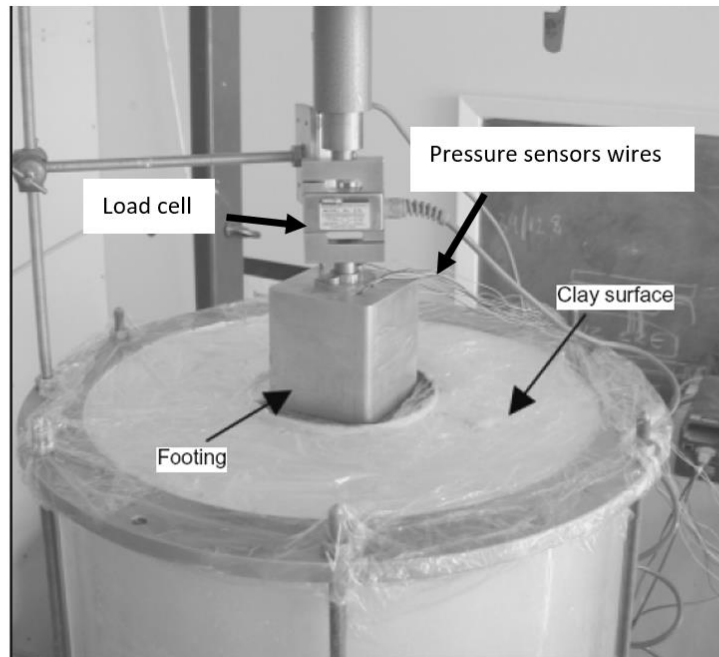
Figure 6: Foundation loading with instrumentation used (McKelvey et al. 2004)
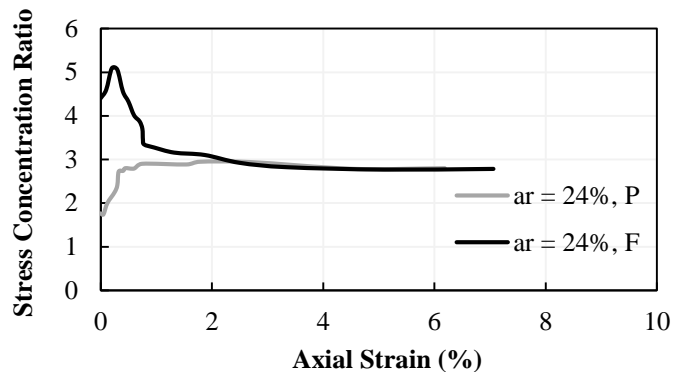
Figure 7: Variation in the stress concentration ratio with axial strain for long and short columns (Modified from McKelvey et al. 2004)

White et al. (2007) conducted four footing load tests on single and group rammed aggregate piers having a diameter of 0.76 m and installed to depths of 2.79 m and 5.10 m in a site characterized by a 13-m thick deposit of soft alluvial clay (CL) overlying glacial till and shale. The full scale tests were conducted using steel reaction

beams secured to helical anchors. All tests were stress-controlled in which the

displacement under each load increment was allowed to reach a steady value before

adding another increment. Results of the load tests on single and group columns

indicated that shorter columns developed more tip movement than the longer columns.

The instrumentation included the installation of multiple 23 cm diameter stress

cells: at the top of the piers in the center, at a certain depth of the pier and above the

clayey soil. The aim of this distribution was to measure the vertical stress distribution.

As for the stress concentration ratio, it was calculated as the ratio of the contact stress

on top of the pier to the contact stress of the matrix soil without denoting which stress

cells were used for this calculations and without showing the contact stress graphs. The

instrumentation also included telltales to measure pier deformations and inclinometers

to measure lateral movement. Figure 8 below shows the instrumentation and the array

configuration of the stress cells used.
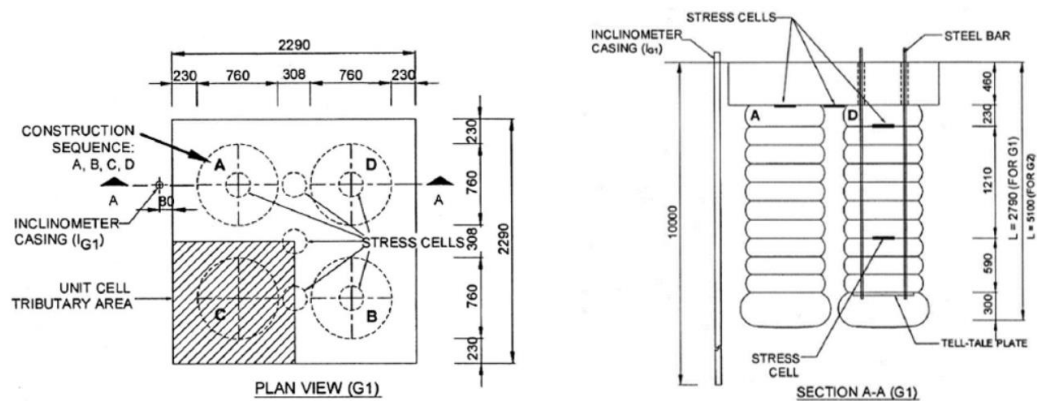
Figure 8: Instrumentation on field for rammed aggregate loading (White et al. 2007)

The mobilized stresses were not large given that tests were stopped at axial strains around 3% to 4%. The reported stress concentration ratio was for an area replacement ratio of 35% and showed a peak at low axial strains of 5.5 (Figure 9), after which the stress ratio did not show a dramatic drop, when compared to laboratory tests, and this might be attributed to the fact of having a stiffer, rammed aggregate piers in this study.
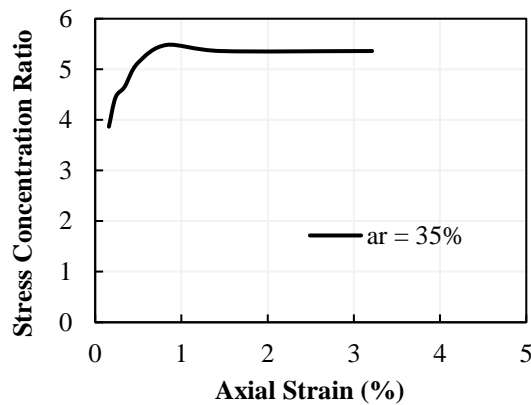
Figure 9: Stress concentration ratio variation with axial strain for rammed aggregate piers loaded in drained conditions (Modified from White et al. 2007)

Murugesan and Rajagopal (2010) conducted laboratory model tests on stone columns installed in a clay bed prepared in a large-scale testing tank (Figure 10a). The model tests were performed on single and group stone columns, with and without encasements. The authors aimed at quantifying and qualifying the effect of different encasements on the axial load capacity and load-sharing mechanism, where they developed, based on the results of their experimental testing program, guidelines for the design of geosynthetic encased stone columns.

As for the instrumentation of the testing program, four pressure cells were used to measure contact stresses above three sand columns with the fourth being above the central clay, which was between the loaded columns. The accuracy of the cells were 0.1 kPa, but no information about the type and geometry was mentioned. The cells were positioned at the bottom of the loading plate (Figure 10b) and were maintained flush with the loading surface. The stress concentration ratio for different tests were observed to study the effect of encasements of stone columns on the mobilization of stresses inside. It showed (Figure 11) that for ordinary stone columns (OSC) the peak stress concentration ratio was around 6.0 at low axial strains, which decreased to 2.0 at high axial strains. This is a typical observation between the performed studies in literature. On Figure 11 also, results for two different encasement type stone columns showed that the peak could reach up to 12.0 when encasing the stone columns with geosynthetics. The residual stress concentration ratios for both tests with encased stone columns was around 4.0.
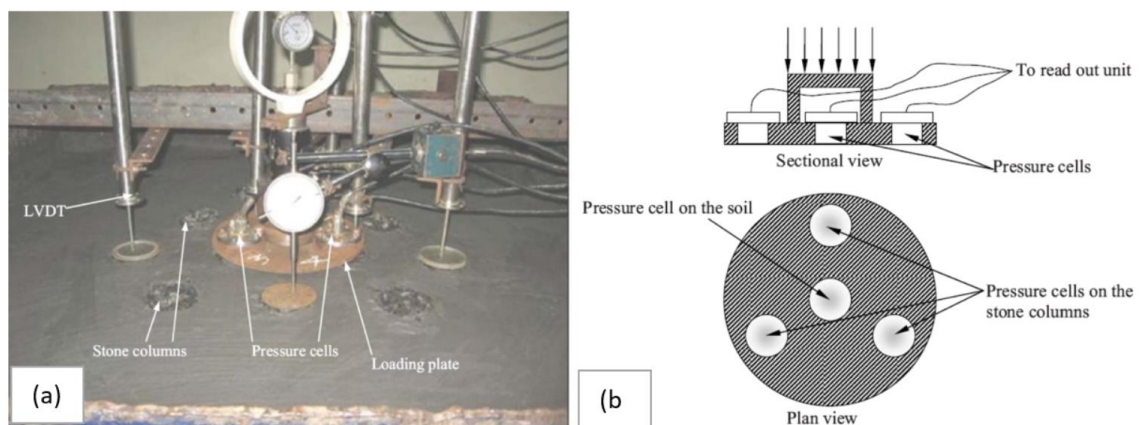
Figure 10: Instrumentation of the large scale testing tank showing (a) loading frame above the soil; (b) schematic of the loading plate with pressure sensor position (Modified from Murugesan and Rajagopal 2010)
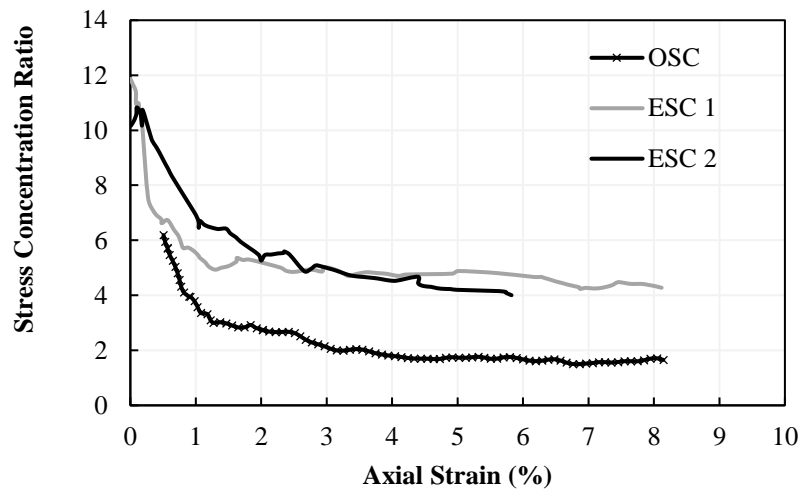
Figure 11: Stress concentration ratio variation with axial strain for tests on ordinary and two different encasement type stone columns (Modified from Murugesan and Rajagopal 2010)

Cimentada et al. (2011) conducted 1-g consolidation tests on a unit cell that is comprised of kaolin reinforced with single ordinary gravel columns with diameters of 8.47 cm and 6.35 cm. The kaolin was consolidated from a slurry in a Rowe-Barden cell with a diameter of 25.4 cm and a depth of 14.6 cm, resulting in area replacement ratios of 11.11% and 6.25 %. Figure 12a shows a schematic of the loading plate with the pressure sensors and instrumentation. The schematic shows that three pore pressure transducers and four contact pressure sensors were used at different radial distances to measure the pore water pressure as well as the contact stresses, respectively. XPM10-10G-LC1 (quality by measurement, QBM) pressure cells of 8 mm diameter were used for measurements in the clay, and XPM10-50G-HA-LC1 cells with the same diameter were used for measurements in the stone column. The calibration for all sensors was

done first with water, and then with both soil materials. The calibration showed, as mentioned by the authors, good results in the measurements. The authors touch on the fact of saturated soils being used for calibration of the pressure cells in kaolin clay, and this could be thought of as minimizing the point loading of the soil grains with the active part of the sensors, thus minimizing measurement noises and errors.
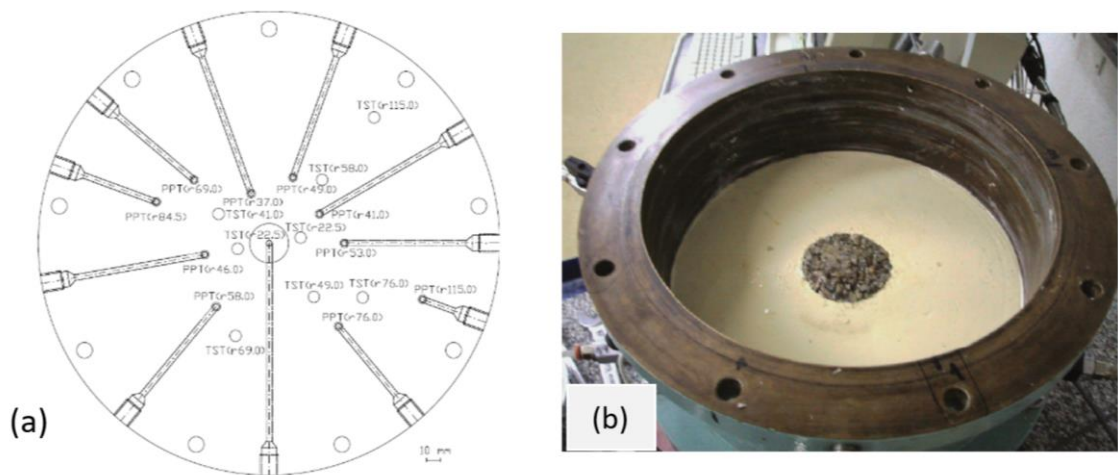
Figure 12: Rowe-Barden cell with (a) instrumentation of the base and (b) single column reinforced kaolin sample in place (Modified from Cimentada et al. 2011)

The reported stress concentration ratios for the low area replacement ratios of 6.25% and 11% were extremely high, reaching values up to 16.6 at low loading steps, but ranging on average between 2.5 and 7.0, at higher stress levels, which is also considered higher than the reported values in the literature, especially for this low area replacement ratios without any use of encasements. This might be due to the fact of applying a stress controlled test and waiting for longer than usual times. Moreover, the sensors (8 mm in diameter) used above the gravel column could be a major source of

error, as the grain size of this material is incompatible with the size of the sensors' active part, and could easily lead to inaccurate measurements. This type of sensors uses the elastic deformation of the metallic surface of the active part as basis for measurement, and, theoretically, it is best used for liquid, as the pressure is distributed all over the sensor surface area. However in the case of measuring stresses over a gravel column, it is expected to get a considerable variability in the measurements for the same loading increment.

Fattah et al. (2011) conducted laboratory 1-g tests on CL soil (10 % sand, 42 % silt, and 48 % clay) that was compacted at a water content of 24–35 % in a 1.1 m × 1.0 m × 0.8 m steel tank (Figure 13a) and reinforced with single and group (2, 3, or 4) crushed stone columns (density = 16.3 kN/m^3) having a diameter of 5.0 cm and lengths of 40 cm (fully penetrating with L/D = 8) and 30 cm (partially penetrating with L/D = 6). The area replacement ratios were as thus 5%, 10%, 15% and 20%. The loading was stress controlled with a 22-cm diameter loading plate with each loading step applied at 2.5 min until the settlement was 5 cm.

Different foundation plates were designed to cater for the loading of different column configurations (single vs. group) as shown in Figure 13b. Every configuration has its own loading distributors and proving rings, as indicated by the authors. The loading distributor shown in Figure 13b is for the two column configuration, which could have a different geometry (1, 3 or 4 loading distributors) for the different configurations. The instrumentation used consists of: dial gauges with proving rings to measure the stresses on the sand alone as well as the clay annulus connected on the reference beam for strain compatibility. The loading was done on stress increments and continuous measurements of contact stresses were measured. The stress concentration

ratio was thus calculated based on the measured contact stresses from the dial gauges.

Two main conclusions with regards to the stress concentration ratio were drawn from this analysis: (1) long columns mobilize higher stresses when compared to shorter columns (Figure 14) and (2) for low area replacement ratio ($a_r = 5\%$), the stress concentration ratio was between 1.0 and 1.8 only, depicting low to no efficiency when using an a_r lower than 10%.
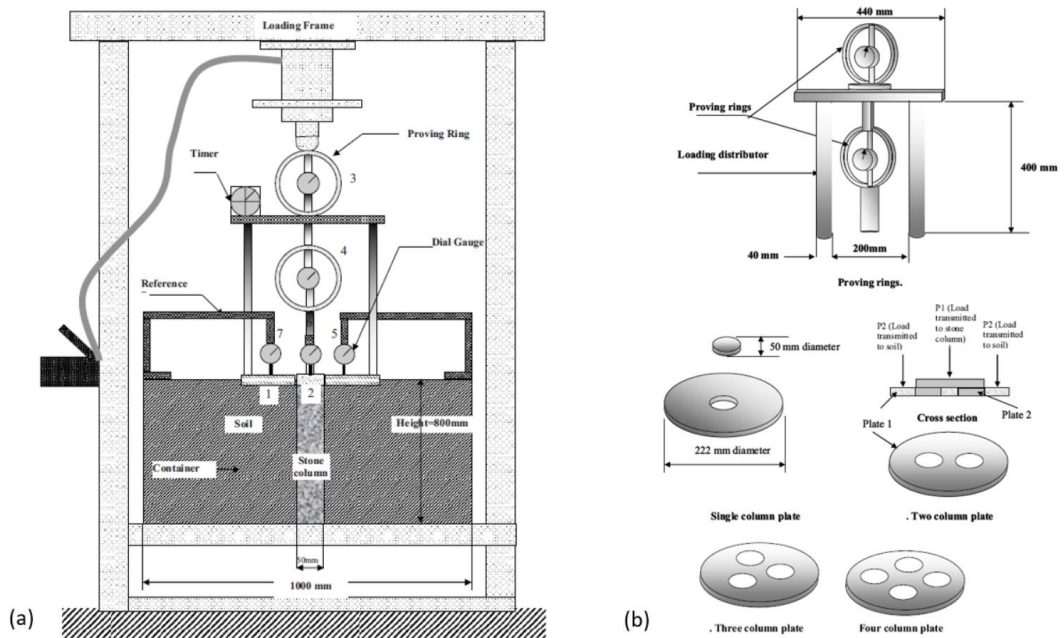
Figure 13: Schematic diagram of the experimental setup showing (a) steel tank with soil and (b) different plates for different configurations
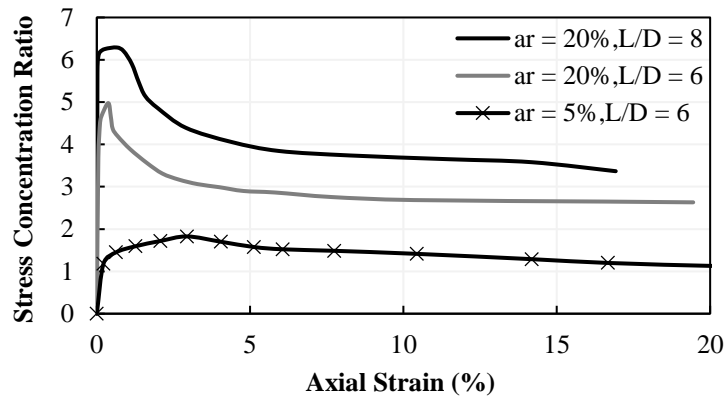
Figure 14: Stress concentration ratio with axial strain for different a_r and L/D (Modified from Fattah et al. 2011)

Ghazavi and Afshar (2013) conducted a series of large 1-g laboratory tests on soft clays (CL) reinforced with single or group stone columns in a large test box (Figure 15a). The granular inclusions were either ordinary or encased with different types of geotextiles. The tests were strain controlled with a rate of 1 mm/min to ensure drained conditions. The instrumentation used in this testing setup included one miniature load cell ($\varphi = 50\ mm$), other than the main load cell, with no information about the accuracy and calibration of the sensor was mentioned. The miniature load cell was mounted flush to the bottom of the loading pad as seen in Figure 15b. This allowed for measuring the total stress applied as well as the stress in either the column or the clay matrix, depending on the configuration used. Thus, the stress in the stone column was calculated when the contact stress above the clay was measured, and vice versa. This allowed for the calculation of the stress concentration ratio, and was done for all performed tests. Note that the diameter of the columns ranged between 60, 80 and 100 mm while ensuring a length to diameter ratio of 5 and an area replacement ratio of 16%, through varying the spacing between the columns.
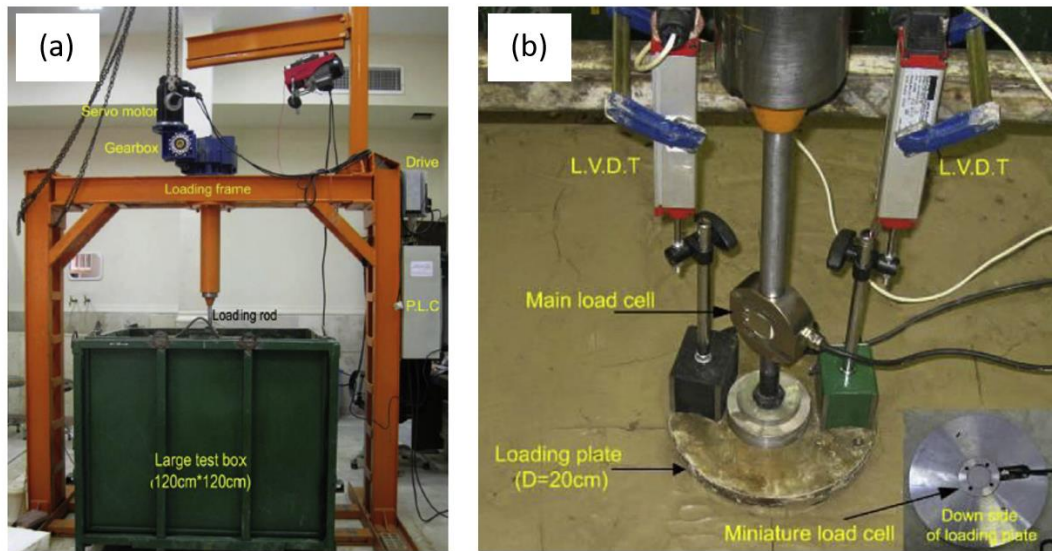
Figure 15: Testing setup showing the (a) large test box with the actuator and loading frame, and (2) instrumentation with load cells and LVDT's mounted over and inside the loading plate (Modified from Ghazavi and Afshar 2013)

The testing program allowed for observing the following: (1) the encasements reduce the bulging due to the additional confinement provided, which also in its turn increases the stiffness/strength of the column, (2) the stress concentration ratio increases with the use of the encasements, having higher peaks and higher residual values(3) the stress concentration ratio goes over a peak at low axial strain for both the encased and ordinary stone columns after which it decreased to a residual value at high axial strains, and this was true for both the OSC and ESC as shown in Figure 16.
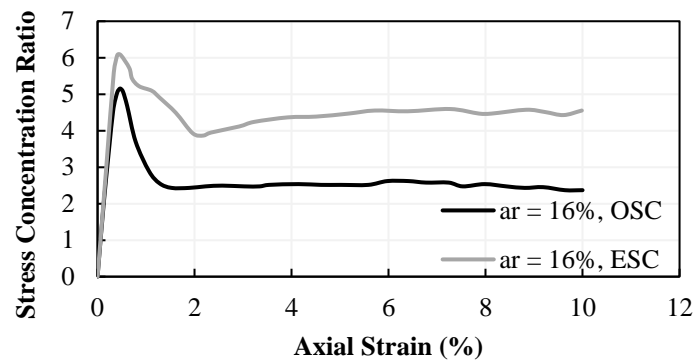
Figure 16: Stress concentration ratio with axial strain for ordinary and encased stone columns under drained conditions (Modified from Ghazavi and Afshar 2013)

Miranda et al. (2017) conducted three 1-D consolidation tests in a large instrumented Rowe-Barden oedometric cell which is the same used by Cimentada et al. (2009) as shown in Figure 12. The paper presents the influence of geotextile encasements on the behavior of the stone columns reinforcing soft soils. The soil used is also kaolin clay prepared in a bed and consolidated after that, with the columns being limestone gravel. The diameter of the columns was 8.5 cm corresponding to an area replacement ratio of 11% only.

Results of stress distribution, pore pressure and soil settlement were presented. The authors concluded that encased columns supported vertical stresses 1.7 times that supported by ordinary columns. The range of the stress concentration factor was between 11 and 25 for the encased columns while this ratio ranged between 3 and 10 for the ordinary stone columns. Pore pressure dissipation which was related to the degree of consolidation and was higher in the two experiments with encasements as compared to the ordinary one. No graphs were presented for the stress concentration ratio and the data provided was not enough to plot manually the stress concentration ratio with axial

strain as the settlements/axials strains were not that clear, so graphs were basically interpolated with few points, based on one axial strain value for one applied stress; this is shown in Figure 17 below. The reported values for the stress concentration factor in this study for just an 11% area replacement ratio are too high, even though with the use of encasements. Values in the range of 15-25 means that merely the clay is feeling the load applied and all the load is carried by the stone column. The reported results are also, as in the case of the results presented by Cimentada et al. 2011, quite off from those found in the literature. Both researches used the same setup and sensors (pressure sensors with dimeter of 8 mm used over gravel columns) and this could kind of justify the reason of having similar results.
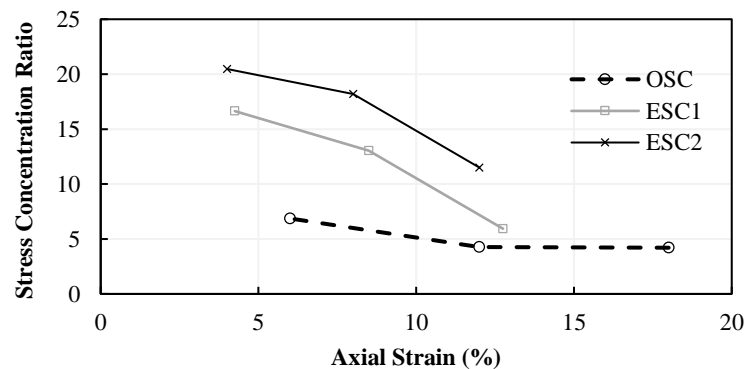
Figure 17: Stress concentration for encased and ordinary stone columns at $a_r = 17\%$ (Modified from Miranda et al. 2017)

NazariAfshar et al. (2019) conducted 1-g laboratory tests on group of long and short stone columns to study the bearing capacity with the use of granular blankets above the columns (thickness 7.5 cm). The testing setup, instrumentation and materials used were the same as in the paper of Ghazavi et al. (2013). Geotextiles and geogrids

were used to reinforce the stone columns and their effect on the bearing capacity was studied. The columns were all 6 cm in diameter and the area replacement ratio was maintained at 19%. Figure 18 below summarizes the main finding for the stress concentration ratio of both encased and non-encased stone columns. The results comply with those presented previously in the literature in terms of: (1) the use of encasements increase the contribution of granular columns to carrying more load and (2) fully penetrating columns mobilize more stresses than partially penetrating columns. The effect of encasements decreased though when using short columns, this is shown as having the ordinary fully penetrating column carrying more stresses than the encased partially penetrating, depicted in Figure 18 as higher stress concentration ratio for the former.
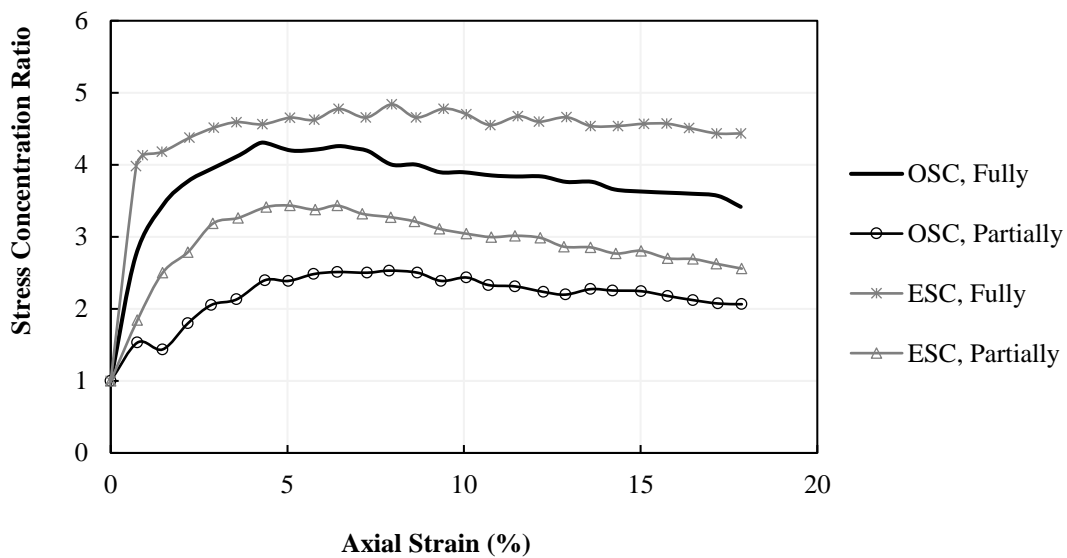
Figure 18: Stress concentration ratio with axial strain for short and long stone columns with and without encasements (Modified from Nazari Afshar et al. 2019)

2.2.2 Remarks on Sensors, Contact Stress Measurements and Stress Concentration Ratio

The literature review conducted focused on the different setups and instrumentation systems (pressure sensors and load cells) used to measure or calculate the contact stresses above/below granular columns and the surrounding clay. It also presented all the work done in an attempt to evaluate the stress concentration ratio. Table 1 summarizes most of the relevant information from all published studies that targeted measuring the stress concentration ratio in a laboratory setting (Charles and Watts 1983, Bachus and Barksdale 1984, Juran and Guermazi 1988, Muir Wood et al. 2000, McKelvey et al. 2004, Murugesan and Rajagopal 2010, Cimentada et al. 2011, Fattah et al. 2011, Ghazavi et al. 2013, Miranda et al. 2017, and Nazariafshar et al. 2019). The information presented in Table 1 leads to the following observations and conclusions:

1. The contact stress measurement could be done using a load cell, pressure cell or even a miniature pressure sensor that is usually used for fluid pressure measurements.

2. Calibration of the sensors is critical, as it should be done on water, clay and sand; however, the soil should be saturated to minimize point load concentrations.

3. If the granular column is not a poorly graded fine sand (like well-graded sand, gravel or stone column) the use of miniature load cells should be avoided as it is accompanied with high source of errors, and could generate misleading stress data.

4. There are no data for the actual measured contact stresses above the different soils tested. The only data available in the literature is in the form of stress concentration ratios only.

5. The stress concentration ratio is not a constant for a given reinforced clay system (given area replacement ratio and given column length/penetration) since it depends on the strain level, magnitude of the applied stress relative to the failure stress, time from the application of the load, and drainage conditions.

6. The reported stress concentration ratio for fully penetrating columns under drained conditions and an area replacement ratio between 7 % and 25% showed an early peak at low axial strains in the range of 4.0 to 6.0, after which it decreased to residual values between 2.0 and 3.0.

7. The post peak strain softening behavior for fully penetrating columns under drained conditions in the sand column is related to a load transfer to the nearby soil from the yielding column. Drainage and progressive consolidation of the soil affects the total bearing capacity as well as the load sharing between the column and the soil.

8. Encasing the granular columns with geosynthetics or geogrids could increase the stress concentration ratio by a factor of 1.5 to 2.0, which actually increases the contribution of granular columns in load carrying through providing additional confinement.

9. Little to no data is available for stress concentration ratio measurements under undrained loading. Most of the studies focus on drained/prolonged loading.

10. The vast majority of the studies did not quantify the effect of the drainage conditions and rate of loading on the reported stress concentration factors.

11. All the studies, except Juran and Guermazi (1988), utilized laboratory-scale 1-g model setups or large-scale odometers as a basis for testing. Limitations to such tests were clearly stated in previous sections.

12. Even though Juran and Guermazi (1988) utilized triaxial setup to measure the stress concentration ratio, the authors only utilized single columns rather than column groups.

Table 1: Experimental research programs with stress concentration factors reported

Reference	Type of Experiment (S = single, G = group)	Loading Conditions (Stress = stress controlled, Strain = strain controlled D=drained, U=undrained)	Area Replacement Ratio (%)	Sensor used for stress measurement (LC = load cell, PS = pressure sensor) m = miniature	Stress concentration factor, n (U = undrained, D = drained F = fully pen., P = partial pen.)
Charles and Watts (1983)	1-g Cons.[a] (S)	Stress (D)	21, 33	PS	a_r=33%, n = 4.8 a_r=21%, n = 2.2
Bachus and Barksdale (1984)	1-g (S/G)	Stress (D) Strain (D)	7, 25	LC	S - n = 2.8-4.2 G - n = 2.5-4.0
Juran and Guermazi (1988)	TX (S)	Strain (D/U)	4	LC	n_D=6.0, n_U=3.0
Muir Wood et al. (2000)	1-g (G)	Strain (D)	10, 30	-	n_P=6
McKelvey et al. (2004)	1-g (G)	Strain (U)	24	m-PS	n_F = 5.2, n_P=2.8
Murugesan and Rajagopal (2010)	1-g (G)	Stress (D)	23	PS	n = 7.0-9.0
Cimentada et al. (2011)	1-D Cons.[a] (S)	Stress (D)	6.25, 11	m-PS	n = 2.5-9.0
Fattah et al. (2011)	1-g (S/G)	Stress (U)	5, 20	Gauges	n = 1.4-6.0
Ghazavi et al. (2013)	1-g (S/G)	Strain (D)	16	m-LC	n = 5.5-6.2
Miranda et al. (2017)	1-g Cons.[a] (S)	Stress (D)	11	m-PS	n= 3.0-6.0
Nazariafshar et al. (2019)	1-g (G)	Strain (U)	19	m-PS	n = 2.2-4.3

Table 1 shows that 10 out of the 11 reported studies utilized laboratory-scale 1-g model setups or large-scale odometers as a basis for testing. Limitations related to such tests were clearly stated in the previous paragraphs. As indicated in Table 1, the only triaxial-based study that measured the stress concentration factor utilized single columns rather than column groups. Finally, results in Table 1 show that the vast majority of the studies did not quantify the effect of the drainage conditions and rate of loading on the reported stress concentration factors. There are no studies that aimed at measuring stress concentration factors within triaxial settings for soft clays that are reinforced with column groups under different drainage conditions. Any advancements that were made/documented in the literature on this issue are still at nascent stages.

2.3 Transparent Soil

2.3.1 Materials Used

The use of transparent synthetic soils in laboratory testing programs emerged as a non-intrusive technique for the visualization of internal displacements (Iskander, 2010; Ganiuy et al., 2016). Transparent aggregate soils have been produced by saturating a transparent aggregate with a pore fluid with matching refractive index, thus creating a homogeneous medium (Iskander and Liu, 2010; Peters et al., 2011). A variety of transparent materials have been used in this regard, including amorphous silica powder (e.g. Sadek et al., 2002; Liu et al., 2003), silica gel (Iskander et al., 2002; Liu & Iskander, 2010) and fused quartz (e.g. Ezzein and Bathurst, 2011; Ferreira & Zornberg, 2015; Peng & Zornberg, 2019). The pore fluids used to match the refractive index of these transparent aggregates include liquids such as mineral oils, white oil, paraffinic oil or even a blended mixture of two or more of these liquids.

The amorphous silica powder, which requires the use of oil as pore fluid, has been used as a transparent material to model clay-like soils. This dates back to the work of Lai et al. (1994). However, one main disadvantage of using this aggregate material is the contingency of getting a transparent medium only when oil is used. Also, researchers faced challenges when using amorphous silica to model soft and highly plastic clays, due to its low plasticity. Here rose the need for another type of aggregate material that behaves like soft clays, yet without the strict need for using oil as the pore fluid.

Recently, and after the work of Wallace et al. (2015), a new material has emerged, called Laponite, which behaves like clays when mixed with water to match its refractive index. There is no need to use different oil mixes to produce and match the refractive index of Laponite; just by simply adding water to the white powder, transparent clay-like material will be formed. In fact, Laponite presented a series of advantages when used as a transparent soft clay surrogate in geotechnical physical models, in terms of plasticity, rheology, and transparency.

The use of transparent like soils could be really informative in the context of geotechnical engineering when it comes to tracking displacement and stress fields of soils in a non-intrusive manner. Studies have shown that tracking particles could be done with laser aided imaging or simply using particles as references without the need for a laser. The laser is mainly used (e.g. Black et al. 2015; Peng & Zornberg, 2019) when the soil-like material behaves like sands i.e. silica gel or crushed fused quartz (Figure 19a). The application of the laser allows for capturing the edges of the particles, and thus tracking their movement could be easily done using digital processing techniques for the consecutive captured images. However, when no laser is used, and if

there is no other non-transparent material, like natural sand or geosynthetics, some use the "seeding particles" that could be followed/tracked successively (Ads et al. 2020). Seeding particles could be anything small in volume and colored (e.g. black fine sand particles) that can float in the clay matrix, and could be tracked during testing (Figure 19b). The installation of these particles should be done in a predetermined vertical plane, so that the analysis/tracing is done in two-dimensional coordinate system.

The two famous image processing techniques that are used for analysis are: digital image correlation (DIC) and the particle image velocimetry (PIV). Both techniques provide the same output, i.e. vector fields for displacement of particles, with the only difference being the approach/tools used for analyzing the images. These methods are used for images taken with and without laser.
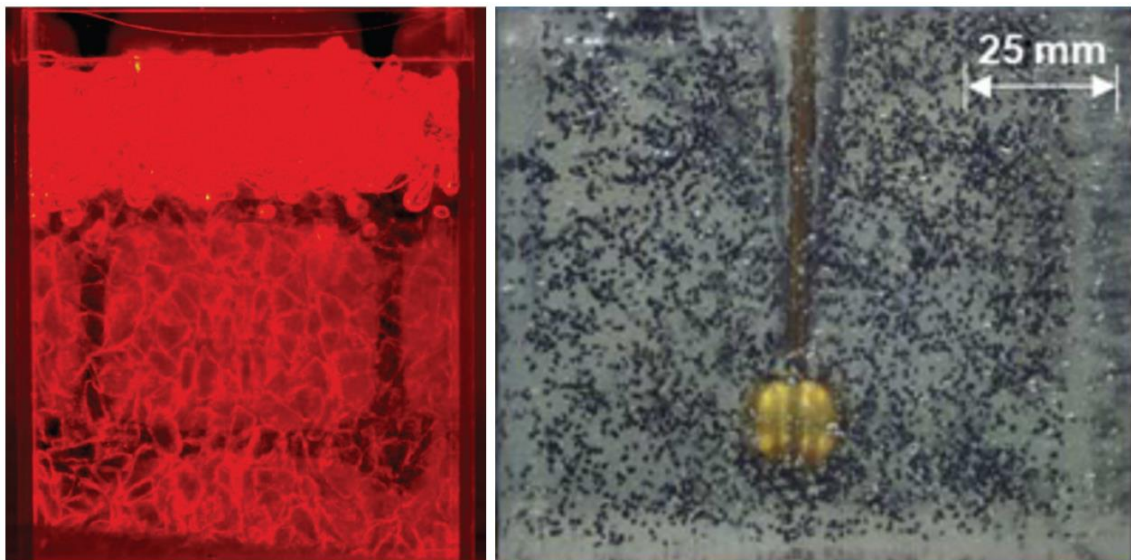
Figure 19: Image capturing with the use of (a) laser in fused quartz and (b) using black sand particles in Laponite mixture without the use of laser (Modified after Peng & Zornberg, 2019 and Ads et al. 2020)

2.3.2 Laponite Clay Surrogate

As mentioned earlier, Laponite is a white powder that forms a transparent clay surrogate when mixed with water. This material has a very low undrained shear strength, which makes it comparable to that of marine soft clays. In the past couple of years, attempts have been made with the Laponite material to characterize its geotechnical properties (Wallace & Rutherford 2015), assess its transparency (Yi et al. 2018) and quantify its shear strength using miniature ball penetrometer tests (Ads et al. 2020). Laponite was also used for physical modeling of geotechnical systems, such as the work of Wallace & Rutherford (2015), through utilizing laser techniques and image processing to visualize failure surfaces after loading caisson foundations.

Laponite is characterized as having thixotropic behavior, which is defined by Mitchell (1960) as a time-dependent change in strength for a non-equilibrium state in inter-particle forces after mixing, remolding or compaction, and is common in highly sensitive clays. In the technical literature, thixotropy has been referred to as aging, thixotropic hardening and structuration (Mitchell 1960; Rodriguez & Santamarina 1999), and is a reversible, time-dependent strength gain. Mitchell & Soga (2005) reported two sources of shear strength gain: a fixed remolded strength and a reversible aged strength. Since Laponite exhibits a thixotropic behavior, meaning that Laponite mixtures can go back and forth between gel and liquid state when left to age or mixed, respectively, both sources of shear strength gain may be anticipated.

One major practical limitation of Laponite is that mixtures cannot be prepared in high concentrations, partly because of the comparatively rapid gelation process. Consequently, the use of additives was proposed as a solution to this problem in order to retard the time of gelation of the Laponite when mixed with water during sample

preparation (Beemer et al. 2016). A specific additive, Sodium Pyrophosphate (SPP), has been used in recent studies in order to facilitate the preparation of Laponite mixtures at comparatively higher concentrations, which has in turn produced mixtures of comparatively higher shear strength and stiffness. However, only a relatively small number of mixtures has been investigated so far that would allow assessment of the impact on geotechnical properties of factors such as laponite content, SPP dosage or aging time. This would be particularly relevant because variables such as SPP dosage, which facilitate the preparation of mixtures at higher Laponite content, may also result in a decreased thixotropic behavior. Consequently, the impact of increasing SPP dosage on the geotechnical properties of laponite is unclear.

2.3.3 Applications of Laponite

Many geotechnical experiments could be more informative if the researcher visualize internally the displacement of particles, mainly if it is related to describing qualitatively the mode of failure during loading/shearing. As such, Laponite could replace natural/synthetic clays in many geotechnical laboratory applications from which are: (1) pullout tests, (2) large-scale beds with group granular reinforcement (3) modeling fault failure, (4) modeling slope failure, (5) triaxial testing and much more.

In the context of this research, using Laponite as a replacement to typical clays when reinforced with granular columns would be really valuable. This is true in the shearing phase to analyze continuously the mode of failure with axial strains. Determining the mode of failure for typical soils tested in laboratories is normally determined by slicing the samples in half, or by looking macroscopically to determine

the overall failure (whether bulging or failing along a sheared plane). However, when using transparent soil as a replacement to typical clay material, this will allow for non-intrusive measurements of the failure mode, through studying the displacement vector fields from the continuous captured images during shearing.

In summary, Laponite is still a new material that is being studied in geotechnical laboratories. There is still a clear need to study the behavior of this material under different concentrations conduct geotechnical experiments to better understand the undrained shear strength, thixotropic behavior, permeability, and consolidation parameters, among others.

CHAPTER 3

LARGE-SCALE INSTRUMENTED TRIAXIAL SETUP FOR INVESTIGATING THE RESPONSE OF SOFT CLAY REINFORCED WITH SAND COLUMN GROUPS

3.1 Introduction and Background

The use of granular inclusions in the form of sand drains or gravel (stone) columns is a common ground improvement solution in many geotechnical engineering applications, particularly those involving relatively light to moderately loaded systems extending over large areas (Najjar et al. 2010). This ground modification technique consists primarily of replacing a certain area of weak soft clay with stiff granular columns. The area replacement ratio could be anywhere between 5% up to 40%, with optimum replacement ratios mostly in the range of 30% to 40%, above which the interaction between the soil matrix and the granular columns may become inefficient (Black et al. 2011).

Granular columns are designed and constructed in groups rather than as individual elements. Given that, there is a clear need to study the group effects and load sharing under various drainage condition. Most of the studies reported in the literature focused on the response of soft clays reinforced with a "single" granular column. Experimental investigations were predominantly based on tests conducted in large one-dimensional (1D) loading chambers (Najjar 2013). Such testing arrangements may be considered to be non-representative of actual field conditions. This is true due to the inability to control the drainage conditions and rate of loading to mimic the field loading, in addition to the inability to model the correct field stress state, which differs

significantly from the stress levels encountered in such model experiments. As a result, findings from laboratory scale model tests, even if conducted on specimens reinforced with column groups, cannot be generalized or extrapolated to the field scale.

In order to overcome these limitations, significant interest was shown by researchers to use a triaxial testing setup to investigate the response of specimens that are reinforced with sand (or stone) columns while controlling the stress state, the global drainage conditions, and the loading rate. Triaxial testing conditions allow for the control of (1) drainage during testing (drained, undrained, or partially drained) and (2) confining stresses that could be selected to be in the same order of magnitude as those expected in the field. Many researchers studied the behavior of granular columns installed in soft clays in triaxial testing setups. This includes the work of Juran and Guermazi (1988), Sivakumar et al. (2004), Black et al. (2006), Black et al. (2007), Kim et al. (2007), Andreou et al. (2008), Najjar et al. (2010), Black et al. (2011), Sivakumar et al. (2011), and Almikati et al. (2020). The vast majority of the above-mentioned triaxial studies involve soft clays that are reinforced with a single central granular column rather than column groups.

The existing works available in the literature that specifically addressed column groups include the efforts of Bachus and Barksdale (1984), Muir Wood (2000), Black et al. (2006, 2007), White et al. (2007), Murugesan and Rajagopal (2010), Fattah et al. (2011), Miranda et al. (2017), and Aslani et al. (2018). The majority of these studies utilized large one-dimensional (1D) loading chambers to investigate the effects of (1) spacing between adjacent columns, (2) configuration of columns in the group, (3) column diameter and penetration depth, and (4) area replacement ratio, on the response of the composite.

The measurement of contact stresses on granular columns and the surrounding clay annulus has been identified as a key element in understanding the stress transfer mechanism between the granular inclusions and the surrounding matrix (Aslani et al. 2018). Contact stress measurements at different stages of loading allow for determining the stress concentration ratio, which is defined as the ratio of the stress in the granular column to the stress in the clay. This ratio is a key parameter when designing reinforced soft clay systems. Several parameters and factors affect the magnitude of the stress concentration ratio from which are: the relative stiffness of the column and clay material, drainage conditions, slenderness of the column, area replacement ratio and other construction details (Hu, 1995).

Table 1 summarizes results from all published studies that targeted the measurement of the stress concentration ratio in a laboratory setting (Charles and Watts 1983, Bachus and Barksdale 1984, Juran and Guermazi 1988, Muir Wood et al. 2000, McKelvey et al. 2004, Murugesan and Rajagopal 2010, Cimentada et al. 2011, Fattah et al. 2011, Ghazavi et al. 2013, Miranda et al. 2017, and Nazariafshar et al. 2019). In these studies, continuous measurement of the contact stresses on the column and clay using miniature pressure sensors and load cells allowed for the investigation of the buildup of stress concentration in the granular column with axial strain. The tests in Table 1 are limited to loading setups involving axial compression, including triaxial compression, footing loading, and area loading.

Information in Table 1 indicates that 10 out of the 11 reported studies utilized laboratory-scale one dimensional model setups or large-scale odometers as a basis for testing. As indicated in Table 1, the only triaxial-based study that measured the stress concentration factor utilized a single column rather than column groups. Finally, results

in Table 1 show that the vast majority of the studies did not quantify the effect of the drainage conditions and rate of loading on the reported stress concentration factors. As such, there appears to be a clear need for additional studies that are aimed at measuring stress concentration factors within triaxial settings for soft clays that are reinforced with column groups under contrasting drainage conditions. The objective of this study is to address the above-mentioned need.

Table 2: Experimental research programs with stress concentration factors reported

Reference	Type of Experiment (S = single, G = group)	Loading Conditions (Stress = stress controlled Strain = strain controlled D=drained, U=undrained)	Area Replacement Ratio (%)	Sensor used for stress measurement (LC = load cell, PS = pressure sensor) m = miniature	Stress concentration factor, n (U = undrained, D = drained F = fully pen., P = partial pen.)
Charles and Watts (1983)	1-g Cons.[a] (S)	Stress (D)	21, 33	m-PS	a_r=33%, n = 4.8 a_r=21%, n = 2.2
Bachus and Barksdale (1984)	1-g (S/G)	Stress (D) Strain (D)	7, 25	LC	S - n = 2.8-4.2 G - n = 2.5-4.0
Juran and Guermazi (1988)	TX (S)	Strain (D/U)	4	LC	n_D=6.0, n_U=3.0
Muir Wood (2000)	1-g (G)	Strain (D)	10, 30	m-PS	n_P=6
McKelvey et al. (2004)	1-g (G)	Strain (U)	24	m-PS	n_F = 5.2, n_P=2.8
Murugesan and Rajagopal (2010)	1-g (G)	Stress (D)	23	PS	n = 7.0-9.0
Cimentada et al. (2011)	1-D Cons.[a] (S)	Stress (D)	6.25, 11	m-PS	n = 2.5-9.0
Fattah et al. (2011)	1-g (S/G)	Stress (U)	5, 20	LC	n = 1.4-6.0
Ghazavi et al. (2013)	1-g (S/G)	Strain (D)	16	m-LC	n = 5.5-6.2
Miranda et al. (2017)	1-g Cons.[a] (S)	Stress (D)	11	m-PS	n= 3.0-6.0
Nazariafshar et al. (2019)	1-g (G)	Strain (U)	19	m-PS	n = 2.2-4.3

[a]Large-scale odometer

To achieve this objective, a newly developed fully instrumented large-scale triaxial test setup is utilized to investigate the overall response of the composite with particular emphasis on monitoring pore water pressure and contact stresses over sand columns and the surrounding clay. The metrics for assessing the success in achieving this objective are based on showing that the proposed test setup is capable of quantifying the distribution of the stresses between the sand columns and the surrounding clay at different levels of axial strain, while controlling drainage and enforcing confining stress levels that are consistent with field applications. A major constraint in designing the test setup was the need to test soft clay specimens that are reinforced with column groups rather than a single column. This constraint necessitated the utilization of a triaxial setup capable of accommodating large diameter cylindrical matrix samples. Details about the novel test setup including the design of the cap, sensors, instrumentation and data acquisition are presented in the following section.

It should be noted that the large scale reinforced specimen that was used in this study extends the unit cell triaxial model to a more realistic group model that could reflect the interaction among the different columns in the group. The triaxial boundary conditions in the case of the group do not diverge from the triaxial boundary conditions of the unit cell in Najjar et al. (2010 and 2020) since the reinforced clay specimen in both cases is confined by a constant confining pressure (σ_3) and is allowed to bulge in the radial direction during triaxial compression. The benefit of large cell tests with groups is that they allow for multiple arrangements of columns at various replacement ratios while modeling the interaction between the columns in the group and the surrounding clay. The normalized spacing between the sand columns (s/d) and their location within the specimen were carefully chosen so that the reinforced specimen will

represent the area replacement ratio and the s/d ratio of a subset of a large group in the field. It is anticipated that the setup and results presented herein will facilitate the development of design methodologies of clays reinforced with column groups.

3.2 Triaxial Test Setup and Instrumentation

A Humboldt triaxial cell capable of testing cylindrical specimens with a diameter of 145 mm and a height of 300 mm was customized (see Fig. 20a) to allow for the collection of data from: Three miniature contact pressure sensors, three pore pressure sensors, a volume change apparatus with a linear variable differential transformer (LVDT), a load cell, and a displacement sensor (LVDT). The setup was designed to allow for testing soft kaolinite clay specimens that were reinforced with up to four sand columns arranged in a square configuration as indicated in Fig. 20b.

3.2.1 Upper Cap Design

An upper cap with a diameter of 145 mm was designed and fabricated from a solid aluminum block to include housings for three access ports for water sources in addition to housings for three miniature contact pressure sensors (Fig. 21a). Porous stones were fitted into the housings of the pore water ports and they were maintained flush with the bottom side of the cap. Similarly, the active part of the pressure sensor (Fig. 21b) was maintained flush with the bottom side of the upper cap.
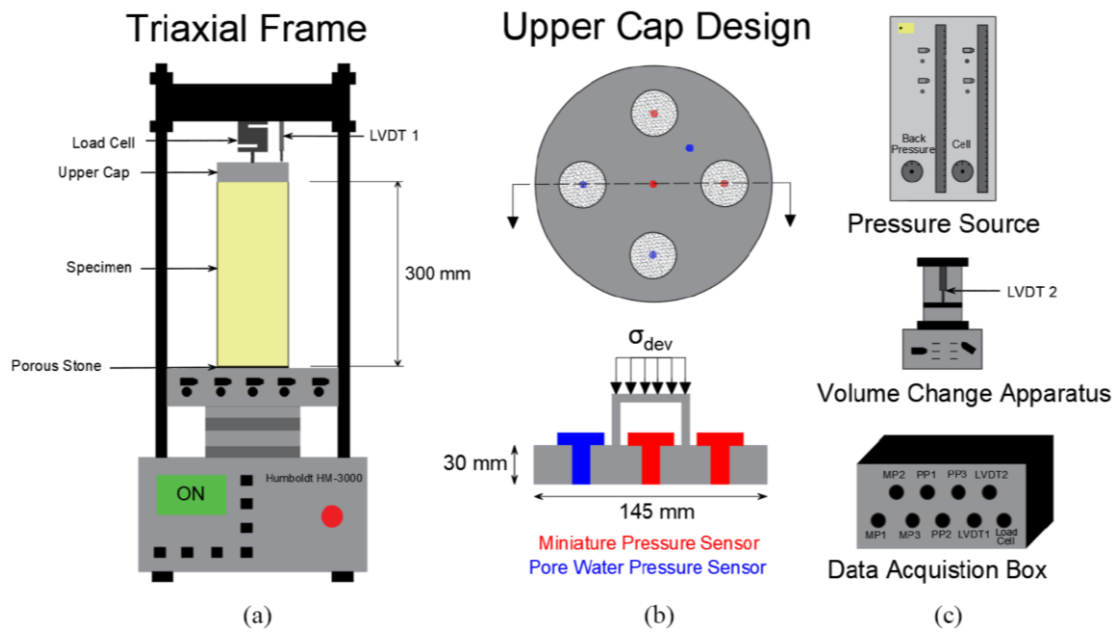
Figure 20: Testing setup showing (a) upper cap design with dimensions; (b) testing frame with sample dimensions; and (c) data acquisition box, pressurized water source and the volume change apparatus.

Two miniature pressure sensors (MP1 and MP2) and two pore water ports (WS and PP3) are arranged in a square configuration 44 mm away from the center of the cap, with a third miniature pressure sensor (MP3) located at the upper cap's center. The third pore water port in the upper cap (PP2) is located between MP1 and MP2 in order to allow for the measurement of the pore pressure in the clay matrix between two sand columns. The pore water port (WS) allows for the application of backpressure from the top side of the specimen in addition to the measurement of volume change in the consolidation and drained shearing stages. Although most of, if not all, the sensors are installed within the upper cap, an additional pore water pressure sensor (PP1) is connected to one of the tubes that accesses the lower porous stone at the base of the specimen.
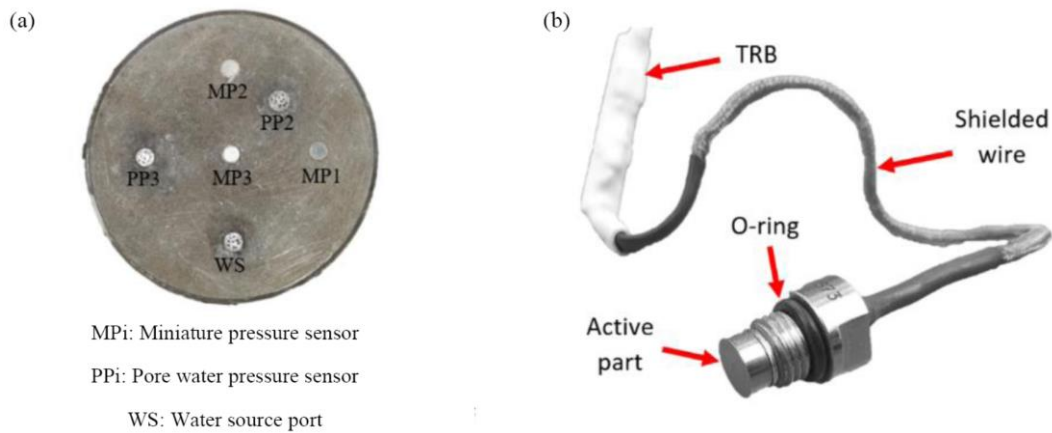
Figure 21: Upper cap setup showing (a) bottom view of the top cap with miniature pressure sensors and porous stones; and (b) Omega miniature pressure sensor used.

A three-dimensional side view of the upper cap (Fig. 22) shows the complete assembly of the upper cap with sensors, fittings and tubing. The miniature pressure sensors' electronic board is close to the active part of the sensor (Fig. 21b), which prohibits installing the sensor without proper isolation of the electronic board from the sensor itself. As such, it was critical to ensure complete water tightness of the fittings to eliminate the possibility of cell water leakage into the sensor chambers through any of the tubing and connections.

3.2.2 Pressure Control and Volume Measurements

As shown in Fig. 20c, two water pressure lines control the stress state in the triaxial cell. The first is a pore water line that is connected to a volume change device that allows for the measurement of volumetric change during the different testing stages. The second is a cell pressure line that is directly connected to water in the triaxial chamber to control the isotropic confining pressure around the specimen.

Figure 22: Side view of the upper cap showing the fittings and tubing to completely isolate the cell pressurized water from leaking towards the sensors and the specimens.

The volume change apparatus has a double acting piston for measuring volume change during consolidation or drained shear with a capacity of 100 ml. It is equipped with a displacement transducer that is calibrated to measure the volume of water passing through the chamber. A T-connection is used to connect the volume change device to the appropriate pore water ports in the upper and lower caps in contact with the soil specimen, thus allowing for the application of a controlled backpressure to both ends of the specimen. The back-pressure and the cell pressure are controlled from a panel that is pressurized using compressed air.The Humboldt HM-3000 master loader and frame was used to run the triaxial tests. It is capable of loading large soil specimens up to 145 mm in diameter and 300 mm in height. The allowable shearing rates range between 0.1 mm/min and 75 mm/min. The cell chamber can withstand pressures up to 1200 kPa.

3.2.3 Sensors, Data Acquisition, and Calibration

The miniature pressure sensors used in the setup are manufactured by OMEGA Engineering Company and have a capacity of 1400 kPa (Fig. 21b). The transducer diaphragm and sidewalls are made of stainless steel. The main application for these sensors is to detect and measure pressures from fluids. Their intended use in the testing setup described is to measure contact pressures above the clay matrix and above the sand-reinforcing column. In order to verify their ability to provide reliable measurements of contact stresses with soils (kaolinite clay and sand), the sensors were calibrated under three conditions: (1) contact with water, (2) contact with kaolin clay, and (3) contact with sand. Under conditions of water contact and kaolin clay contact, the sensors exhibited a linear response and showed repeatable calibration coefficients. This was somewhat expected given the clay's very small particle size, plasticity, and saturation, where minimal variations and noises were detected in the measurement of contact stresses above the clay matrix.

Conversely, the calibration of the sensors using the dry Ottawa sand yielded non-linear results. This was attributed to large contact forces between the sand grains, which are larger than the clay particles, and the sensor's membrane. Further calibration using saturated sand interface resulted in a more-or-less linear response in the pressure range of interest. Since all specimens in the test program were backpressure saturated prior to shearing, it was considered that the pressure sensors would yield reliable measurements for both the sand and the clay in the large-scale composite specimens, provided the respective calibration constants were applied.

It should be noted that calibration using pressurized water was done using an enclosed triaxial chamber, with the pressure sensors mounted flush with the bottom side

of the loading cap. The calibration of the sensors using kaolin clay or sand was done using a custom made one-dimensional odometer consolidation upper cap that has a central manufactured space for the pressure sensors to be mounted in. The one-dimensional setup has a closed-loop pressure option that helps maintain a uniform applied pressure.

The electric signals from the pressure sensors exhibited some noise due to issues related to connections, wiring, and soldering. The noise in the voltage was found to be minimal during calibration in water. The voltage output from clay and sand calibrations gave linear and repetitive results. The noise was filtered using in-line amplification with a TL072CP operational amplifier from Texas Instrumentation. The TL072CP was also used to amplify the output to values in the order of 0.5-3 volts that is suitable for the data acquisition module.

The pore pressure sensors did not present any problems or challenges given that the active component of the sensor is outside the triaxial setup. All tubes connected to the pore pressure sensors were maintained saturated at all times. The pore pressure sensors incorporated in the testing setup are from Ametek Co. with a maximum capacity of 1,400 kPa. All sensors were connected to a data acquisition box that houses the data acquisition modules, signal conditioning, signal amplification and noise filtering. The modules used are from National Instruments and the interface adopted for data collection was LabVIEW. A custom-designed graphical user interface was used to control data collection from all nine sensors and provide real-time plots the data during the test.

3.3 Material Characterization

The materials used in this testing program are Kaolin clay and Ottawa sand. Detailed properties of these materials are presented in the following sections.

3.3.1 Kaolin Clay

The kaolin clay (Supreme China Clay) was sourced from the United Kingdom. It has a liquid limit of 65%, plasticity index of 19%, and specific gravity of 2.56. A one-dimensional consolidation test was conducted on a 50 mm diameter specimen trimmed from a sample consolidated from slurry under a vertical stress of 100 kPa. Seven loading and three unloading increments were used to determine the e-log p curve, where each increment was left for 24 hours to complete the primary consolidation stage. The resulting e-log p curve for the kaolin clay is presented in Fig. 23. The recompression (C_r), compression (C_c) and swelling (C_s) indices were determined to be 0.19, 0.50 and 0.17, respectively. The preconsolidation pressure was determined to be 92 kPa using Casagrande (1936) method, indicating that the 100 kPa consolidation pressure that was applied to the slurry in the 1D consolidometers may not have fully transferred to the specimen due to frictional losses along the mold surfaces.
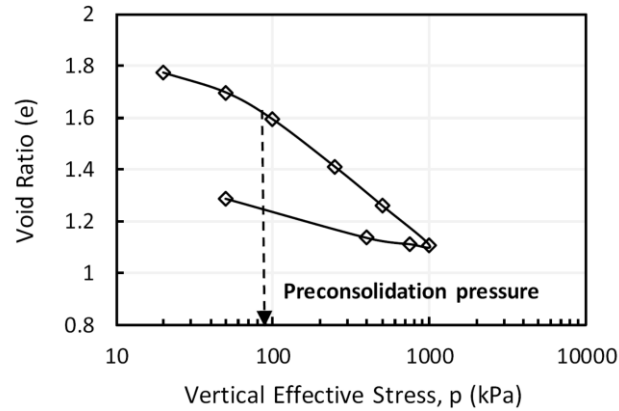
Figure 23: e-log σ'ᵥ for normally consolidated kaolin clay.

In order to characterize the shear strength of the kaolin clay, three isotropically consolidated undrained (CU) tests and three consolidated drained (CD) tests were conducted on back-pressure saturated specimens with a height of 142 mm and a diameter of 71 mm at effective confining pressures of 100, 150 and 200 kPa. The results of the drained and undrained triaxial tests on kaolin clay are presented on Figs. 24a and 24c, respectively.

The stress-strain response from the consolidated drained tests (Fig. 24a) indicated a strain hardening effect for all confining pressures up to an axial strain of 16%, where a peak deviatoric stress was reached. The volumetric change indicated contractive behavior that is typical of soft normally consolidated clay specimens that are sheared in a drained condition towards critical state. The effective drained Mohr-Coulomb failure envelope was used to determine the drained shear strength parameters of the kaolin clay. The measured effective strength parameters for kaolin clay were $c' = 0$ kPa and $\varphi' = 21.8°$.

For the consolidated undrained tests, the variation of the deviatoric stress and the excess pore water pressure with axial strain (Fig. 24c) indicates that the kaolin clay used in this experimental program softens at axial strains in the order of 10% to 12%. The maximum deviatoric stresses were 56.9, 79.4 and 100.4 kPa corresponding to $s_u/(\sigma'_3)_0$ ratios of 0.28, 0.26 and 0.25 respectively, where s_u represents the undrained shear strength and $(\sigma'_3)_0$ represents the initial effective confining pressure. These $s_u/(\sigma'_3)_0$ ratios are typical of normally consolidated clays sheared in undrained conditions (Lin and Penumadu, 2005). For the different effective confining pressures of 100, 150 and 200 kPa, the maximum recorded pore water pressures were 60.0, 92.9, and 119.3 kPa, corresponding to Skempton pore pressure parameters "A_f" of 1.06, 1.13 and 1.19, respectively (Skempton, 1954).

(a) Kaolin – CD	(b) Sand – CD	(c) Kaolin – CU	(d) Sand – CU
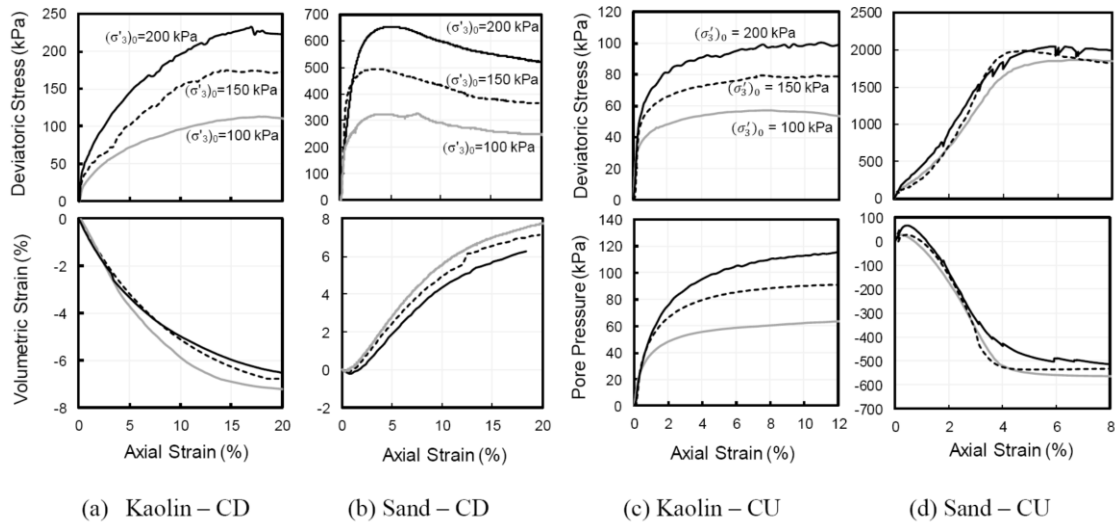
Figure 24: Results of consolidated drained (CD) and consolidated undrained (CU) triaxial tests on Kaolin clay and Ottawa sand.

3.3.2 Ottawa Sand

The sand used in the test program is classified as poorly graded Ottawa sand (SP) according to the Unified Soil Classification System. The physical and mechanical properties of the sand are presented in Table 2. The sand shear strength was determined using isotropically consolidated drained and undrained triaxial tests that were conducted on specimens with a height of 142 mm and a diameter of 71 mm at initial confining pressures of 100, 150, and 200 kPa. The specimens were prepared at a dry density of 1.74 Mg/m^3 corresponding to a relative density of 85%, and a void ratio of 0.53. All sand columns used in the testing program had a density of 1.74 Mg/m^3 ± 0.01 Mg/m^3 ensuring high consistency during testing.

Table 3: Physical and mechanical properties of Ottawa Sand.

Soil property	Value
D_{10} (mm)	0.22
D_{30} (mm)	0.3
D_{60} (mm)	0.5
Specific gravity	2.65
Coefficient of uniformity (D_{60}/D_{10})	2.3
Coefficient of curvature (D_{30})²/($D_{60}*D_{10}$)	0.82
Maximum void ratio; e_{max}	0.75
Minimum void ratio; e_{min}	0.49
Angle of internal friction (φ)°	39

The drained triaxial test results presented in Fig. 24b show stress-strain and volumetric responses that are typical of dense sand. Clear peaks were exhibited in the stress-strain responses at axial strains in the order of 3 to 5%, followed by softening all the way to critical state. The softening was associated with the dilation of the dense

sand during drained shear. The drained tests indicated that the sand can be characterized with a $c' = 0$ kPa and $\varphi' = 39.0°$. The consolidated undrained test results in Fig. 24d reflect the dilative tendency of the dense sand through the generation of large negative excess pore water pressures during undrained shearing.

3.4 Laboratory Testing Program

The testing program is summarized in Table 3. In total, three isotropically consolidated drained (CD) and three isotropically consolidated undrained (CU) triaxial tests were performed on specimens having a diameter of 145 mm and a length of 295 mm. Tests were performed on control specimens and specimens reinforced with a group of four non-encased, fully penetrating dense sand columns with diameters of 30 and 40 mm, representing area replacement ratios of $a_r = 17.1\%$ and 30.4%, respectively. The columns were installed in predrilled holes using a square arrangement at 44 mm offset from the specimen center. The holes were drilled using a custom-fabricated augering apparatus. All specimens were saturated using a back pressure of 300 kPa and isotropically consolidated under an effective confining pressure of 100 kPa. Skempton B values were around 0.98 for all tests (Skempton, 1954), indicating adequate degrees of saturation. All tests were strain controlled and terminated at axial strains of ~20%. The strain rate chosen for every test was function of t_{50} as per the ASTM standards.

3.4.1 Clay Specimen Preparation

Kaolin clay (China Clay) powder was mixed with water at two times its liquid limit (i.e. 130% water content) to form a slurry. The mixture was then poured into custom-fabricated split PVC pipes and subjected to 1-D consolidation using a

sequenced application of dead weights. Three 1-D consolidometers were fabricated for this purpose (Fig. 25). Custom-fabricated split PVC pipes functioned as split molds 3 mm thick, 500 mm high, with an internal diameter of 145 mm. Slurry was placed inside the well-tightened PVC pipe segments (Fig. 26a). High strength duct tape and metallic bands were used to confine the split PVC while maintaining negligible lateral strains during one-dimensional consolidation of the slurry under a vertical applied pressure of up to 100 kPa.

The advantage of using split molds is that an undisturbed, relatively soft, homogenous clay specimen could be retrieved (Fig. 26) with minimal disturbance. Perforated metallic upper and lower caps with filter paper served as porous boundaries. Dead weights were seated on a circular steel plate that transferred the load to the top of the clay through a cylindrical steel rod. Dead weights were added gradually and in increments based on the time schedule presented in Table 4.

Table 4: Laboratory testing program and results

Test number	Drained (D) or Undrained (U)	Diameter of sand column (mm)	Number of sand columns	Area replacement ratio A_c/A_s (%)	Maximum deviatoric stress (kPa)	Excess pore pressure (kPa)	Volumetric strain (%)	Increase in deviatoric stress (%)	Reduction in excess pore pressure (%)	Reduction in volumetric strain (%)
1	U	0	0	0	56.6	61	-	0.00	0.00	-
2	U	30	4	17.1	78.3	45	-	38.4	26.2	-
3	U	40	4	30.4	146.5	12	-	158.8	80.3	-
4	D	0	0	0	119.0	-	6.44	0.00	-	0.00
5	D	30	4	17.1	128.1	-	4.57	7.65	-	29.0
6	D	40	4	30.4	166.4	-	0.97	40.0	-	84.9

Figure 25: Custom fabricated 1-D consolidometers.

The loading schedule was selected using trial and error to achieve repeatable and uniform samples with minimal disturbance. The quality of the specimens thus formed was evident in (1) the uniformity in the final specimen height (~ 315 mm) and (2) consistency in the water content along the specimen length. This consistency was verified through a trial experiment in which a specimen was sliced into 6 pieces and the water content and void ratio determined for each slice. The variation of the water content and void ratio along the height of the specimen as presented in Fig. 27 indicates a relatively uniform degree of consolidation along the specimen height.
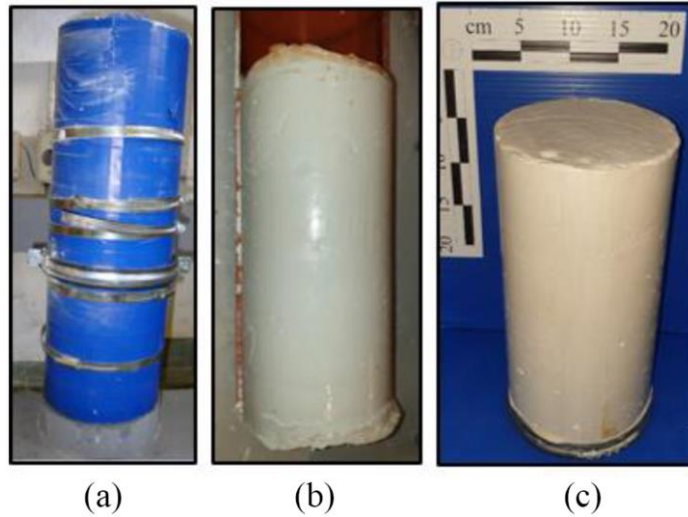
Figure 26: (a) Sealed PVC split sections; (b) dismantling of PVC sections; and (c) kaolin specimen consolidated to 100 kPa.
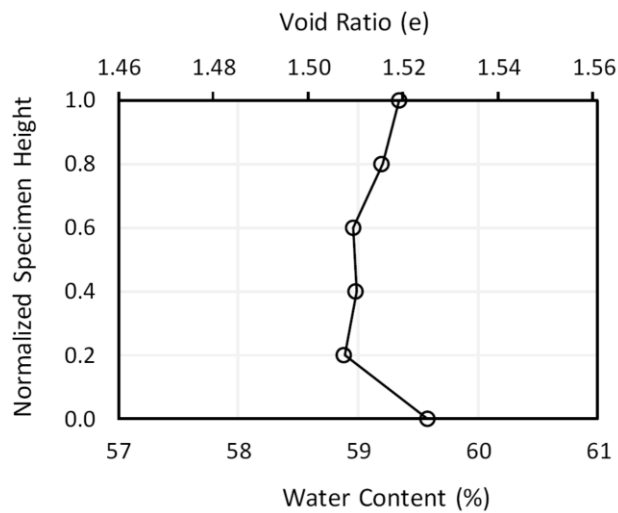
Figure 27: Variation of water content and void ratio along the height of the sample after 1D consolidation.

All samples were subsequently isotropically reconsolidated at 100 kPa in the triaxial cell, which eliminated any one-dimensional stress history that might have existed in the sample following consolidation in the 1D consolidometers.

Table 5: Loading sequence during 1-D consolidation

Test information	S1	S2	S3	S4	S5	S6	S7
Applied weight (kg)	0	10	20	40	80	120	170
Applied pressure (kPa)	0	6	12	24	48	71	101
Duration (hr)	12	24	24	24	24	24	24

Note: S1 refers to Stage No. 1 and so on

3.4.2 Construction of Sand Columns

After dismantling the cylindrical kaolin specimen from the PVC

consolidometers and trimming it to the specified final height of 295 mm, the sample

was placed in a custom-fabricated augering apparatus that is capable of drilling up to

300 mm inside the soil specimen (Fig. 28). Two auger bits were then used to drill either

30 mm or 40 mm diameter holes in the clay specimen to form the column group. Pre-

prepared frozen sand columns were then placed in their respective predrilled holes. The

sand columns were frozen in prefabricated 3D-printed tubes. The tubes were printed as

split molds with a total height of 300 mm and a wall thickness of 2 mm. The freezing

method was used for the preparation of sand columns (e.g., Sivakumar et al. 2004;

Black et al. 2007) as it has shown good repeatability and consistency in terms of the

relative density of the sand columns (Najjar et al. 2010).

The sand split tubes were held in place using high strength duct tape to ensure

no lateral strains during sand freezing. The sand was filled in layers while vibrating the

tubes from the outside to achieve a final dry density of $1.74\ Mg/m^3 \pm 0.01\ Mg/m^3$,

corresponding to 85% relative density. Following densification, water was added to

achieve a water content of around 20%. The columns were then placed in the freezer for

at least 24 hours. After drilling each hole, a sand column is removed from the freezer, the tubes split and the column inserted into the drilled hole and allowed to thaw (Fig. 28).

Figure 28: Drilling holes in kaolin specimen and sand column installation.

3.5 Test Results and Analysis

The modified triaxial test setup with its newly devised instrumentation was used to run large scale drained and undrained triaxial tests on control clay specimens and specimens that were reinforced with a group of four sand columns distributed in a square arrangement. All samples were isotropically consolidated under an effective confining pressure of 100 kPa prior to the shearing stage, after ensuring saturation through applying an incremental backpressure of 300 kPa. The test results are presented in Table 1 and include two tests on control clay specimens, two tests on specimens reinforced with an area replacement ratio $a_r = 17.1\%$, and two tests on specimens reinforced with an area replacement ratio $a_r = 30.4\%$. The analysis focused on the effect of sand columns on: (1) consolidation, (2) bearing capacity and stress

distribution, (3) reduction in volumetric strain and pore pressure during shearing and (4) development of stress concentration within the sand columns.

The drained and undrained triaxial tests were conducted in accordance with ASTM standards. In the consolidated drained tests, the rate of shearing was calculated as $\dot{\varepsilon} = \frac{\varepsilon_f}{120 t_{50}}$, where ε_f represents the axial strain at failure (chosen as 10%) and t_{50} is the time corresponding to a degree of consolidation of 50%. For the consolidated undrained tests, the rate of shearing was calculated as $\dot{\varepsilon} = \frac{\varepsilon_f}{10 t_{50}}$ to achieve equalization of pore water pressure throughout the height of the specimens. As a result, the strain rate that was adopted in the consolidated drained tests ranged from 0.1 to 1.2 mm/hr, while the rate adopted for the undrained tests ranged from 1.1 to 28.5 mm/hr. It should be noted that in the drained tests, fully drained conditions during shearing were confirmed by monitoring the excess pore water pressure at three locations (See Fig. 20). The excess pore pressures were always in the range of $-2\ kPa \leq u_p \leq +2\ kPa$, indicating complete dissipation of excess pore water pressure in the specimens.

3.5.1 Consolidation Stage

The isotropic consolidation response of the six test specimens under an effective confining pressure of 100 kPa is presented in Fig. 29. Three observations can be made from the volumetric strain versus time curves: (1) The incorporation of sand column groups in the reinforced clay specimen reduced the volumetric strain of the control specimen by about 35% and 46%, with a higher percent reduction for the higher area replacement ratio ($a_r = 30.4\%$), (2) The time required for consolidation to be completed decreased significantly as the area replacement ratio increased, with the time

corresponding to 50% consolidation t_{50} decreasing from around 670 minutes in the case of the control clay specimen to 15 minutes and 4 minutes for the specimen reinforced at $a_r = 17.1\%$ and 30.4%, respectively, and (3) the difference in the consolidation response between identical drained and undrained specimens (whether control or reinforced) was little indicating a high level of repeatability and consistency in sample preparation, testing, and instrumentation.

The reductions observed in the volumetric strain and consolidation time are expected given the dual role that sand columns play in (1) increasing the overall stiffness of the composite specimen, and (2) enhancing radial drainage by functioning as vertical drains that reduce the horizontal drainage paths of water leaving the clay. In the control clay specimens, the drainage was mainly vertical with the maximum drainage distance being equal to half of the specimen height (~ 145 mm). In the reinforced specimens, the drainage direction is pre-dominantly radial with maximum drainage distances in the order of 35 mm and 25 mm in the case of $a_r = 17.1\%$ and 30.4%, respectively. Since consolidation times are roughly proportional to the square of the maximum drainage distance, the reductions observed in the primary consolidation times in the reinforced specimens may be considered reasonable.
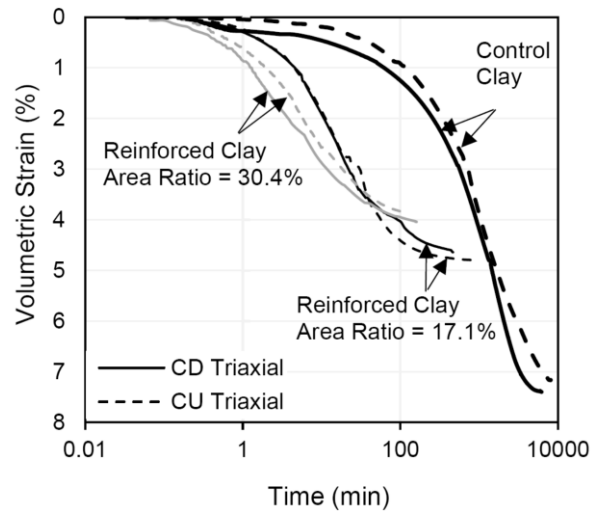
Figure 29: Variation of volumetric strain with time during isotropic consolidation of control and reinforced specimens.

3.5.2 Stress-Strain Response

The stress-strain curves for the control and reinforced clay specimens are presented in Fig. 30a and 30b, for the CD and CU triaxial tests, respectively. Irrespective of the drainage conditions, results as presented in Fig. 30 indicate that the sand column group improved the bearing capacity and stiffness of the soft clay. The maximum deviatoric stress measured in the control clay specimen increased by 8% ($a_r = 17.1\%$) and 40% ($a_r = 30.4\%$) in the drained tests and by 39% ($a_r = 17.1\%$) and 159% ($a_r = 30.4\%$) in the undrained tests.

For reinforced clay specimens, the stress-strain curves in Fig. 30 show signs of strain softening starting from axial strains in the order of 5 to 10%, particularly in specimens reinforced at the higher area replacement ratio of 30.4%. This response reflects the dominant role of the dense sand columns, which are expected to dilate during shear, particularly in the drained tests. The dilative tendency of the sand columns and its role in dominating the response of the composite is clearly exhibited in Fig. 30 through the variation of the volumetric strain (drained tests) and the excess pore water

pressure (in undrained tests) with axial strain. Reinforcing the clay with the sand column group reduced the compressive volumetric strain at failure in the CD tests from 6.5% to 4.6% ($a_r = 17.1\%$) and 1.0% ($a_r = 30.4\%$), and reduced the excess positive pore water pressure in the CU tests from 60 kPa to 45 kPa ($a_r = 17.1\%$) and 10 kPa ($a_r = 30.4\%$), respectively.

It should be noted that although the consolidated undrained tests could be considered to be "globally undrained", exchange of pore water between the dilating sand columns and the surrounding compressive soft clay is inevitable. This local exchange will lead to partial drainage of the sand columns in the group and the surrounding clay leading to local volume change. Evidence of this partial drainage in the consolidated undrained tests is clear in the stress-strain response, which shows clear signs of strain softening. Had the sand columns been totally undrained, the generation of large negative pore pressures in the sand would have prohibited strain softening in the reinforced clay specimen.

In the consolidated undrained tests, excess pore water pressure was measured at three locations, namely above one sand column, above the clay annulus between two sand columns, and at the bottom as a global measure for the composite soil. For all tests, the pore pressure sensors gave similar results, irrespective of their position in the specimen. This indicates that even with the relatively high rate of loading that was used in the undrained tests, equilibration of pore water pressure occurred within the test specimen leading to the same pore water pressure measurement in the sand and the clay. As a result, data from only one pore water pressure sensor was included in Fig. 30 for the undrained tests.
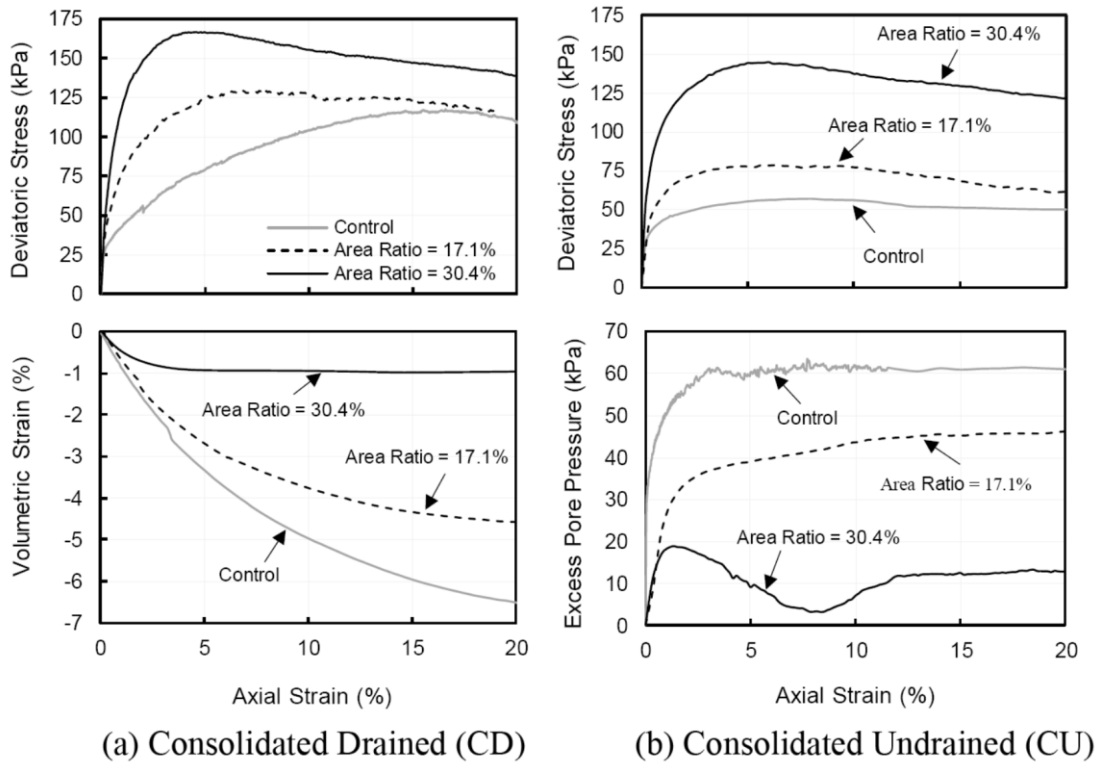
Figure 30: Results of the large scale triaxial tests (a) Drained and (b) Undrained.

For the particular case of the a_r = 30.4% specimens, Fig. 30b clearly shows that at relatively small strains, the dilative tendency of the large diameter columns results in a significant reduction in the overall positive pore pressure generation during shearing. However, as strains accumulate towards significant values of about 10%, the gradual reduction in the pore pressure is clearly interrupted and reversed. This could be attributed to excessive shear stress/strain concentrations along the failure surface leading to a tendency for dislocation of the sand columns and interruption of their continuity. This explanation of the observed response is supported by the pictures shown in Figs. 31d and 32d which show the magnitude of distortion and bulging that was induced in the sand columns at large strains.

3.5.3 Mode of Failure

An investigation of the mode of failure of control and reinforced clay specimens indicated that the mode of failure was affected by the drainage conditions. For the three drained tests (Fig. 31), the controlling mode of failure was uniform bulging along the height of the clay specimens. At the onset of reaching a peak in the deviatoric stress, formation of a failure plane was observed in control and reinforced specimens, followed by strain softening all the way to critical state conditions. On the other hand, undrained specimens (Fig. 32) that were reinforced with column groups showed localized bulging that was concentrated in the upper half of the specimens with no evidence of the formation of a failure plane (unlike the control clay undrained specimen which showed a clear failure plane).

To examine the internal mode of deformation of the sand columns in drained and undrained tests, the specimens reinforced with 40 mm sand column groups ($a_r =$ 30.4%) were cut along a vertical section passing through two of the sand columns in an attempt to expose the columns and the surrounding clay. The cross sections are presented in Fig. 31d and 32d for drained and undrained tests, respectively. For the drained test, the cross-section clearly shows the failure plane cutting the sand columns along a pre-defined direction. No such failure plane was evident in the undrained test on the reinforced specimen. However, it is interesting to note that the sand columns in the undrained tests showed asymmetrical bulging, with the columns showing signs of outward bulging towards the exterior of the specimen and almost no inward bulging towards each other. The restraining action that internal sand columns exhibit within a column group was observed in the group tests conducted by Bachus and Barksdale (1983), among others.

(a) Control Clay   (b) a_r=17.1%   (c) a_r = 30.4%   (d) Cross Section (a_r=30.4%)
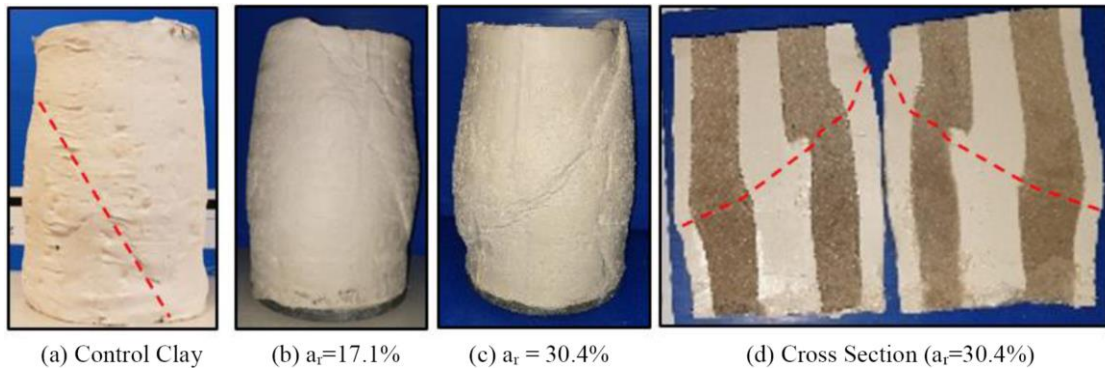
Figure 31: External and Internal Mode of Failure in Consolidated Drained Triaxial Tests.

(a) Control Clay   (b) a_r=17.1%   (c) a_r = 30.4%   (d) Cross Section (a_r=30.4%)
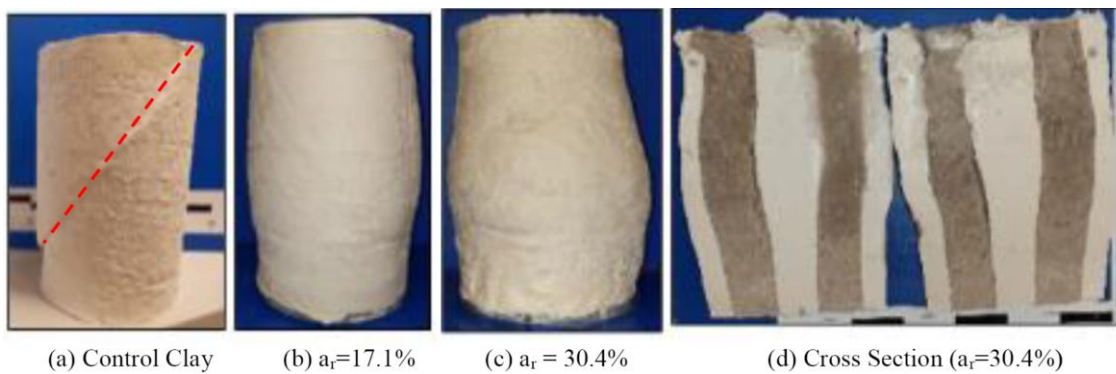
Figure 32: External and Internal Mode of Failure in Consolidated Undrained Triaxial Tests.

3.5.4 Measured Contact Stresses

Local contact stresses were measured using miniature pressure sensors located over two sand columns and over the clay at the center of the upper cap. The variation of the measured contact stresses with axial strain is presented in Fig. 33 for all test specimens. Also shown in Fig. 33 are the curves representing the variation of the overall global deviatoric stress with strain as measured using the global load cell.

For the control clay specimens, measuring contact stresses using the miniature pressure sensors allowed for testing the effectiveness and reliability of the miniature pressure sensors in measuring stresses under drained (Fig. 33a) and undrained (Fig. 33b) conditions. These contact stresses for the case of the control clay indicated that the three pressure sensors gave reliable and repeatable results compared to the global deviatoric stresses measured by the load cell. As expected, the stresses measured by the miniature pressure sensors at three locations exhibited some natural variability that was quantified to be within 5 to 10% of the measured global deviatoric stress at least for axial strains below 10%. This observation is important since it indicates that the utilized sensors can be effectively used to monitor stresses in the drained and undrained normally consolidated kaolin clay with minimal errors.

As for the reinforced specimens, the square configuration of the four sand column group permits stress measurement in two sand columns and in the central clay. The variations of these measured contact stresses with axial strain are presented in Figs. 33c,d and Figs. 33e,f for specimens reinforced with 30 mm and 40 mm sand column groups, respectively. Results from stress measurements above the sand columns (MP1 and MP2) indicated that: (1) the stiff sand columns attracted stresses that are much larger than those measured in the clay, irrespective of the drainage conditions and area replacement ratio, (2) some variability in the contact stresses is observed between the sand columns in the same composite specimen, and (3) the magnitude of the measured sand stresses in the columns is affected by the drainage conditions and the area replacement ratio.
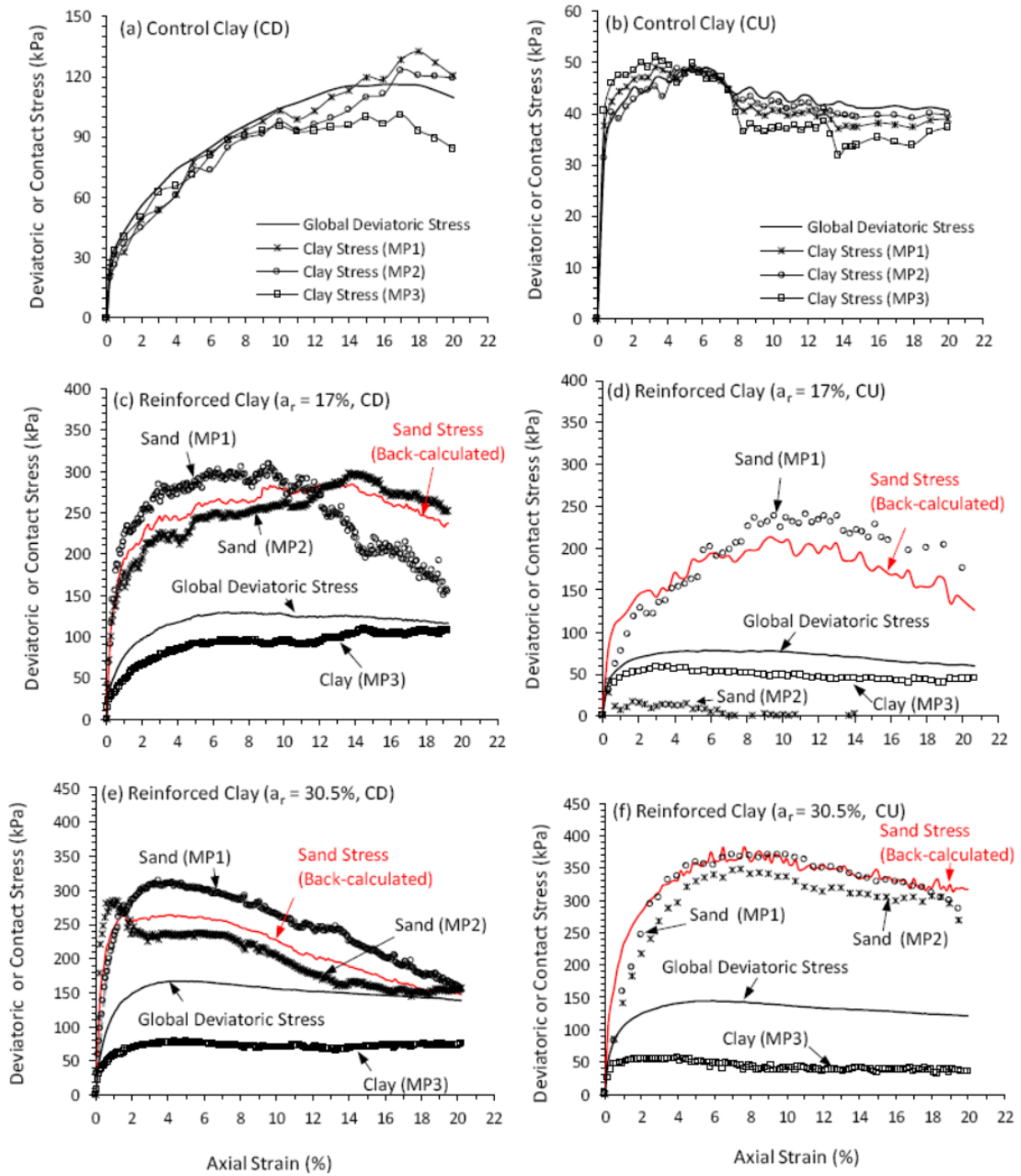
Figure 33: Variation of deviatoric and contact stresses with strain for control and reinforced clay specimens under drained and undrained loading conditions.

The inherent variability in the response of identical sand columns within the same composite specimen can be attributed to multiple factors. First, slight variations in relative density between the columns in the group could affect the uniformity or lack of in the stress distribution between the columns. Second, the stresses may have been

affected by slight possible rotations in the upper cap, particularly at larger strains (10% to 20%) following the formation of distinct failure planes or excessive bulging. The reliability of the sensor readings can be considered as somewhat degraded by the large movements. However, all tests were continued to axial strains of 20% to get a sense of what is happening well beyond the peak response since it was assumed that even with large distortions, the measurements still give a sense of the distribution of the loads. It should be noted that the contact stresses measured by sensor MP2 in the case of the consolidated undrained test that was conducted on the sample reinforced at an area replacement ratio of 17.1% were flawed (See Fig. 33d). As a result, these measurements were disregarded from the analysis.

In order to validate and verify the applicability and reliability of the stress measurements in the sand columns, the clay stresses that were measured by MP3 and the global deviatoric stresses for the composite clay specimen were used to back-calculate the average stress in the sand columns in the group. The variation of the back-calculated stresses in the columns with axial strain is presented in Fig. 33 in red. The back-calculated stresses were calculated using Equation 1 by assuming that the global deviatoric stress on the composite specimen (σ_d) was shared by the stress in the clay (σ_{clay}) and the average stress in the four sand columns (σ_{sand}) such that:

$$\sigma_d A_{sample} = \sigma_{clay} A_{clay} + \sigma_{sand} A_{columns} \tag{1}$$

Where A_{clay} and $A_{columns}$ are the area of the clay and the area of the sand columns in the reinforced clay specimen, while A_{sample} is the total cross sectional area of the composite specimen. Given the global deviatoric stress (σ_d) and the measured stress (MP3) in the clay (σ_{clay}), Equation 1 was used to back-calculate (σ_{sand}). Interestingly,

results on Fig. 33 indicate that the variation of the back-calculated average stresses in sand (σ_{sand}) with axial strain (red curves) compare well with the stresses in sand measured using MP1 and MP2. In fact, the back-calculated stresses in sand constitute a realistic representation of the average stresses measured by MP1 and MP2, irrespective of the area replacement ratio and drainage conditions. These results are important since they indicate that the stresses measured by the miniature pressure sensors are reliable and reflective of the true stress distribution in the composite specimen.

To scrutinize the mechanics of load sharing between the sand columns in the group and the surrounding clay and its dependence on the area ratio and drainage conditions, the stresses mobilized in the clay (MP3) for the control and reinforced specimens were plotted on the same figures (Fig. 34a and 34b for CD and CU tests) for comparison. Similarly, the stresses mobilized in the columns in the composite specimens were compared to the deviatoric stress measured from the triaxial tests conducted on the control sand specimens (Figs. 34c and 34d).

Results presented in Fig. 34 lead to many interesting observations that show the effect of drainage conditions and area replacement ratio on the mechanics of load sharing between the sand and the clay and its dependence on the strain level. First, results for the stresses in clay (Figs. 34a, b) indicate that the clay under drained conditions was able to carry higher stress than the undrained case. In fact, the stresses mobilized in the clay surrounding the columns in the drained tests approached the maximum deviatoric stress mobilized in the drained control clay specimen, without reaching it. For the case with the lower area replacement ratio ($a_r = 17.1\%$), the variation of the stress in clay with strain was closer to the drained stress-strain response of the control clay specimen, indicating that the failure mechanism was dominated by

the clay. In the composite specimen with the higher area replacement ratio ($a_r = 30.4\%$),

the stresses in clay were lower indicating that the response was governed by the stiff

larger diameter sand columns.
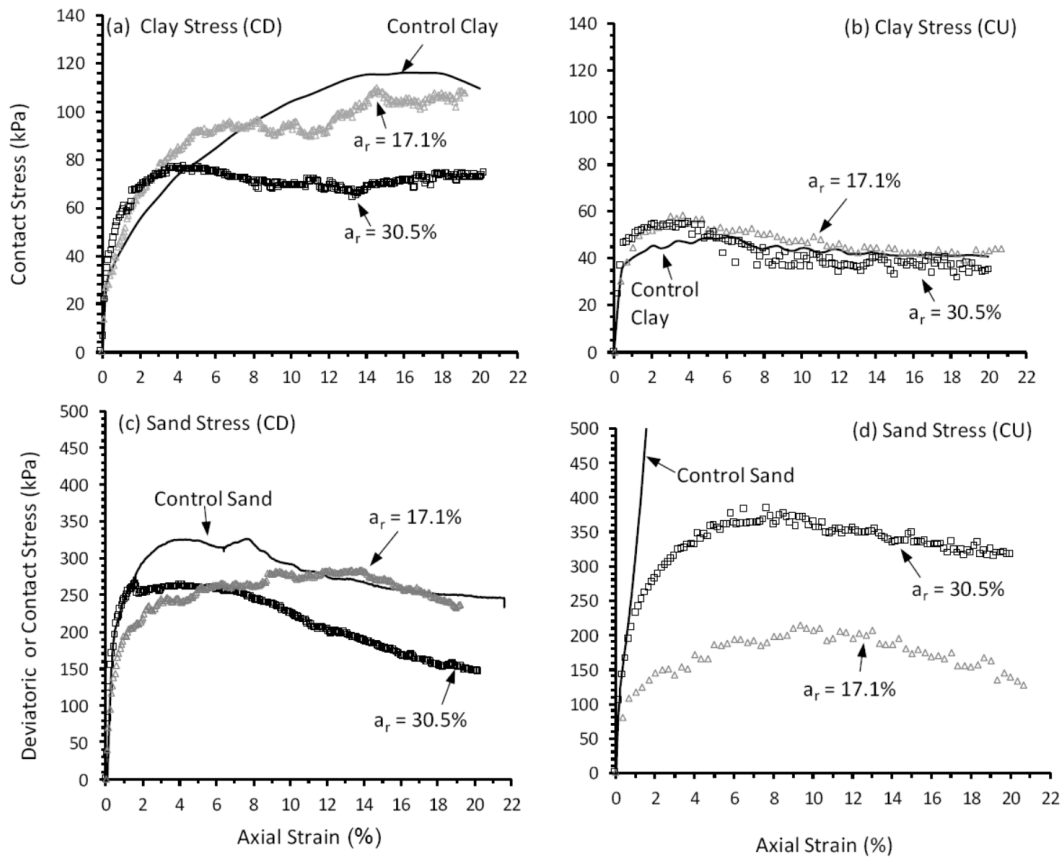
Figure 34: Effect of area replacement ratio and drainage conditions on the mobilized clay and sand contact stresses.

On the other hand, results for the undrained tests indicate that the stresses in clay

in the composite specimens were (1) insensitive to the area replacement ratio and (2)

consistent with stresses measured in the control clay specimen. These observations

indicate that the undrained response in the composite clay specimens was largely

governed by the relatively low undrained shear strength of the clay and that the

presence of sand columns did not affect the undrained shear strength of the surrounding clay. It is interesting to note that in the range of axial strain of 4% to 6%, the measured stresses in clay in the composite specimens were slightly larger than those observed in the control clay specimen. This slight increase could be due to partial local radial drainage from the clay into the sand columns, leading to slight local increases in the strength of the surrounding clay, despite the fact that the tests were globally undrained.

An investigation of the gradual stress buildup in the sand columns in Figs. 34c and 34d leads to two main observations: (1) the average stresses in sand in the column group were highly dependent on the area replacement ratio, particularly in the composite specimens that were sheared undrained, and (2) the stresses in sand mobilized in the "globally undrained" tests show clear evidence of local water exchange between the sand columns and the surrounding clay, leading to significant reductions in the mobilized stresses in sand compared to the stresses in sand observed in the control sand specimen that was sheared under true undrained conditions. This local partial drainage in the case of composite specimens is expected to prohibit the dense sand columns from generating negative pore water pressure even under fast loading rates. Unlike the undrained control sand specimen that exhibited a maximum peak deviatoric stress of about 1800 kPa (not shown on Fig. 34d so as not to distort the scale of the y-axis), the maximum stresses in sand in the sand columns did not exceed 210 kPa for the composite specimen with $a_r = 17.1\%$ and 375 kPa for specimens with $a_r = 30.4\%$. In fact, the stresses in sand in the case of $a_r = 17.1\%$ (undrained test) were smaller than the stresses in sand observed in the identical drained test. The combination of low undrained shear strength in the surrounding clay and the inability to generate negative

88

pore water pressure in the columns due to partial drainage resulted in extremely small stresses in sand in the undrained test involving an a_r of 17.1%.

3.5.5 Stress Concentration Ratio

The stress concentration ratio was calculated for all composite specimens by dividing the average measured stresses in sand (MP1 and MP2) by the stresses in clay measured with sensor MP3 at all strain levels, except for the undrained test under an a_r of 17.1%, where the measured stress in sand from sensor MP1 was only used in the analysis. The variation of the stress concentration ratio with axial strain is presented on Figs. 35a and 35b for the drained and undrained tests, respectively.

Results on Fig. 35 reveal a clear distinction between the mechanics of load sharing in drained and undrained conditions. For the drained tests, the variation of the stress concentration ratio with strain shows a sharp increase in the ratio at relatively low strains, reaching maximum values of 4.5 and 6.3 for area replacement ratios of 17.1% and 30.4%, respectively. After the peak, the stress concentration ratio decreases gradually to reach values as low as 1.5 at large axial strains. Conversely, the variation of the stress concentration ratio with strain in undrained tests indicates a gradual monotonous increase leading to peaks in the order of 6.5 and 9.5, for area replacement ratios of 17.1% and 30.4%, respectively. These peaks are observed at relatively large strains (greater than 13%). It should be noted that irrespective of the drainage conditions, the cases with the higher area replacement ratios resulted in the higher stress concentration ratios, which is in line with the work of Bachus and Barksdale (1984).
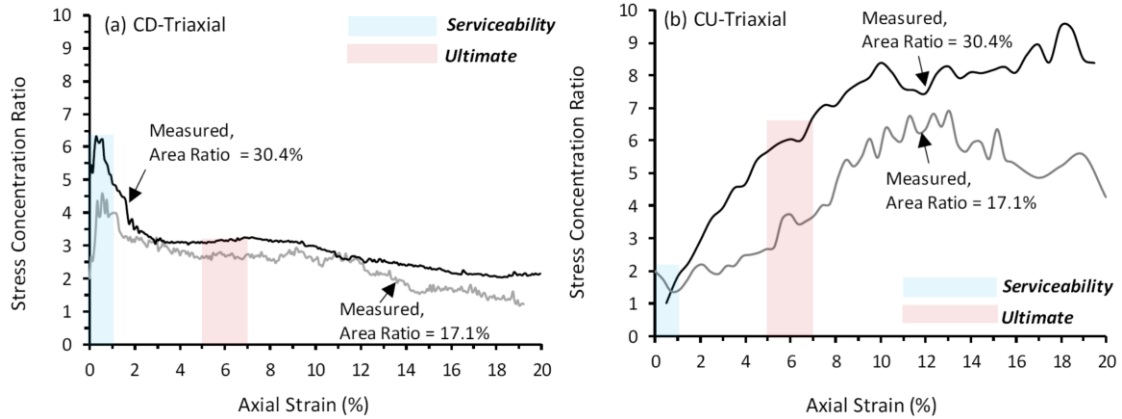
Figure 35: Variation of stress concentration ratio with axial strain for the drained and undrained tests.

For the drained tests, the early peaks in the stress concentration ratio and the gradual but significant reduction that follows can be attributed to two main factors: (1) the softening that is observed in the sand columns which dilate and soften at relatively small strains, and (2) the progressive gradual strain hardening that is exhibited in the clay surrounding the columns as the clay consolidates and compresses during drained shear (Black et al. 2011). These two factors lead to an initial early peak in the stress concentration ratio followed by a significant reduction at large strains.

For the undrained tests, the monotonous increase in the stress concentration ratio with strain and the significantly larger stress concentration ratios in the specimens reinforced at the higher area replacement ratio of 30.4% can be attributed to two main factors: (1) the undrained conditions that governed the response of the clay in the composite specimens leading to the mobilization of relatively low undrained stresses in the clay, irrespective of the area replacement ratio (See Fig. 34b), and (2) the gradual increase in the mobilization of stresses in sand with strain (up to strains in the order of 10%) and the clear superior response of the 40 mm sand columns compared to the 30

mm columns (see Fig. 34d). The superior response of the sand columns in the specimen reinforced at an area replacement ratio of 30.4% is a direct consequence of the drainage conditions within the composite specimen and the role that the large diameter sand columns played in reducing the overall generation of positive pore water pressure in the composite specimen.

The results on Fig. 35 point to several implications that could affect the design of clay systems that are reinforced with granular columns in practical field applications. The first implication is the importance of identifying the strain range that is relevant to practical design, given the significant variations that the stress concentration ratios exhibited in Fig. 35. For applications in which serviceability limit states are expected to govern the design of the reinforced clay system, results on Fig. 35 indicate that stress concentration ratios in the range of 3 to 4 ($a_r = 17.1\%$) and 5 to 6 ($a_r = 30.4\%$) should be adopted in quantifying the load sharing between the clay and the sand column group if drained conditions are expected to govern. The stress concentration ratios pertain to estimated axial strains that are less than 1% in the blue shaded area in Fig. 35. If the designer is interested in the ultimate limit state (failure of composite system), the strain range of interest shifts to around 5 to 7% (see Fig. 30). In this strain range, the stress concentration factors that should be adopted in design assuming drained conditions reduces to around 2.5 to 3.0 (see red-shaded area in Fig. 35).

If fast loading conditions that will result in an "undrained" response in the clay are expected to govern the design, results on Fig. 35 indicate that for serviceability considerations, stress concentration factors as low as 1.5 to 2.0 are required to model the load sharing between the sand and the clay. For ultimate limit state considerations

that involve undrained failure, stress concentration factors as high as 2.5 to 3.5 (ar =

17.1%) and 5.5 to 6.5 (ar = 30.4%) should be adopted to realistically model the stress

distribution. It should be noted that these ranges for the stress concentration factor apply

to the clay and sand used in this study and should not be generalized to cases involving

different soil conditions.

3.6 Conclusions

In this paper, a newly developed fully instrumented large triaxial system is

introduced to examine the behavior of soft clay specimens reinforced with group

granular columns under both drained and undrained conditions. An innovative upper

cap with three miniature pressure sensors and two pore water pressure sensors was

designed with proper calibration of the contact pressure sensors on different soil types

and conditions.

Tests on large control clay specimens and specimens reinforced with a group of

four sand columns at two area replacement ratios ($a_r = 17.1\%$ and 30.4%) were

conducted under drained and undrained conditions. The stress measurements were used

to investigate the mechanics of the stress distribution and load sharing between the sand

column group and the surrounding clay, with emphasis on identifying the variation of

the stress concentration ratios with strain and their dependence on the drainage

conditions and area replacement ratio. Based on the results, the following conclusions

can be made:

1. The newly developed instrumented large-scale triaxial setup allowed for

    collecting reliable data on pore pressures, volume change, overall deviatoric

stress, and development of local stresses in the clay and the surrounding columns. The measurements were repeatable and reliable for studying the mechanism of the interaction between the sand column group and the surrounding clay under different drainage conditions and rates of loading.

2. The use of dense sand columns to reinforce soft kaolin clay at area replacement ratios of 17.1% and 30.4% could increase the drained ultimate strength of the specimen by 8% and 40%, and the undrained strength by 39% and 159%, respectively. This increased strength is attributed to the dense columns' ability to carry additional stresses. This was proved by the miniature pressure sensors' measurements placed above dense sand columns that showed mobilized stresses as high as 350 kPa. In comparison, the miniature pressure sensors above the clay annulus indicated stresses as low as 50 kPa to 60 kPa.

3. Local stress measurements indicated that the stress concentration ratios varied significantly with strain, rate of loading, and area replacement ratio. At very low axial strains and under drained conditions, stress concentration ratios between 4 and 6 could be mobilized. These relatively high ratios decrease to about 1.5 at relatively large strains. For the case of undrained loading, the stress concentration factors are very low (1.5 to 2) at small strains and increase to values as high as 6.5 and 9.5 for cases involving area replacement ratios of 17.1% and 30.4%, respectively.

It should be noted that the measured stress concentration factors pertain to the particular case of a clay specimen that is reinforced with a group of four sand columns. For a given area replacement ratio, there is a possibility that the measured stress concentration factor might be affected by the number and configuration of the columns

93

in the group (triangular vs square configurations). Possible differences in the response for single and multiple column cases can be related to differences in the slenderness ratio of the columns (length to diameter ratio). In a triaxial setup, a single large-diameter central column will exhibit a smaller slenderness ratio compared to multiple columns. In addition, clay specimens that are reinforced with a single column may exhibit an internal state of stress that may locally diverge from that exhibited in the multiple column case, where the shear plane will have to interact with multiple columns. Moreover, the stress state in the two cases might be affected by local differences in the internal drainage conditions and column stiffness. The effect of these parameters on the response of the composite and particularly on the stress concentration factors will be studied in future work.

The sand columns used in this research are of direct relevance to applications related to the use of granular columns as vertically draining elements (sand drains) or as reinforcing elements (sand compaction piles). As far as the comparison to stone or gravel columns and the potential size (or scale) effects, the use of sand columns instead of gravel or stone columns in physical modeling is dictated by testing constraints. The size of specimens that can be accommodated in triaxial setups is limited even in the large triaxial cell used in this study. Nevertheless, results from published studies indicate that the type of material used to construct the granular column (gravel, sand, or a mixture of both) does not change the mechanics of the interaction between the columns and the surrounding clay. The reported stress concentration ratios in this study are very much needed for a better understanding of the load-transfer mechanism between the clay matrix and granular columns in applications involving both short and long-term stability of foundations.

CHAPTER 4

STUDYING THE EFFECT OF PARTIAL DRAINAGE ON THE RESPONSE OF SOFT CLAYS REINFORCED WITH SAND COLUMN GROUPS

4.1 Introduction and Background

Reinforcing soft clays with columnar inclusions has proven to be an effective and economical ground improvement technique as it enhances the stiffness, strength, permeability and consolidation times of the composite soil system (e.g. Bachus and Barksdale 1984; Muir Wood 2000; Najjar 2013; Najjar et al. 2020; Almikati et al. 2020). For soil improvement applications involving preloading/surcharging of soft clay, the role of radial drainage in facilitating the dissipation of pore pressure in the clay surrounding the column/drain is well known among practicing engineers. However, the role of radial drainage in increasing the "short-term" bearing capacity of foundations or embankments that are supported on clays reinforced with granular columns (sand, gravel, or stone columns) is yet to be fully explored/quantified.

Common design practice for soil improvement schemes involving granular columns is based on bounding the stability problem by the fully undrained or fully drained loading conditions. In reality, loading rates and drainage conditions in the clay surrounding the columns will govern the response of the composite. If we consider typical/practical construction rates, the assumption that the clay around the columns will respond in fully undrained conditions does not reflect the true drainage conditions in the soil, as consolidation and pore pressure dissipation will inevitably occur as a result of radial drainage. The degree of partial drainage will depend on the rate of loading, the

permeability of the clay, the spacing and diameter of the sand/gravel columns, and the possibility of smearing of the clay around the column during installation (Najjar 2013). Current design procedures lack a systematic approach for quantifying the effect of partial drainage and accounting for it in design. Disregarding the positive effect of partial drainage on the short-term ultimate bearing capacity of the composite system will inevitably lead to over-conservative designs (Najjar et al. 2010).

Studies pertaining to the investigation of partially drained behavior of clay-reinforcing granular columns systems are relatively scarce (Juran and Guermazi 1988; Andreou et al. 2008; and Bou Lattouf 2013). Juran and Guermazi (1988) studied the effect of partial drainage of a silty soil sample reinforced with river sand using a modified triaxial cell. The authors allowed the sand column to drain freely in one series of tests and blocked drainage from the columns in another. The freely drained column had a maximum load carrying capacity of about twice that of the undrained column. Andreou et al. (2008) conducted triaxial tests on Kaolin samples reinforced with single columns of Hostun sand and gravel. They observed clear reductions in strength when the rate of loading was "accelerated" with drainage allowed (partially drained) relative to slower rates of loading (fully drained). However, the measured strength remained higher than that of the reinforced "fully" undrained sample. Bou Lattouf (2013) conducted triaxial tests on Kaolin clay samples reinforced with Ottawa sand columns. They varied the drainage conditions and loading rates (3.5%, 40%, and 80% strain per hour). For the partially drained tests, the stress-strain curves obtained were bounded by the undrained (lower bound) and drained (upper bound) results. The main conclusion from previous work is that the undrained behavior generally underestimates the strength

of soft clay reinforced with sand columns and that partial drainage could significantly improve the short-term strength/bearing capacity.

The key to understanding the impact of partial drainage on the response of a clay/column composite is to investigate the buildup of contact stresses and pore water pressure in the column and the surrounding clay during loading. Measurement of contact stresses is critical for understanding the stress transfer mechanism between the columns and the clay matrix (Aslani et al. 2018). Contact stress measurements at different stages of loading allow for the determination of the stress concentration ratio, defined as the ratio of the stress in the granular column to the stress in the surrounding clay (Charles and Watts 1983, Bachus and Barksdale 1984, Wood et al. 2000, Black et al. (2006), Cimentada et al. 2011, Fattah et al. 2011, and Almikati et al. 2021). Local pore water pressure measurements at different time intervals also reflect the impact of radial drainage on the response and provide useful data on the degree of consolidation of the soft clay at different stages of loading (e.g. Juran and Guermazi 1988; Sivakumar et al. 2004).

Almikati et al. (2020) designed and implemented an innovative large-scale triaxial experimental setup that is capable of independently measuring excess pore water pressure above a group of granular columns and above the surrounding clay. In addition, the setup comprised miniature pressure sensors that collect data on the development of stresses in the columns and the clay concurrently. Such a setup presents a unique opportunity to study the impact of partial drainage on the development of contact stresses and pore water pressures within a reinforced clay specimen in an effort to quantify the global response of the composite clay/sand column system and the stress concentration factor.

Despite the advancement in sensing and instrumentation in large scale triaxial testing (Almikati et al. 2020), available test setups only allow for the collection of data from sensors that are in "external" contact with the soil sample (pore pressure sensors, miniature pressure sensors, LVDTs, load cells). The only/primary tool that is available for examining "internal" stresses, strains, and pore pressure generation/dissipation for reinforced clay systems is numerical analyses. Several studies targeted analyzing the radial consolidation problem of soft clays reinforced with vertical drains (Lei et al. 2017). Barron (1948) proposed an analytical solution for radial consolidation. Since then, multiple researchers presented modifications to Barron's solution to account for different boundary conditions, different types of materials, and loading scenarios (Table 6). The majority of available models utilize the axisymmetric unit cell concept in analyzing the response, with few analyzing the problem as a plane strain model (Tan et al. 2008). In almost all the cases considered, results from numerical and analytical analyses are validated with data from 1-D consolidometers rather than triaxial setups. One-dimensional consolidometers do not allow for modeling the true response of reinforced clay specimens under true foundation/shearing loads. Thus, there is a need for validating the effectiveness of available models in predicting the radial consolidation response of soft clay specimens that are reinforced with sand column groups under controlled triaxial shear conditions.

This paper aims at investigating the impact of partial drainage on the response of large-diameter soft clay specimens that are reinforced with a group of sand columns. A newly developed fully instrumented large-scale triaxial test setup is utilized to investigate the overall response of the composite, with particular emphasis on monitoring contact stresses over the sand columns and the surrounding clay. Drained,

undrained, and partially drained tests were conducted on 14.5 cm-diameter clay specimens reinforced with a group of four fully penetrating 3cm-diameter dense columns. Partial drainage is enforced by prohibiting drainage from the bottom of the clay and allowing it only through the miniature porous stones in the upper cap of the triaxial cell. Different shearing rates were used to represent relatively quick loading (strain rate of 40% per hour), slow loading (a strain rate of 0.5% per hour) and average loading (strain rates of 3% and 10% per hour). All tests were performed on slurry-consolidated, back-pressure saturated, clay specimens at a confining pressure of 100 kPa.

The main objectives of the test program were to (1) compare the behavior of partially drained samples to that of fully drained and fully undrained samples under similar conditions, and (2) establish a relationship between the mobilized partially drained strength and the theoretical estimates of the degree of consolidation calculated using finite difference solutions that take into consideration the radial dissipation of pore pressures in the partially drained tests. Continuous measurements of contact stresses on the clay and above sand columns will allow for the evaluation of the impact of partial drainage on the stress concentration ratio and will provide valuable data that could guide and facilitate the development of design methodologies for reinforced clay systems under different drainage conditions and rates of loading.

4.2 Experimental Program

4.2.1 Large-Scale Triaxial Test Setup

The testing setup used to run the experimental program is shown in Figure 36. A large triaxial frame capable of testing cylindrical soil samples as large as 145 mm in diameter and 300 mm in length was modified for this study testing. An upper cap with

housings for miniature pressure sensors and pore water pressure sources was designed and fabricated. The upper cap is made from aluminum and has an outer diameter of 145 mm. The innovative upper cap was designed to include housings for three miniature pressure sensors (MP1, MP2 and MP3) and three water sources, two of which (PP2 and PP3) were used for pore water pressure measurement above a sand column and the clay, whereas the third water source was used for back pressure saturation and volume change measurements. A third pore water pressure sensor (PP1) was connected to the bottom porous stone.

Table 6: Various research studies to study the radial drainage in reinforced soft clays with vertical drains

Reference	Free Strain or Equal Strain	Unit Cell (U) or Plane Strain (PS)	Smear Zone and Well Resistance Consideration	Vertical Drainage Consideration with Radial Drainage	Analysis Type: Experimental (E) Numerical (N) or Analytical (A)	Prefabricated Vertical Drain (PVD) or Granular Drain (GD)
Barron (1948)	Equal	U	✓	X	A	PVD
Hansbo (1981)	Equal	PS	✓	✓	A	PVD
Atkinson et al. (1985)	Equal	U	X	X	E (Triaxial)	GD (Sand)
Hird et al. (1992)	Free	U and PS	✓	X	N (Finite element)	PVD
Indraratna and Redana (2000)	Equal	PS	✓	✓	N (Finite element)	PVD
Han and Ye (2001)	Equal	U	X	✓	A	PVD
Seah and Juirnarongrit (2003)	Equal	U	X	X	E Consolidometer)	PVD
Leo (2004)	Equal	U	✓	✓	A	PVD
Tan et al. (2008)	Equal	PS	X	X	N (Finite element)	GD (Stone)
Conte and Troncone (2009)	Equal	U	✓	✓	A	PVD
Bo et al. (2016)	Equal	U	X	X	E Consolidometer)	PVD

Volume change and back pressure saturation lines can be connected to both the upper and lower caps via a T-connection. The back-pressure (pressurized water) comes from the pressure source controller to the volume change device then reaches the sample through either/both the upper and lower lines. The measurement of volume change is done using a volume change apparatus that has a double acting piston connected to a linear variable differential transducer (LVDT 2).

The instrumentation includes, in addition to the aforementioned sensors, a load cell and an LVDT connected to the top of the sample. All sensors and transducers are connected to a central data acquisition box. The data logging is done on LABVIEW software.
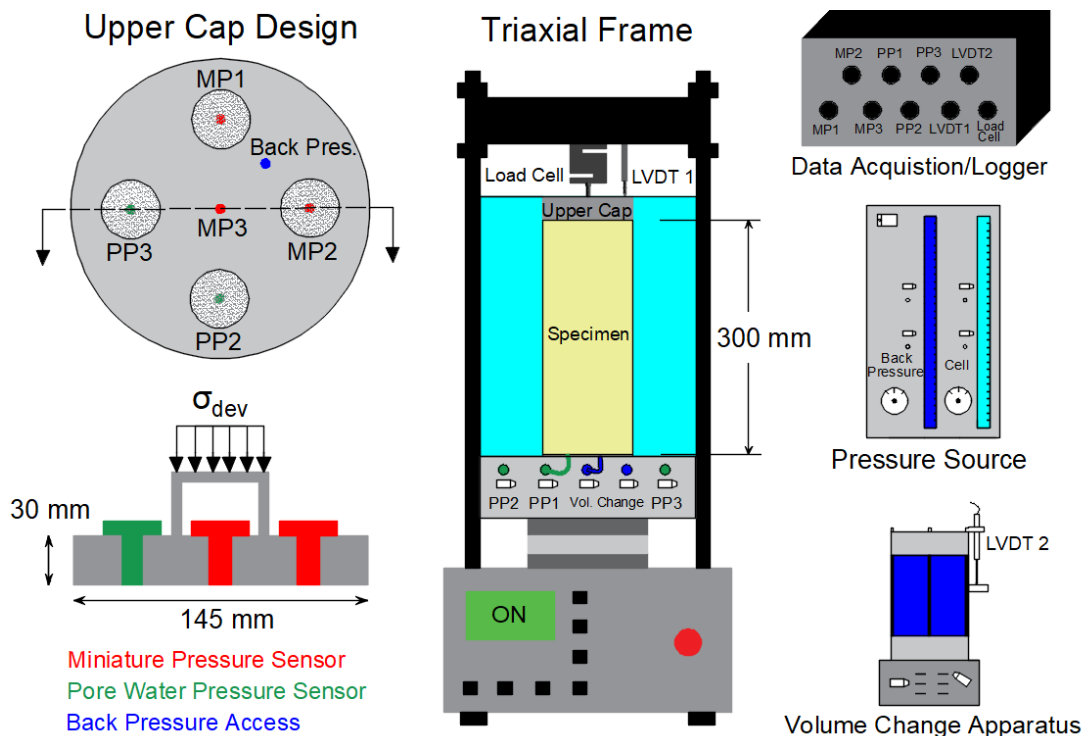
Figure 36: Testing setup with all sensors and equipment used in triaxial testing

4.2.2 Materials

Kaolin clay and Ottawa sand were used in the triaxial testing program. General properties of both materials are presented in the following sections. Additional information about the soils used can be found in Almikati et al. (2020).

The clay used in this experimental study is Kaolin clay (Supreme China Clay) sourced from the United Kingdom. The liquid limit and plasticity index of the clay are 65% and 29%, respectively, with a specific gravity, $G_s = 2.56$. The consolidation parameters were determined from a one-dimensional consolidation test and the recompression (C_r), compression (C_c) and swelling (C_s) indices were found to be 0.19, 0.50 and 0.17 respectively. Isotropically consolidated drained and undrained triaxial tests were performed on the Kaolin clay under three confining stresses (100, 150 and 200 kPa) to determine the effective shear strength parameters, yielding $c' = 0$ kPa and $\varphi' = 21.8°$. Pore water pressure measurements yielded Skempton pore pressure parameters "A_f" of 1.06, 1.13 and 1.19, for effective confining stresses of 100, 150 and 200 kPa, respectively (Skempton, 1954).

Ottawa sand, used in this testing program, is classified as poorly graded sand (SP) as per the Unified Soil Classification System. The specific gravity of this sand is 2.65, with minimum void ratio of 0.49 and maximum void ratio of 0.75. Additional physical and mechanical properties of the Ottawa Sand are found in Almikati et al. (2020). Consolidated drained and undrained triaxial tests were also done on Ottawa sand at a relative density of 85%, which is the density chosen for the granular columns. Dilative behavior was predominant for the drained tests, while negative pore water pressures were measured in the undrained tests. For a range of confining stresses

between 100 and 200 kPa, results indicated that the effective friction angle of the dense sand is $\varphi' = 39°$.

4.2.3 Specimen Preparation

Sample preparation consisted of mixing kaolin powder with water at twice the liquid limit. After proper mixing, the slurry was poured in custom fabricated, well-tightened PVC split pipes that are 500 mm in length and have an internal diameter of 145 mm. Dead weights were used to consolidate the clay in a one-dimensional setting under a normal stress of 100 kPa while allowing upper and lower drainage. Ottawa sand was used for the preparation of the dense sand columns at a relative density of 85% using the freezing method as per the recommendation of Black et al. (2007), Najjar et al. (2010), and Almikati et al. (2020).

The final length of all specimens after trimming was 290 mm (Figure 37a) with a diameter of 145 mm, representing a length to diameter ratio $L/D = 2$. The sand columns were prepared to the target density one day prior to testing and left in the freezer. They were removed from the freezer and installed directly in the predrilled holes (Figure 37b), after which they were left to thaw prior to testing. A total of four 30-mm diameter columns were installed in a square configuration representing an area replacement ratio $a_r = 17\%$ (Figure 37c).
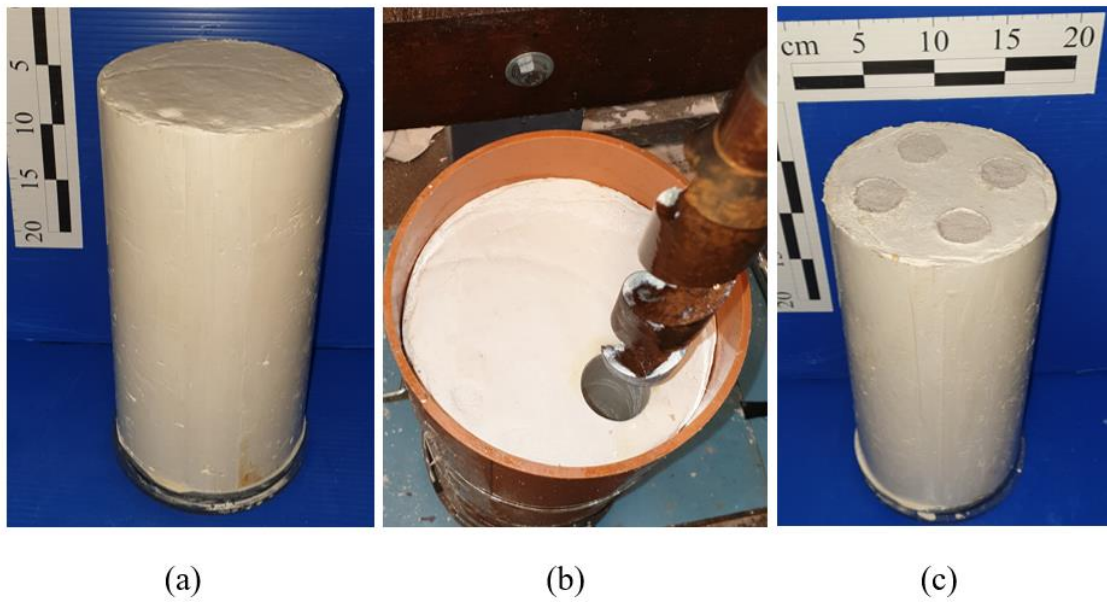
Figure 37: Sample preparation showing (a) kaolin prior to drilling; (b) drilling process and (c) reinforced sample ready for testing with four sand columns installed

4.2.4 Testing Program

The large triaxial testing setup was used to conduct six triaxial tests on Kaolin specimens that were reinforced with a sand column group. The tests comprised four partially drained tests (PD), one consolidated drained test (CD) and one consolidated undrained (CU) test. In addition to the tests on reinforced specimens, two additional tests were conducted to determine the drained and undrained response of unreinforced clay specimens (control specimens).

The main difference between the partially drained tests and the consolidated drained and undrained tests is the drainage pattern. In all partially drained tests, drainage was prohibited from the bottom side of the specimen to enforce a drainage pattern that is predominantly radial. Drainage from the upper cap was facilitated by the placement of a cylindrical filter at the top of the sample which connects the columns to

the "small" outlet/porous at the base of the upper cap. For the CU and CD tests, two-way drainage was allowed during consolidation (CU, CD) and drained shearing (CD). Volumetric change was monitored during consolidation (for all tests) and shearing (drained and partially drained tests) to quantify the volumetric strains. For undrained and partially drained tests, pore water pressures were measured below the porous stone in the base cap below the clay matrix. All tests were isotropically consolidated to an effective confining pressure of 100 kPa (back-pressure of 300 kPa and a cell pressure of 400 kPa). The shearing rates chosen for the consolidated drained and consolidated undrained tests were as per ASTM standards. For partially drained tests, the loading rates were selected to cover/create different scenarios of partial drainage. Strain rates of 40%/hour, 10%/hour, 3%/hour and 0.5%/hour were selected for tests PD1, PD2, PD3 and PD4, respectively.

4.3 Experimental Test Results

Table 7 shows the values of peak deviatoric stresses, pore water pressures, and volumetric strains for all reinforced clay specimens tested. In order to link the results to the drainage conditions that dominated within each specimen, the volume change data that was collected during the isotropic consolidation stage was used to determine t_{50}, the time required for 50% consolidation to be achieved (see Table 7). The time to failure ($t_{failure}$) of each specimen was determined and normalized by the associated t_{50} value and reported in Table 7. The ratio $t_{failure}/t_{50}$ is an important indicator that is expected to correlate to the degree of consolidation that is achieved in each partially drained test, at failure.

Table 7: Test results for drained, undrained, and partially drained reinforced clay specimens

Test* Type	t_{50} (min)	Strain Rate (%/hour)	$t_{failure}$ (min)	$t_{failure}/t_{50}$	Peak Deviatoric Stress (kPa)	Stress Improvement Factor (%)	Peak Excess Pore Water Pressure (kPa)	Volumetric Strain ε_v (%)	$\varepsilon_{v(PD)}/\varepsilon_{v(D)}$ (%)	Finite Difference U_f (%)
CU	51.0	1.20	-	-	78.5	-	43.81	0.00	-	-
PD1	87.0	40.00	13.33	0.17	85.5	13.9	41.30	0.33	7.2	9.4
PD2	85.0	10.00	53.33	0.71	96.2	35.0	29.41	1.53	33.5	28.2
PD3	82.0	3.00	178	2.44	111.6	65.5	17.84	2.94	64.3	59.5
PD4	84.0	0.50	1,067	14.29	130.0	101.2	1.40	4.22	92.3	94.5
CD	47.0	0.067	-	-	129.4	-	0.00	4.57	-	-

* CU: Consolidated Undrained, CD: Consolidated Drained, PD: Partially Drained

4.3.1 Stress-Strain and Volumetric Strain Response

Curves showing the variation in the deviatoric stress, excess pore water pressure, and contractive volumetric strain with axial strain are shown in Figures 38a to 38c for all reinforced specimens. The stress-strain curve of the control clay specimen that was sheared under undrained conditions is also included in the plot to serve as a reference for quantifying the improvement brought by the inclusion of the sand column group.

The stress-strain curves exhibited consistent increases in deviatoric stresses with strains as the samples were sheared towards critical state conditions. All tests exhibited clear peaks indicating failure at axial strains varying between 8% and 12%. The measured global volumetric strains (partially drained and drained tests) were all contractive. The pore water pressures (partially drained and undrained tests) were positive and increased as the deviatoric stresses reached their maximum values and then decreased or leveled out at larger strains. In fully drained tests, the compressive volumetric strain that was measured in the unreinforced clay specimen (~ 6.5% at large strains) was reduced to around 4.6% for samples reinforced with the 3cm diameter sand

column group. As expected, this reduction in contractive behavior was more significant for the partially drained tests, particularly for faster shearing rates. This higher reduction in contractive behavior for the specimens sheared at a fast strain rate is associated with higher pore pressures that did not have enough time to dissipate.

The deviatoric stress versus axial strain plots show that the all those corresponding to the partially drained specimens lie between two bounding curves, the higher is that of the fully drained test, while the lower is that of the undrained test. These results are consistent with the findings of Andreou et al (2008). As the strain rate increased, a clear reduction in the peak deviatoric stress was observed in partially drained tests. The reduction in the peak deviatoric stresses with faster loading rates in partially drained tests is linked to the decreased degree of consolidation associated with radial drainage that can develop during the shearing phase. Even at the highest strain rate of 40% per hour, the stress-strain and volumetric strain curves show that some degree of drainage has occurred in the tested specimen despite the fact that the ratio of $t_{failure}/t_{50}$ was relatively low (0.23). In the somewhat slower partially drained tests (PD2 and PD3) with $t_{failure}/t_{50}$ of 1.4 and 4.7, it is clear from the results that the sand columns acted as drainage boundaries that allowed significant pore water pressure dissipation predominantly through radial drainage. As the shearing rate decreases, the partially drained curves become closer to the fully drained curve. Interestingly, the slowest partially drained test (PD4) with $t_{failure}/t_{50}$ of about 15 yielded a stress-strain response that was almost identical to that observed in the fully drained CD test.
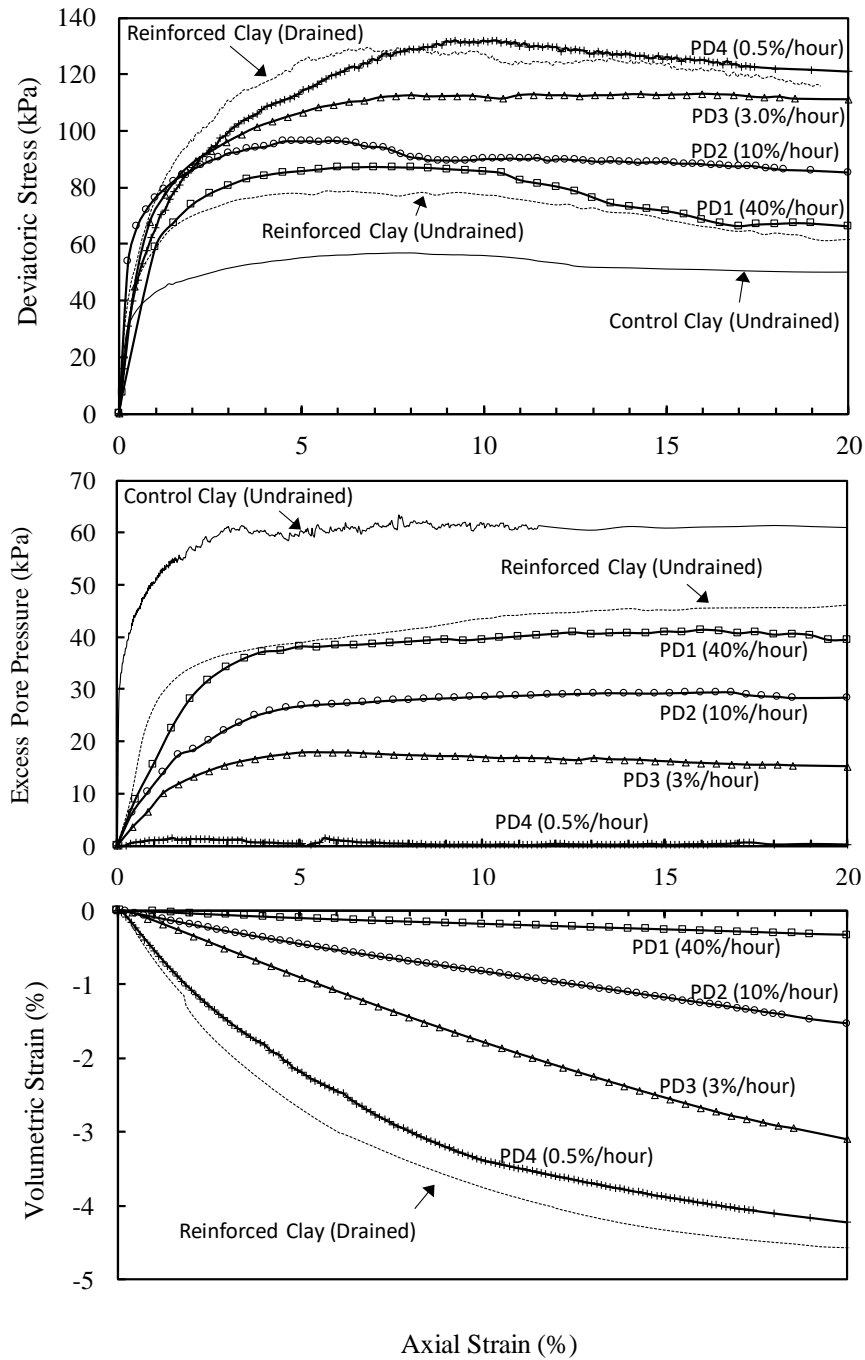
Figure 38: The variation of (a) deviatoric stress, excess pore water pressure, and (b) volumetric strain with axial strain

It is important to note that although "global" volumetric strains and pore water pressure generation in the reinforced clay specimens indicated a net contractive tendency (positive excess pore pressure and compressive volumetric strain), it is

hypothesized that the dense sand columns exhibited a dilative tendency that was masked by the contractive tendency of the soft clay matrix. Given the relatively low area replacement ratio (17%), it is likely that the positive pore water pressures in the clay satisfied the negative pore pressures in the sand, resulting in a net positive pore pressure response at the lower porous stone. This is supported by the measured volumetric strains which reflected the overall contractive volume change in the sample. Volumetric strains that approach zero indicate that enough compressive strains have occurred in the clay to balance the dilative volumetric strains that inevitably occurred in the freely draining dense column. Unfortunately, the local pore pressure sensors that were incorporated in the upper cap of the triaxial cell to measure local pore pressure in the sand column and the clay matrix did not yield reliable local pore pressure data that could be used to isolate the pore pressure response in the sand columns from the response of the clay matrix.

4.3.2 Mode of Failure

An investigation of the failure mode for the reinforced drained, undrained and partially drained tests indicated that all samples failed along a well-defined shear plane regardless of drainage condition (Figure 39). The formation of the failure plane is consistent with peaks exhibited in the stress-strain responses (Figure 38a), irrespective of the drainage conditions and loading rate.

For the drained tests, the formation of a failure plane could be traced to the dilative tendency of the dense sand columns, which is expected to dominate the failure mode of the composite specimen. Drained triaxial tests on dense Ottawa sand (Almikati

et al. 2021) clearly indicate a strain softening behavior with an associated formation of a failure plane as the sand dilates during shear. On the other hand, for the undrained tests, the soft clay generates positive pore water pressures during shearing, thus a decrease in the effective stresses in the clay matrix and associated softening. Control clay specimens that were sheared under undrained conditions also showed the formation of a failure plane. It could thus be concluded that the formation of a failure plane in the reinforced clay specimens during undrained loading is attributed to the dominant role of the soft clay matrix that controlled the mode of failure. For the partially drained tests, the mode of failure of reinforced specimens was consistent with the drained and undrained cases, as it is somewhere in between the two similar modes of failure.
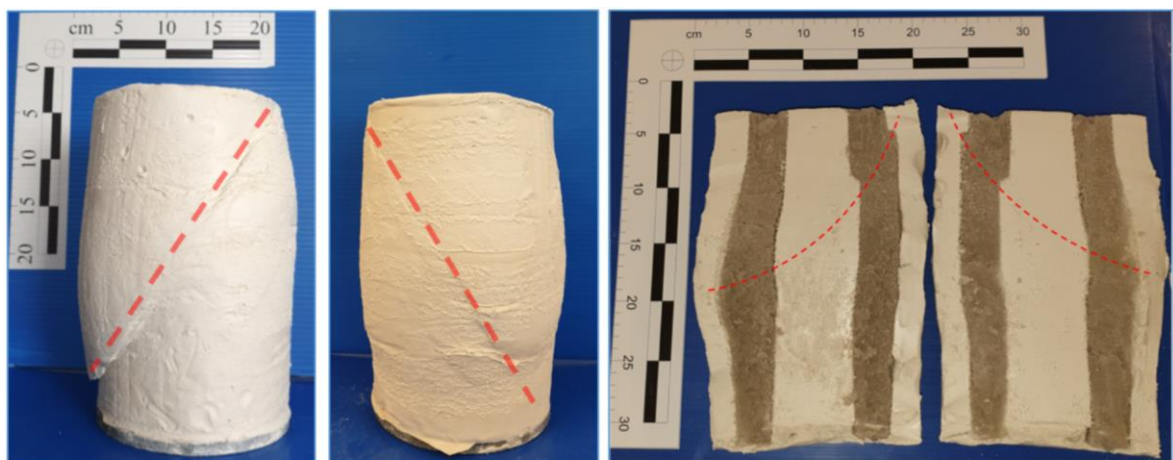
(a) Reinforced Undrained   (b) Reinforced Drained   (c) Cross Section (Reinforced Drained)

Figure 39: Failure mode for reinforced clay specimens (a) CU tests, (b) CD test, and (c) PD test(s) under varying drainage conditions

4.3.3 Effect of Partial Drainage on the Ultimate Strength

Figure 40a shows the variation of deviatoric stresses at failure with the ratio $t_{failure}/t_{50}$ plotted in logarithmic scale. The graphical representation is for the partially drained and fully drained tests, with the fully undrained test represented by red square markers serving as a lower bound to the strength of the composite system. Results in Figure 40a indicate that as the ratio $t_{failure}/t_{50}$ increases, the maximum load carrying capacity of the clay-sand column composite improves. This improvement in shear strength levels off at an approximate $t_{failure}/t_{50}$ of 15, where the measured deviatoric stress of the slowest partially drained test approaches the upper bound strength observed in the fully drained test. It is worth noting that the ratio $t_{failure}/t_{50}$ is typically used to determine the shearing rates required for consolidated drained tests (ratio in the range of 80-120) and for consolidated undrained tests. For the latter the ratio is taken as 10 to ensure pore water pressure equalization.

For comparison, data from partially drained triaxial tests that were conducted by Bou Lattouf (2013) on small-scale triaxial clay specimens (7.1 cm diameter) and that were reinforced with a single central 3-cm diameter sand column are plotted on Figure 40a. The strain rates adopted in the partially drained tests reported in Bou Lattouf ranged from 3.5% to 80%. Despite differences in intrinsic properties (plasticity and permeability) of the clays used in their study in comparison to ours, the results from the Bou Lattouf (2013) also show that partial drainage improves the maximum deviatoric stresses in reinforced specimens compared to the fully undrained reinforced specimen (Figure 40a). The maximum deviatoric stresses in the partially drained tests of Bou Lattouf (2013) increase with the ratio $t_{failure}/t_{50}$ and level off at an approximate $t_{failure}/t_{50}$ of 10 to 30, which is a behavior similar to the one we observed.

111

In order to generalize the results of the partially drained tests and analyze them in a systematic context, we used a normalized stress improvement index, α. This index is defined as the ratio of the difference in the maximum deviatoric stress in a partially drained test and the undrained test $(\sigma_{PD} - \sigma_U)$, to the difference between the maximum deviatoric stresses of the fully drained and undrained tests $(\sigma_D - \sigma_U)$. The strength improvement index, α, is analogous to the liquidity index for clays in the sense that it provides a relative measure of the magnitude of strength that could be mobilized in a partially drained test in reference to the minimum and maximum strengths that could be obtained assuming undrained and drained conditions, respectively. The formula used for the calculation of α is shown in Equation 2:

$$\alpha = \frac{\sigma_{PD} - \sigma_U}{\sigma_D - \sigma_U} \tag{2}$$

The strength improvement index α is plotted against the ratio $t_{failure}/t_{50}$ in Figure 40b. The values of the stress improvement indices of the partially drained tests were 0.14, 0.35, 0.66 and 1.01 for PD1, PD2, PD3 and PD4, respectively. It is interesting to note that although the fastest partially drained test (PD1) portrayed small contractive volumetric strain of 0.34% at the end of shearing, it exhibited a strength improvement index of about 0.14, indicating a 14% increase in strength relative to the fully undrained test. The slowest partially drained test on the other hand (PD4) mobilized the full drained strength of the specimen even at a $t_{failure}/t_{50}$ of about 15, which could be considered to be practical ratio at which the drained strength is mobilized.

Interestingly, the trend between the strength improvement index and the ratio $t_{failure}/t_{50}$ for the partially drained tests conducted in Bou Lattouf (2013) is remarkably similar that observed in this study despite differences in clay type/properties, sample

scale, single versus group column reinforcement, and density of the sand columns.

Based on the data presented in Figure 40b, the ratio of $t_{failure}/t_{50}$ could be seen/adopted as

a practical normalized indicator of the improvement in the deviatoric stress at failure,

for partially drained tests on reinforced clay specimens. This observation will need

further/future validation from additional triaxial tests on different types of clay and sand

columns.

4.3.4 Contact Stresses in Clay and Sand Column

Local contact stresses were measured using miniature pressure sensors located

over two sand columns and over the clay matrix below the center of the upper cap. The

variation of the measured contact stresses with axial strain is presented in Fig. 41 for all

test specimens. Also shown in Fig. 41 are the curves representing the variation of the

overall global deviatoric stress with strain as measured using the load cell connected to

the test frame.

For the control clay specimens, measuring contact stresses using the miniature

pressure sensors allowed for testing the effectiveness and reliability of the sensors in

measuring stresses under drained (Fig. 41a) and undrained (Fig. 41b) conditions.

Contact stresses for the case of the control clay indicated that the three pressure sensors

gave reliable and repeatable results compared to the global deviatoric stresses measured

by the load cell. As expected, the stresses measured by the miniature pressure sensors at

three locations exhibited some natural variability and were within 5 to 10% of the

measured global deviatoric stress. This observation is important since it confirms that

the utilized sensors can be effectively used to monitor stresses in the drained and

undrained normally consolidated kaolin clay with minimal errors.
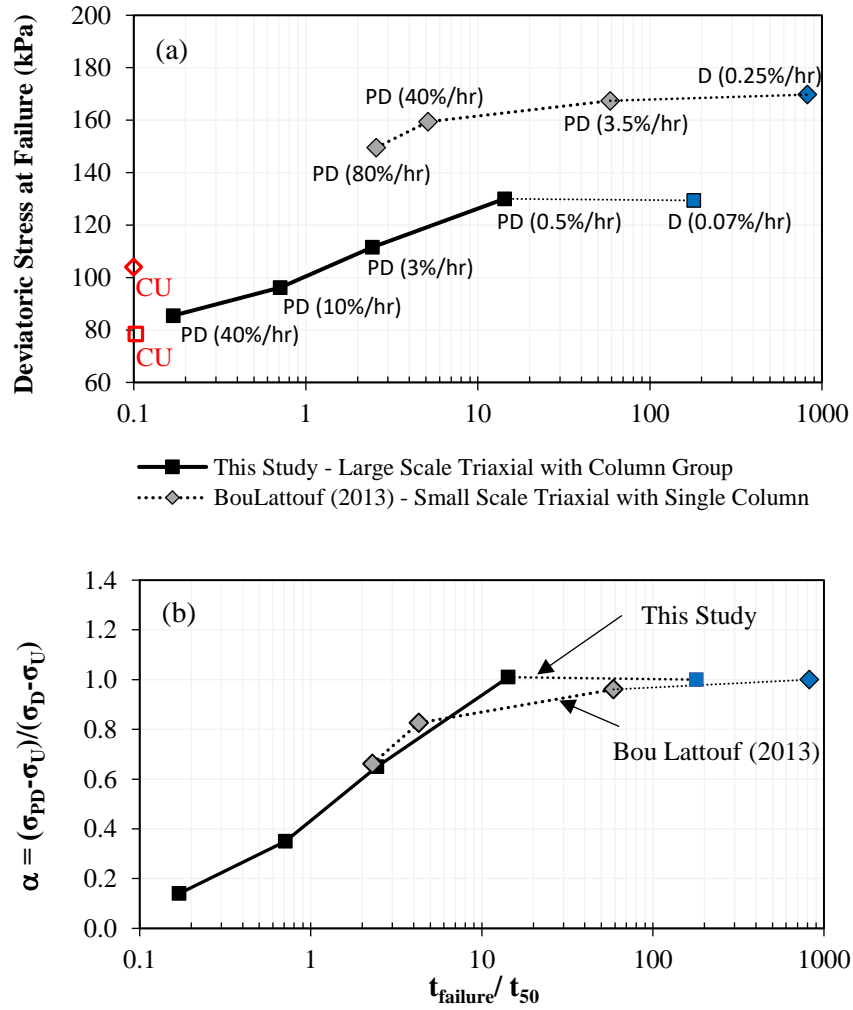
Figure 40: (a) Variation of deviatoric stress with $t_{failure}/t_{50}$ and (b) Variation of normalized stress improvement index with $t_{failure}/t_{50}$

For test involving reinforced specimens, the square configuration of the four

sand column group permits stress measurement for two of the columns and at the

central clay. The variations of these measured contact stresses with axial strain are

presented in Figs. 41c to 41h for specimens tested under different drainage conditions

and rates of loading. Results from stress measurements above the sand columns (MP1 and MP2) indicated that: (1) the stiff sand columns attracted stresses that are much larger than those measured in the clay, irrespective of the drainage conditions, (2) some variability in the contact stresses is observed between the sand columns in the same composite specimen, and (3) the magnitude of the measured stresses in the columns is affected by the drainage conditions and rate of loading.

In order to validate and verify the applicability/reliability of the stress measurements at the sand columns, the clay stresses that were measured by MP3 and the global deviatoric stresses for the composite clay specimen were used to back-calculate the average stress at the sand columns in the group. The variation of the back-calculated stresses at the columns with axial strain is shown in red in Fig. 41. The back-calculated stresses were obtained using Equation 3 by assuming that the global deviatoric stress (σ_d) was shared by the stress in the clay (σ_{clay}) and the average stress at the four sand columns (σ_{sand}) such that:

$$\sigma_d A_{sample} = \sigma_{clay} A_{clay} + \sigma_{sand} A_{columns} \tag{3}$$

Where A_{clay} and $A_{columns}$ are the areas of the clay the sand columns in the reinforced clay specimen, while A_{sample} is the total cross sectional area of the composite specimen. Given the global deviatoric stress (σ_d) and the measured stress (MP3) in the clay (σ_{clay}), Equation 3 was used to back-calculate (σ_{sand}). Interestingly, results on Fig. 41 indicate that the variation of the back-calculated average stresses in sand (σ_{sand}) with axial strain (red curves) compare well with the stresses in sand measured using MP1 and MP2.
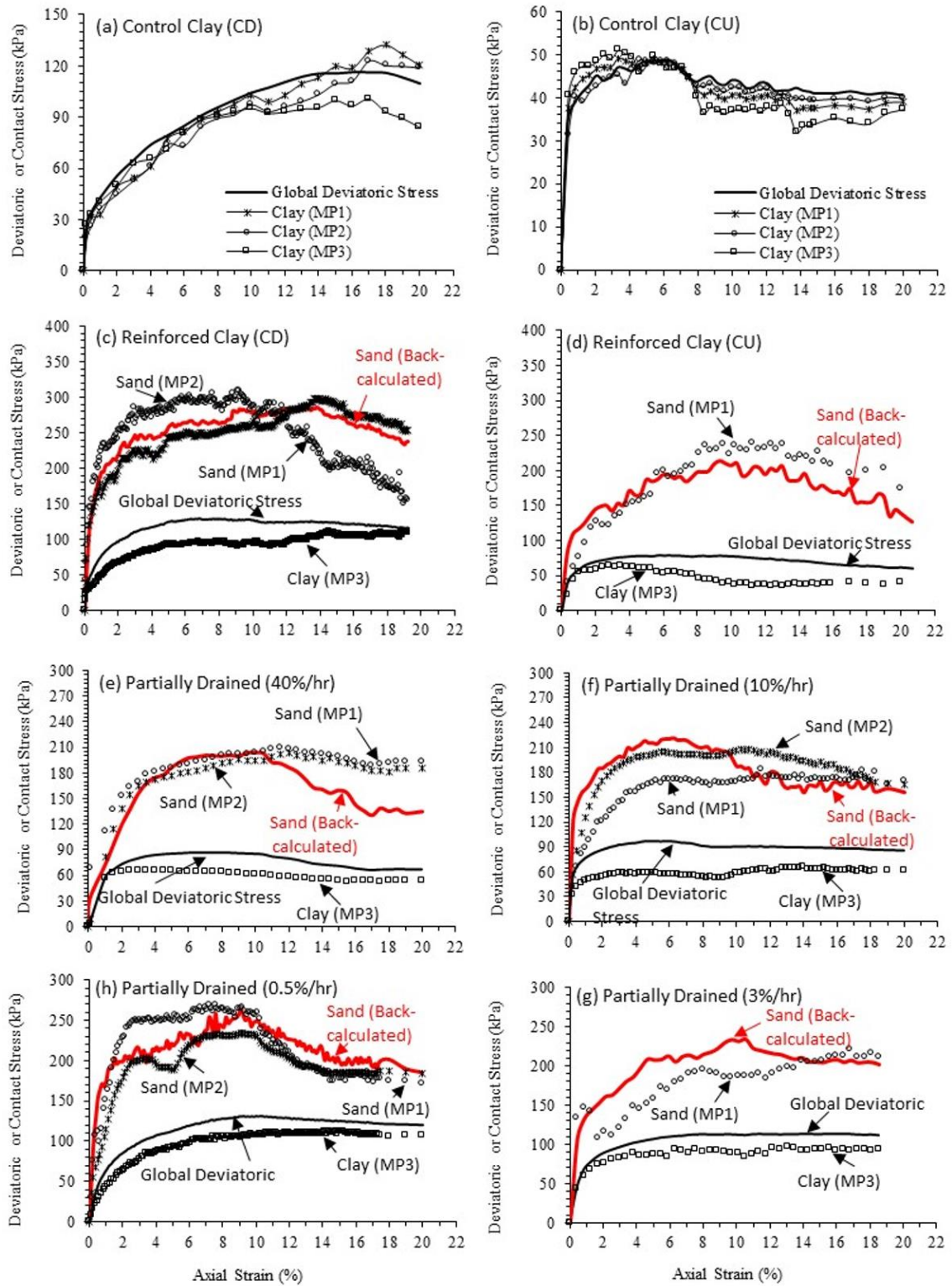
Figure 41: Variation of deviatoric and contact stresses with strain for control and reinforced clay

In fact, the back-calculated stresses in sand constitute a realistic representation of the average stresses measured by MP1 and MP2. These results are important since they indicate that the stresses measured by the miniature pressure sensors are reliable and reflective of the true stress distribution in the composite specimen.

The mechanics of load sharing between the sand columns in the group and the surrounding clay and its dependence on the drainage conditions and rate of loading were further explored by plotting the stresses mobilized in the clay (MP3) and those in the sand columns on Figure 42. The stresses in the clay matrix indicate that the clay was able to carry higher stresses under drained conditions compared to the undrained case. For the drained test, the stresses mobilized in the clay matrix approached, but did not reach, the maximum deviatoric stress mobilized in the drained control clay (Fig 41a). This indicates that the failure mechanism in the drained test was governed by the failure of the sand columns. On the other hand, results for the undrained test indicate that the stress in the clay matrix was consistent with stresses measured in the undrained control clay specimen (Fig. 41b). These observations indicate that the undrained response in the composite clay was largely governed by the relatively low undrained shear strength of the clay matrix. The premature undrained failure in the clay matrix prohibited the sand columns from mobilizing large stresses, with column stresses that were 30% to 40% smaller than the column stresses mobilized in the fully drained test (compare blue lines in Figure 42).

In the partially drained tests, an investigation of the gradual stress buildup in the sand columns and the clay shows clear evidence of the dissipation of positive pore water pressure due to radial drainage from the clay matrix into the sand columns. This increased the effective confinement of the clay and resulted in a clear increase in the

mobilized clay stresses compared to the fully undrained case. The increase in the load carrying capacity of the clay matrix as a result of partial drainage, allowed the sand column group to carry additional stresses as indicated by the measured contact stresses in the sand (Fig. 42). As the rate of loading decreased from 40% per hour to 0.5% per hour, the ability of the sand column and the surrounding clay matrix to carry deviatoric loads increased with the increase in the degree of consolidation until it approached that of the fully drained specimen.
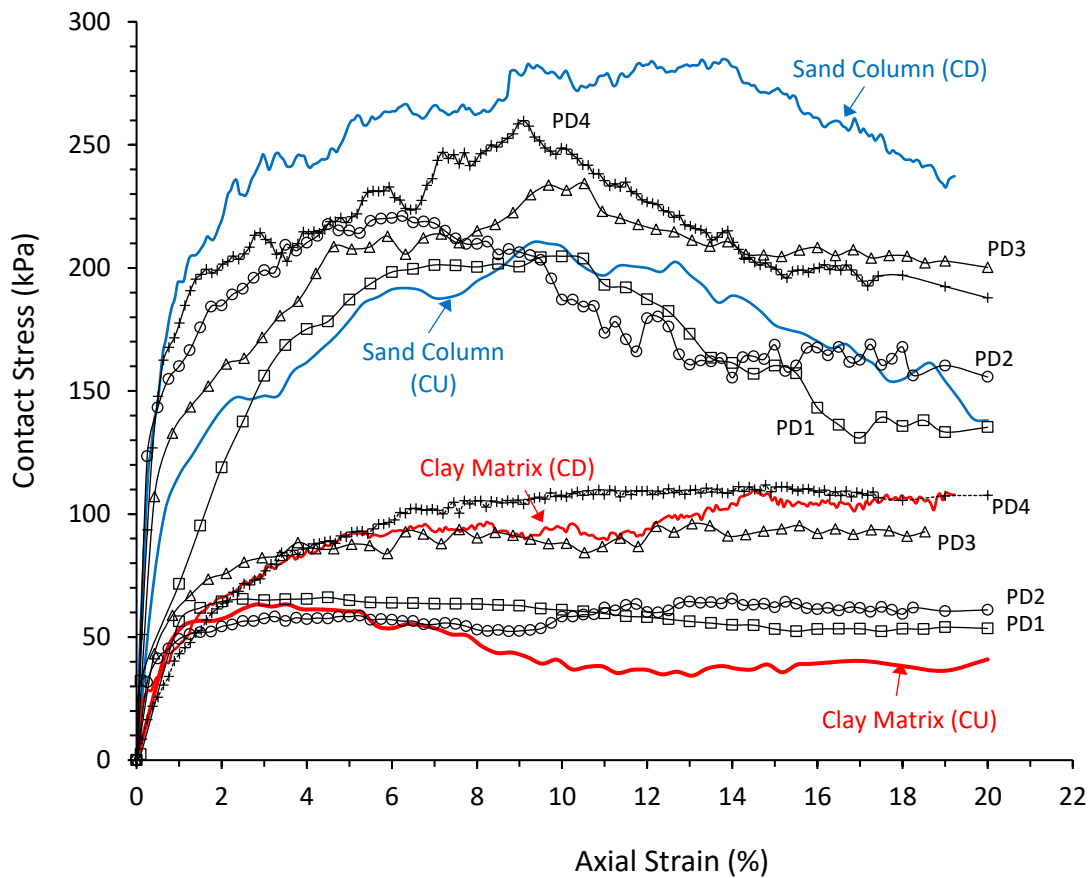
Figure 42: Variation of clay and sand contact stresses with strain for all reinforced specimens

4.3.5 Stress Concentration Factor

The measured contact stresses were used to calculate the stress concentration factor "n" for all composite specimens by dividing the average measured stresses in the sand (MP1 and MP2) by the stresses in the clay measured with sensor MP3 at all strain levels. The variation of the stress concentration ratio with axial strain as presented on Fig. 43 reveals a clear distinction between the mechanics of load sharing in drained and undrained conditions. For the drained test, the variation of the stress concentration ratio with strain shows a sharp increase in the ratio at relatively low strains, reaching maximum values of 4.5 and then decreasing gradually to reach values as low as 1.3 at large axial strains. Conversely, the variation of the stress concentration ratio with axial strain in the undrained test indicates a gradual monotonous increase leading to peaks in the order of 6 to 7 at axial strains ranging from 10% to 15%. The trends of both CD and CU tests are well in line with previous research done on drained and undrained response of soft clays as in the work of Bachus and Barksdale (1984), Juran and Guermazi (1988), Han and Ye (1991) and Fattah et al. (2011).

For the drained test, the early peak in the stress concentration ratio and the gradual but significant reduction that follows can be attributed to two main factors: (1) the softening that is observed in the sand columns which dilate and soften at relatively small strains, and (2) the progressive gradual strain hardening that is exhibited in the clay surrounding the columns as the clay consolidates and compresses during drained shear (Black et al. 2011).
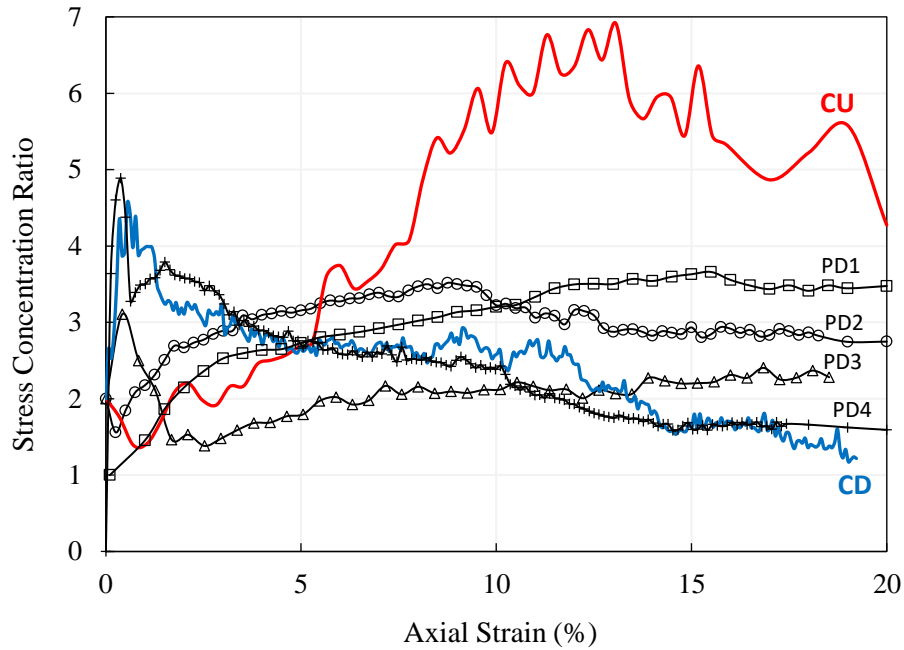
Figure 43: Stress concentration factor variation with axial strain for all conducted tests

For the undrained test, the monotonous increase in the stress concentration ratio with strain can be attributed to two main factors: (1) the undrained conditions that govern the response of the clay in the composite specimen leading to the mobilization of relatively low undrained stresses in the clay, and (2) the gradual increase in the mobilization of stresses in sand with strain (up to strains in the order of 10%).

The variations of the stress concentration factor with axial strain for the CD and CU tests theoretically define the two boundaries of the variation of the partially drained tests. The variation of the stress concentration factor with strain for the slowest test (PD4) was almost identical to the fully drained test although the strain rate in PD4 was six times faster. For the other relatively faster partially drained tests, the stress concentration factors at axial strains less than 10% ranged from 2 to 4, with no particular trend with the applied strain rate. Interestingly, for axial strains exceeding

120

10% where the stress concentration factors in the CU test were as high as 7, stress concentration factors in the PD tests remained relatively low, with average n values of 2.2, 3.0, and 3.6 for PD3, PD2, and PD1, respectively. These results indicate that even minor partial drainage could result in significant reductions in the stress concentration factors at larger strains compared to the fully undrained case. It should be noted that the reductions in "n" due to partial drainage are not attributed to a stress reduction in the columns, but to an increase in the stress that is carried by the clay due to an increased degree of consolidation. Even with the decreased values of "n", the net effect of partial drainage is to increase the deviatoric stress of the composite specimen in comparison to the undrained case.

4.3.6 Effect of Partial Consolidation on Mobilized Strength

Although strong correlation was observed in Figure 40 between the strength improvement index and the ratio $t_{failure}/t_{50}$, the more direct and traceable correlation is expected to be between the strength improvement factor and the average degree of consolidation of the clay matrix, which is in turn correlated to the rate of dissipation of pore water pressure due to partial drainage. The most relevant indicator of the degree of consolidation in the triaxial test measurements is the volumetric strain. Results on Figure 39 clearly indicated that the volumetric strains for cases involving partial drainage were directly correlated to the rate of loading. In the absence of direct measurements of the degree of consolidation in the clay matrix, the measured global volumetric strains in drained and partially drained tests could be utilized to reflect the dissipation of excess pore water pressures and are directly linked to the progression in the consolidation of the clay matrix.

To test this hypothesis, the variation of the strength improvement index with the "volumetric improvement index", defined as the ratio of the volumetric strain measured in the partially drained test to the volumetric strain in the fully drained test $\varepsilon_{PD}/\varepsilon_D$, is plotted in Figure 43. The four data points represent the four partially drained tests while the 45° line serves as the line of unity. The plot indicates a strong correlation between the strength improvement index, α and the volumetric improvement index, $\varepsilon_{PD}/\varepsilon_D$. A similar correlation could also be observed using the partially drained test data reported in Bou Lattouf (2013) and which were added to Fig. 44 for completeness. This finding is significant because it indicates that simple measurements of volumetric strains from a triaxial test could provide valuable feedback on the degree of consolidation that has occurred during shearing, and could be used as a basis for predicting the relative mobilization of shear strength for the partially drained tests relative to the drained and undrained strengths through the strength improvement index.
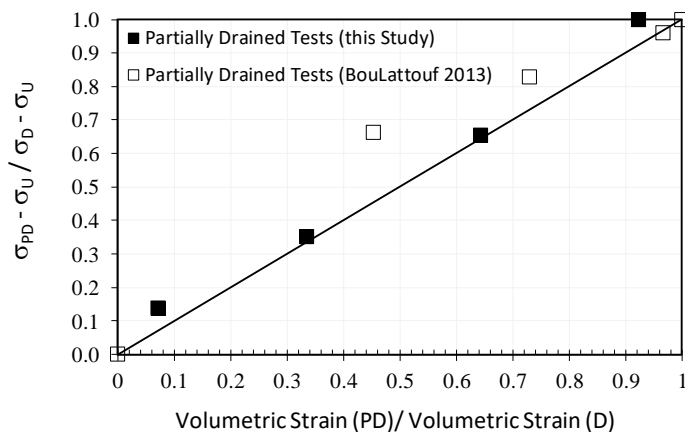
Figure 44: Variation of strength improvement factor with volumetric improvement index

4.4 Finite Difference Analysis

4.4.1 Modeling and Assumptions

In this section, a finite difference analysis is conducted to study the localized progression of consolidation and pore pressure dissipation with axial strains for different shearing rates. The realistic estimation of the degree of consolidation requires a coupled radial and vertical consolidation solution, necessitating the calculation of generated and dissipated pore pressures. For the large-scale triaxial tests conducted in this study, vertical drainage is expected to be negligible given that the length of the sample (290 mm) is significantly larger than the longest radial drainage path (~37 mm) from the furthest clay particle to the nearest sand column (Figure 45a). As a result, the finite difference solution that is adopted involves radial drainage only.

To simplify the problem further, the solution used reduces the 3-dimensional specimen that includes the group of columns to a unit cell that includes a central sand column acting as a drain for the surrounding clay matrix (Figure 45b). The equivalent diameter of the assumed unit cell was selected to be 72.5 mm to yield an area replacement ratio $a_r = 17.8\%$ assuming a sand column with a diameter of 30 mm. The assumed dimensions of the unit cell also ensure a representative area replacement ratio, compared to the area ratio that is typically calculated for the square/hexagonal sand column configuration ($d_e = 1.15s$) that was used in the large-scale triaxial specimens.
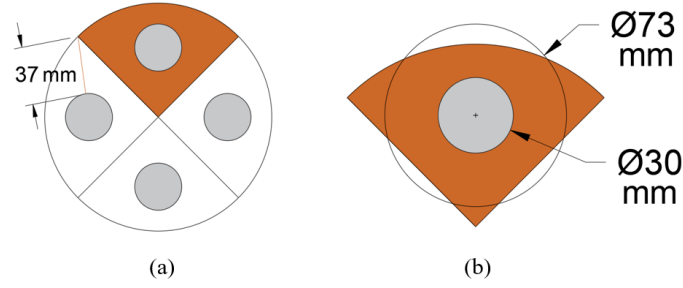
Figure 45: Modeling of (a) sample reinforced with group sand columns as (b) unit cell with equivalent diameter

The explicit finite difference solution to the radial pore water pressure dissipation problem is presented in Equation 4. The unit cell is defined as a matrix of nodes that are spaced at a radial distance Δr of 1 mm and the solution targets a time increment Δt of 5 seconds. The predicted pore water pressure $u_{k,j+1}$ at a radial distance k and at time j +1 is calculated in the finite difference solution such that:

$$u_{k,j+1} = u_{k-1,j}\alpha\left(1 - \frac{\Delta r}{2r_k}\right) + u_{k,j}(1 - 2\alpha) + u_{k+1,j}\alpha\left(1 + \frac{\Delta r}{2r_k}\right) \tag{4}$$

Where:

- $\alpha = \frac{c_R * \Delta t}{\Delta r^2}$

- c_R: horizontal coefficient of consolidation

- r_k: radial distance to node k from the sand column

- $u_{k,j+1}$ is the pore pressure at a radial distance *(k)* and a time *(j+1)*

- $u_{k-1,j}$ is the pore pressure at depth *(k-1)* and a time *(j)*

- $u_{k,j}$ is the pore pressure at depth *(k)* and a time *(j)*

- $u_{k+1,j}$ is the pore pressure at depth *(k+1)* and a time *(j)*

The horizontal coefficient of consolidation, c_R is back-calculated using Equation 5 from the consolidation stage of the triaxial tests using a t_{50} value of 85 mins (see Table 7) as an average between the PD tests. Equation 4 (Olson 1985; Sridharan et al. 1996) assumes only radial drainage occurring from the clay matrix to the sand columns.

The radial coefficient of consolidation is affected by the radius of the sand column (r_w)

the radius of the specimen (r_e) and the ratio between the two such that:

$$c_R = \frac{d_e^2 * F(n) * \ln\left(\frac{1}{1 - U_h}\right)}{8 * t_{50}} \tag{5}$$

Where (de) is the equivalent diameter of the unit cell (72.5 mm), $F(n)$ is a

factor that is determined in Equation 6 as a function of the ratio of the equivalent

diameter of the unit cell and the sand column diameter, and U_h is the degree of

consolidation (50% when t_{50} is used).

$$F(n) = \left[\left(\frac{n^2}{n^2 - 1}\right) * \ln(n)\right] - \frac{3n^2 - 1}{4n^2} \tag{6}$$

$$n = \frac{r_e}{r_s} \tag{7}$$

The back-calculated coefficient of consolidation was 0.032 mm/sec^2, yielding an

$\alpha = 0.16$ assuming a Δt of 5 seconds and a radial distance increments Δr of 1 mm.

The use of Equations 4 to 7 allows for estimating the degree of consolidation

that a partially drained sample undergoes at any time with particular emphasis given

to the time at which failure occurs. The finite difference solution yields values of pore

water pressure during shearing in the clay surrounding the sand column at different

times $(t + \Delta t)$ or $(j + \Delta j)$, and at different radial distances $(r + \Delta r)$ or $(k + \Delta k)$ for

a grid composed of 22 radially-spaced nodes. The generation of the initial pore water

pressure was calculated from the measured contact stresses in the clay multiplied by

Skempton's pore pressure coefficient, A. Figure 46 shows the variation of Skempton's

pore pressure coefficient A with axial strain based on the CU test of the control clay.

The predicted pore pressure in the clay was then input into the finite difference

solution to predict the pore pressure dissipation with time. The average degree of

consolidation at different times and strain levels was then computed by subtracting the

excess pore pressures that remain in the clay from the total excess pore pressures that

were generated up to that time.
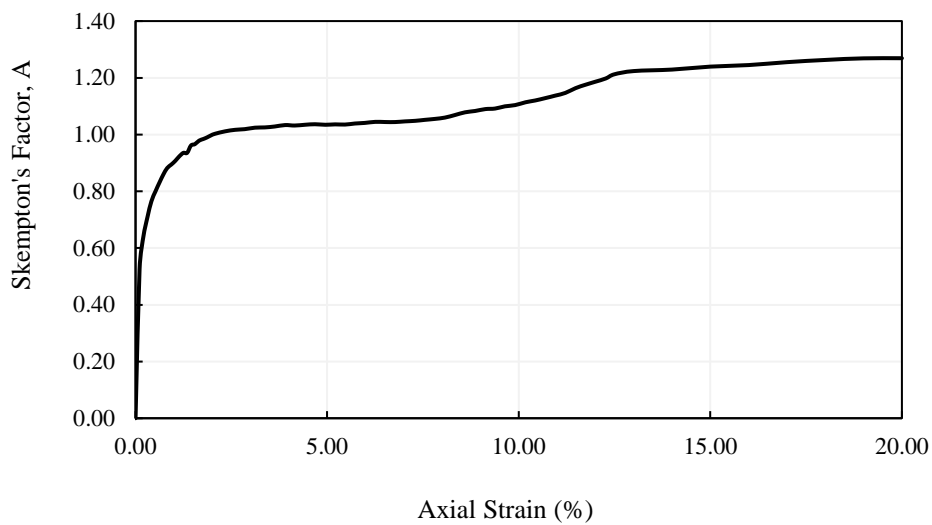
Figure 46: Variation of Skempton's pore pressure parameter A with axial strain

4.4.2 Finite Difference Results

The finite different solution for the radial distribution of excess pore water

pressure in the clay matrix at different strain levels is presented in Figure 47 for the four

partially drained tests. Each curve in Figs. 47a,c,e,g represents the pore water pressure

at nodes spaced radially at 1-mm increments from the edge of the sand column. The

pore pressure results allow for a detailed investigation of the impact of the strain rate on

the extent of partial drainage during shear. The pore pressure data was also used to

calculate the spatial variation in the degree of consolidation in the clay matrix at

126

different radial distances from the central sand drain (Figs. 47b,d,f,h). In the absence of instrumentation that could measure the local distribution and dissipation of pore water pressure in the clay, the finite difference analysis presents a unique tool to achieve this objective.

For the fastest partially drained test (PD1), the pore pressure results on Figure 47a indicate that minimal pore pressure dissipation occurred in the clay matrix. The only exception is the clay that is in direct contact with the sand column (at radial distances of 1 to 5 mm), which showed some pore pressure dissipation given the short drainage path to the sand drain. The associated degree of consolidation for the clay in close proximity to the column was in the order of 10% to 50%. For radial distances that were larger than 5 mm, pore pressure dissipation was minimal, resulting in degrees of consolidation that were generally less than 10%.

The extent of pore pressure dissipation in the clay matrix clearly increased for the lower strain rates applied during shearing in tests PD2, PD3, and PD4. In test PD2, although the clay carried stresses that were similar to those carried in test PD1 (indicating similar initial pore pressure generation), results on Fig. 47c indicate lower magnitudes for the overall positive pore pressure values in the clay matrix, with pore pressures ranging from 20 kPa (close to the sand drain) to 40 kPa (at the outer boundary). These pore pressure values are much smaller than those observed in PD1 (40 kPa close to columns and 70 kPa at the outer boundary). Reductions in pore pressure were associated with higher degrees of consolidation ranging from 30% to 60% in the inner 5-mm clay zone surrounding the column. For clay in the outer zone (5mm to 22mm), the degree of consolidation ranged from 30% to around 10%.
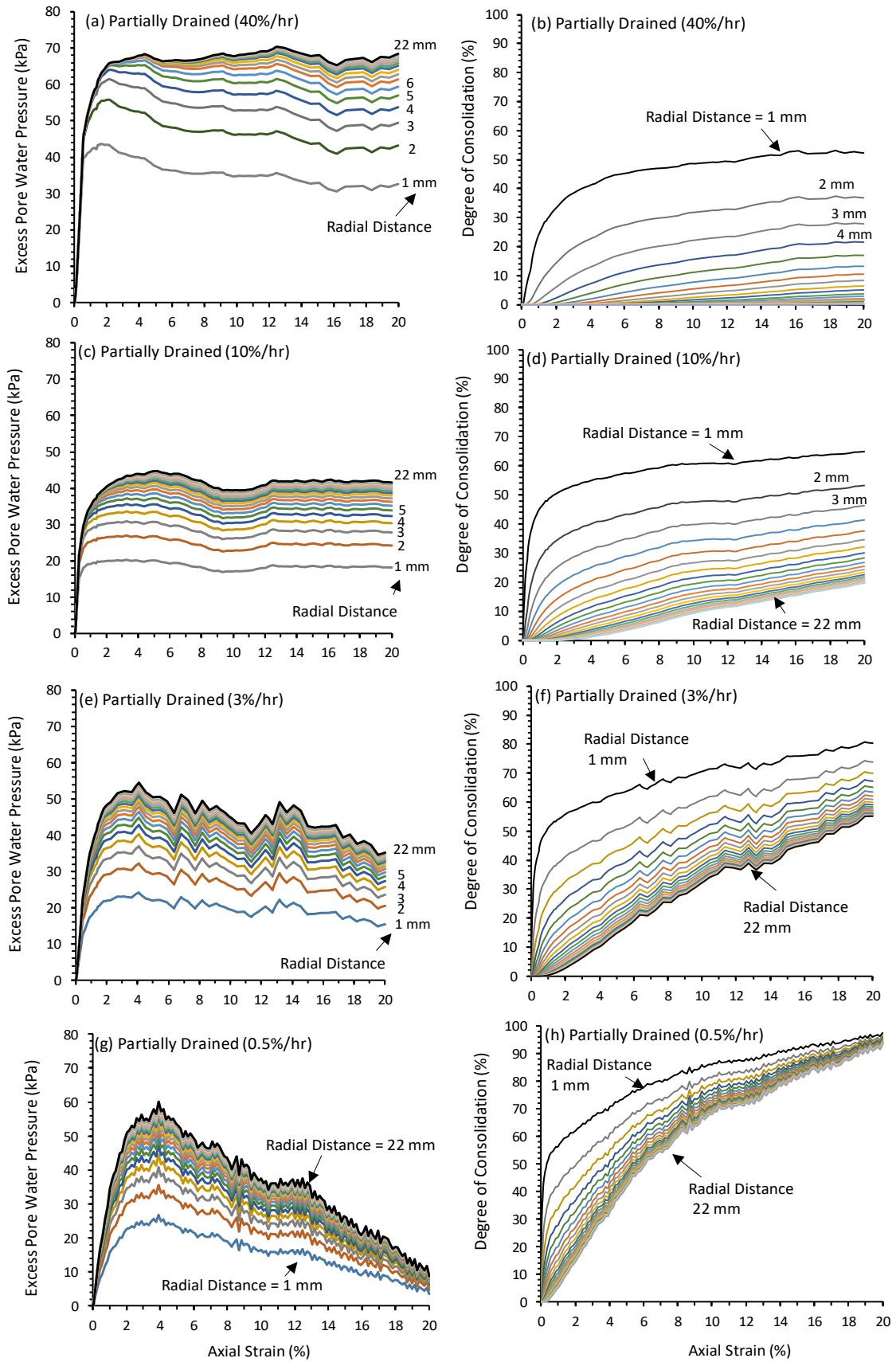
Figure 47: Finite difference solution for pore water pressure and degree of consolidation

In tests PD3 and PD4, the lower applied strain rate allowed for additional pore pressure dissipation that was clearly visible in Figs. 47e and 47g. At these relatively slow rates, a gradual drop in the pore pressure dissipation with axial strain could be observed at any given radial location in the clay matrix. Such a drop was not observed in PD1 and PD2 where the pore pressures at any given point remained relatively constant with axial strain. The reduction in the pore pressure with strain was clearly visible in the case of PD4, with almost complete dissipation of pore pressure occurring at the large axial strains at all radial distances in the clay matrix, indicating a response that is approaching the fully drained response. An investigation of the data showing the degree of consolidation (U) in the clay matrix for tests PD3 (Fig. 47f) and PD4 (Fig. 47h) indicates large degrees of consolidation (between 50% to 80% for PD3 and 90% to 95% for PD4 at large strains) in the clay matrix. For axial strains at which failure occurred (8% to 12%), the degrees of consolidation were about 35% to 70% for PD3 and 70% to 85% for PD4.

To quantify the difference in the overall degree of consolidation in the different test specimens due to differences in the degree of partial drainage, a global degree of consolidation was calculated at every time increment (strain level) by integrating the local degrees of consolidation (through the dissipated pore water pressure) across all the radial distances in the clay matrix. The variation of the global degree of consolidation with strain for the four partially drained test specimens is presented in Figure 48. Moreover, the global degrees of consolidation ($U_{f,avg}$) at the onset of failure (strains between 8% and 12%) are shown in Table 8 for all test specimens, together with the stress improvement index and volumetric improvement index that were determined from the triaxial tests.

The curves on Fig. 48 portray the effectiveness of the finite difference method in quantifying the variation of the degree of consolidation (U_{avg}) with strain as a result of radial dissipation of pore water pressure from the clay matrix to the sand column. Results clearly show that U_{avg} varies with the level of axial strain and is a function of the applied strain rate during shearing. U_{avg} increases with the magnitude of the axial strain since more time is being allowed for the pore pressures generated at small strains to dissipate. This is because excess pore pressure are directly related to the "change" in the deviatoric stress during shearing, which is generally significant at small strains and reduces at larger strains. This explains the significant increase in U_{avg} with axial strain for the relatively slower tests PD3 and PD4, in which enough time is allowed for excess pore pressures to drain at larger strains.

Results on Figure 48 show that the global degree of consolidation for PD1 is almost negligible (less than 10%), irrespective of the applied strain level. This indicates that drainage conditions in PD1 approached the drainage conditions in the fully undrained test. For test PD2, results show U_{avg} values of about 20% and 30%, at axial strains of 10% (around failure) and 20% (at the completion of test.). The associated global U_{avg} values increased to 40 to 60% for test PD3 and 75 to 92% for test PD4, indicating that the drainage conditions in test PD4 approached the fully drained conditions at large strains.
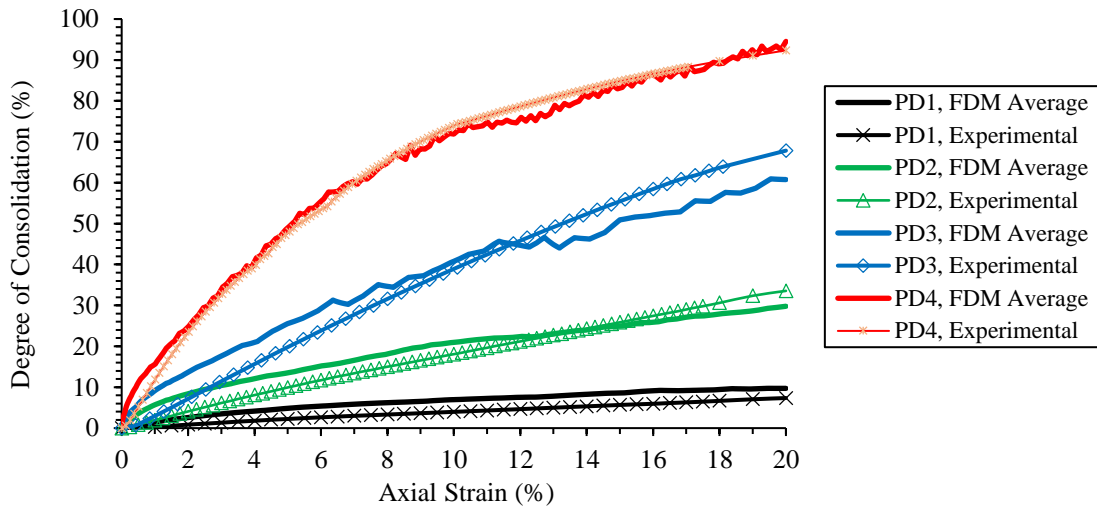
Figure 48: Comparison between the measured volumetric improvement index ($\varepsilon_{v(PD)}/\varepsilon_{v(D)}$) and the numerically computed global degree of consolidation (U_{avg}).

The finite difference results allow for testing the correlation between the global degree of consolidation (U_{avg}) and the strength improvement factor (α). In addition, the calculated global degree of consolidation (U_{avg}) could be used to check whether the volumetric improvement index ($\varepsilon_{v(PD)}/\varepsilon_{v(D)}$) from the triaxial tests of the partially drained tests could be used as a representative estimate of the global degree of consolidation. To test the latter hypothesis, the volumetric improvement indices ($\varepsilon_{v(PD)}/\varepsilon_{v(D)}$) for the four partially drained tests were plotted on the same figure with the calculated (U_{avg}) for comparison (Figure 48). Results show a remarkable overlap between the two parameters at all levels of strain, despite the fact that (U_{avg}) was calculated numerically while ($\varepsilon_{v(PD)}/\varepsilon_{v(D)}$) was measured in the triaxial tests.

Table 8: Finite difference average degree of consolidation with the volumetric and stress improvement indices

Test #	Test Type	FDM Average Degree of Consolidation	Volumetric Improvement Index $\varepsilon_{v(PD)}/\varepsilon_{v(D)}$	Stress Improvement Index α
1	CU	-	-	-
2	PD1	0.094	0.072	0.139
3	PD2	0.280	0.335	0.350
4	PD3	0.595	0.643	0.655
5	PD4	0.945	0.923	1.012
6	CD	-	-	-

The potential correlation between the numerically derived global degree of consolidation (U_{avg}) and the strength improvement factor (α) is tested in Figure 49 for the four partially drained tests. The data shows that strong correlation exists between the two parameters, indicating that simple finite difference analyses could be used to predict the maximum deviatoric stresses for soft clays that are reinforced with sand columns under partially drained conditions, provided that the strengths from fully drained and fully undrained tests are available. This would eliminate the need for conducting relatively complicated triaxial tests with complex drainage conditions that are needed to physically model partial drainage.
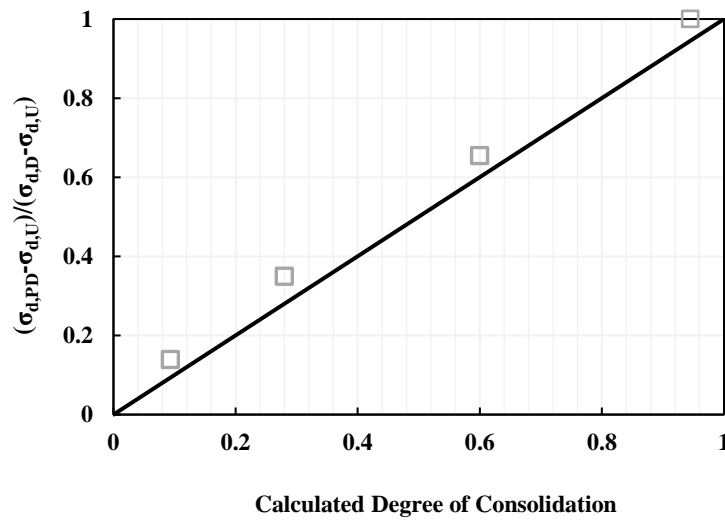
Figure 49: Correlation between the strength improvement index and the calculated degree of consolidation

4.5 Conclusions

This paper studies the effect of radial drainage on the consolidation of soft clays reinforced with vertical sand drains through both an experimental program and a numerical analysis. This was achieved through a series of large triaxial tests on normally consolidated soft clays reinforced with a sand columns group in square configuration using a well-instrumented large triaxial setup. Six tests (fully drained, fully undrained and four partially drained tests) were conducted to quantify the effect of partial drainage on the strength of the composite. The partially drained tests had different loading rates and were allowed to drain only from the top to ensure predominant radial flow from the clay matrix to the sand columns.

Results indicated that the partially drained tests were bracketed between the fully drained and the fully undrained tests that served as upper and lower bounds for the strength of the composite, respectively. Moreover, volumetric strains during shearing

133

showed progressive consolidation with decreased strain rate. Stress concentration ratio results for partially drained tests showed response also bounded between the drained and undrained scenarios, with an average stress factor in between 2.0 and 5.0.

The results also included graphical representation of the normalized improvement index with the ratio of $t_{failure}/t_{50}$. The results showed that a ratio of $t_{failure}/t_{50}$ of 15 seems to be a practical ratio at which the drained strength is mobilized in partially drained tests. Variation of the strength improvement index with the volumetric improvement index correlated well, meaning that one can predict the strength improvement of a partially drained test in a triaxial testing setup based on the ratio of the volumetric strain of the PD tests to the volumetric strain in the fully drained test. This was also verified with a finite difference analysis which showed a similar trend for the calculated degree of consolidation with volumetric improvement index. These findings are expected to serve as a baseline for expanded future research in the field of soil improvement of soft clay using granular columns under partially drained conditions that mimic the real world applications.

CHAPTER 5

THE EFFECT OF SAND COLUMN CONFIGURATION ON THE RESPONSE OF REINFORCED SOFT CLAYS

5.1 Introduction

Ground improvement of soft clays using granular columns has been the subject of numerous studies since the early 1970's. Previous work aimed at studying the factors affecting the field response of the clay/granular column system as a cost-effective ground improvement alternative that could replace deep foundations in some geotechnical applications. Granular columns improve the mechanical properties of soft clays by facilitating radial drainage, increasing stiffness, and improving the bearing capacity of the composite subsurface. When granular columns are intended as radial drains (ex. sand drains), designers typically neglect the resulting potential increase in stiffness and strength (Najjar et al. 2010).

The behavior of soft clays reinforced with granular columns is affected by several factors that include: (1) soil materials and properties, (2) the area replacement ratio (Charles and Watts 1983; Cimentada et al. 2011), (3) the column penetration depth (McKelvey et al. 2004; Fattah et al. 2011), (4) the density of the column (McCabe and Killeen 2017), (5) the column type (Kumar and Samanta 2020), (6) use of encasement (Murugesan and Rajagopal 2020; Miranda et al. 2017), and (7) column configuration/arrangement (Black et al. 2007; Aslani et al. 2018). Among the above factors, the effect of the column arrangement on the response of the composite has been insufficiently studied, particularly under triaxial loading conditions. Recent studies have

shown that laboratory triaxial testing of reinforced clays provide a representative and less costly experimental research alternative when compared to full scale field tests (Najjar et al. 2010; Najjar 2013; Almikati et al. 2020). These testing conditions allow for the control of: (1) drainage during testing (drained versus undrained) and (2) confining stresses that could be selected to be in the same order of magnitude as those expected in the field.

The limited previous work that aimed at studying the effect of stone column configuration on the consolidation rate, bearing capacity and load-sharing mechanism between the granular column and the surrounding clay was mainly based on studying the effectiveness of the unit cell concept in representing column groups. Black et al. (2007) conducted triaxial experiments with single and triangular configurations at the same area replacement ratio. Their results showed that the clay specimens that were reinforced with the single column configuration exhibited a stiffer response compared to specimens that were reinforced with the triangular arrangement. Aslani et al. (2018) conducted large direct shear tests to study the effect of single, triangular and square configurations on the peak shear strength of the composite, while measuring contact stresses using load cells. Results indicated that the stress concentration factors in the sand columns ranged from 1.5 to 5, with the square configuration having the highest stress concentration ratio among the different configurations.

Understanding the load sharing mechanism between the granular columns and the surrounding soft clay has recently become a major objective in research studies (ex. Aslani et al. 2018). The measurement of contact stresses both above the granular columns and the surrounding clay provides insight into the behavior of the clay-granular column hybrid system. Continuous measurement of the contact stresses allows for

investigating the buildup of stress concentration in the granular columns, which could yield effective and efficient designs of column-reinforced clay systems in the field. Advancements that were reported in the literature with specific reference to this issue (Bachus and Barksdale 1984, Black et al. 2006, Nazariafshar et al. 2017, and Almikati et al. 2020) are still in their early/preliminary stages. There is a clear and pressing need for additional studies that are aimed at measuring stress concentration factors within triaxial settings for soft clays that are reinforced with column groups of different configurations and under different drainage conditions.

The objective of this paper is to study the behavior in a triaxial testing setup of large-diameter (145 mm) soft clay specimen that are reinforced with sand columns with different arrangements but with the same area replacement ratio of 17%. Three drained tests were performed with single, triangular and square configurations corresponding to a central 60-mm diameter column, three 35-mm diameter columns with a triangular configuration, and four 30-mm diameter columns with a square configuration, respectively. The upper cap of the triaxial setup was equipped with three miniature pressure sensors to measure contact stresses above the sand columns and the clay annulus. The results included the effect of the different arrangements on (1) the consolidation time and rate, (2) stiffness response related to settlement and (3) contact stresses of the columns and the clay leading to information about the mobilization of the stress concentration factors with axial strain. The tests were restricted to fully drained conditions to highlight the effect of the column configuration on the long-term stability of foundations/embankments that are supported on soft clays reinforced with sand column groups.

5.2 Testing setup and Column configuration

The large triaxial setup used in the testing program is capable of testing specimens that are 150 mm in diameter and 300 mm in length [Figure 50(a)]. A modified upper cap was designed to include housings for miniature pressure sensors with a maximum capacity of approx. 1 MPa. These sensors were installed within/flush with the cap and at a distance of 44 mm away from the center [Figure 50(b)]. This allowed for contact stresses to be measured directly above sand columns and above the surrounding clay for the different column arrangements. Data was collected from three miniature pressure sensors, three pore water pressure sensors, a volume change device, a displacement LVDT, and a load cell through a data acquisition box [Figure 50(c)]. More details about the setup and instrumentation can be found in Almikati et al. (2020).

| (a) | (b) | (c) |
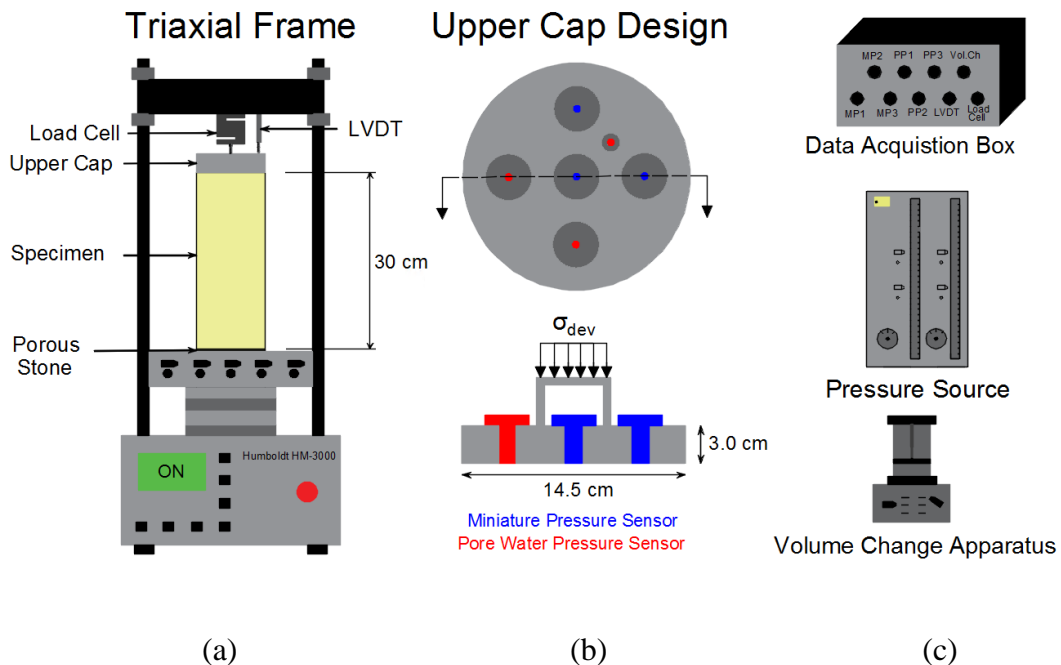
Figure 50: Testing setup consisting of (a) triaxial machine, (b) upper cap design with miniature pressure sensors and water sources in addition to (c) data acquisition box, pressure source for water and volume change device

The three column configurations that were adopted in the experimental program are shown in Figure 51. The alignment of the miniature pressure sensors (red circles) was selected so that the sensors are either above the center of a sand column, or above the surrounding clay. This allowed for actual and reliable measurements of the respective contact stresses from which stress concentration factors were calculated for all tests.
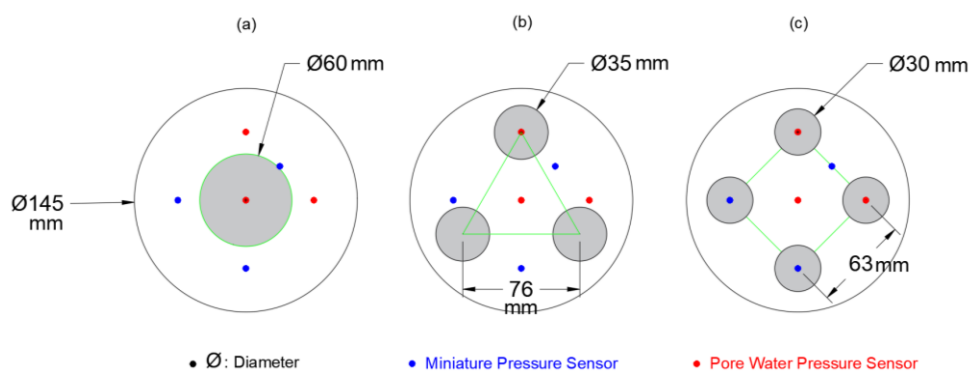
Figure 51: Column configuration for the three performed triaxial tests as (1) single central column, (b) triangular, three columns and (c) square, four columns

5.3 Sample Preparation and Materials Used

Kaolin clay was used as the matrix material in the testing program. The clay powder was mixed with water at a water content of 130% (~twice its liquid limit) using a high rotational speed large mixer. The slurry was then placed in prefabricated 145 mm diameter stiff PVC pipes that were sealed in a one-dimensional large odometer setup. The consolidation stress was applied incrementally through a number of dead weights that were added based on a predetermined loading schedule. The slurry was thus

consolidated from an initial thickness of 500 mm to a final thickness of around 315 mm

at the target applied normal stress of ~100kPa. The 1D-consolidated samples were then

removed from the PVC pipes and trimmed to a final length of 300 mm, placed in the

triaxial chamber and isotropically consolidated in the triaxial machine at a confining

stress of 100 kPa to ensure the elimination of any stress history the sample has

experienced before, during and after sand column placement (Black et al. 2007).

To construct the sand columns, Ottawa sand was used at a relative density of

85%. The sand columns were prepared using the freezing method, which showed

repeatability and consistency in previous studies (Sivakumar et al. 2004; Black et al.

2007 and Najjar et al. 2010, Almikati et al. 2020). Split molds for sand column

preparation were 3-D printed to insure a perfectly circular column cross-section. The

molds were sealed tightly to allow sand filling using multiple layers achieving a target

density of $17.05 \ kN/m^3 \pm 0.10 \ kN/m^3$. The internal diameters of the molds used to

prepare the sand columns were 30, 35 or 60 mm. The drilling method was used to create

vertical, fully penetrating holes of different diameters through the clay sample,

depending on the target test configuration. A custom-designed auguring system was

fabricated for this purpose. The manual augers allowed for a total penetration depth of

300 mm inside the clay specimen. The auger bits were manufactured using the HAAS

Automation CNC machine, with respective diameters of 30.5, 35.5 and 60.5 mm,

allowing for a minimal space for a snug-fit column insertion. Figure 52 shows the

different configurations of the reinforced specimens with sand column installed prior to

the triaxial testing.
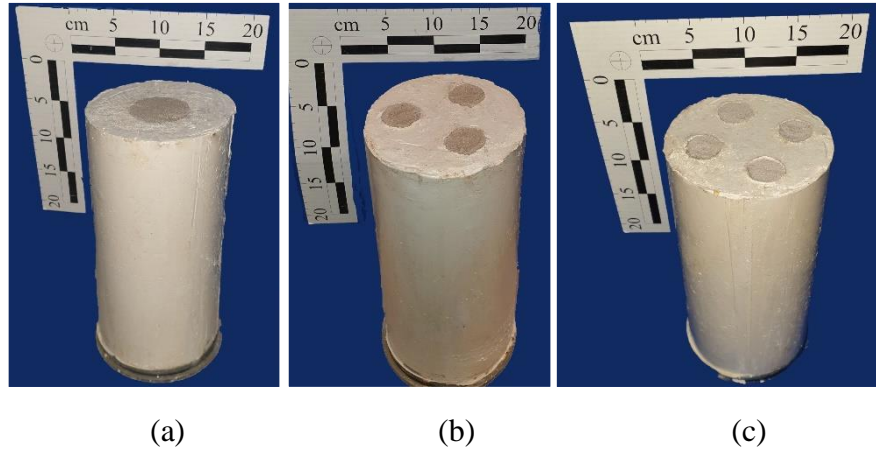
Figure 52: Reinforced kaolin samples with (a) single, (b) triangular and (c) square column configuration at an area replacement ratio of 17%

The Kaolin clay used has a liquid limit of 65%, a plasticity index 26%, and a specific gravity of 2.56. Results from one dimensional consolidation tests yielded recompression (C_r), compression (C_c) and swelling (C_s) indices of 0.19, 0.50 and 0.17, respectively. The pre-consolidation pressure was around 85 kPa, according to the method proposed by Casagrande (1936). The preconsolidation pressure is slightly lower than the target 100 kPa pressure that was applied to the slurry due to inevitable side friction between the slurry and the PVC tubes used in the sample preparation. The Ottawa sand is classified as a poorly graded sand according to the Unified Soil Classification System, USCS. More details about the physical and mechanical properties of the sand can be found in Najjar et al. (2010). Results from the consolidated drained triaxial tests that were conducted on the clay and the sand indicated internal friction angles of $\varphi' = 22°$ for the kaolin clay and $\varphi' = 39°$ for the Ottawa sand, respectively. The drained shear strength parameters were obtained from triaxial tests that were conducted at confining pressures of 100, 150 and 200 kPa.

It should be noted that both unreinforced and reinforced clay specimens were back-pressure saturated using a back pressure of 300 kPa and a cell pressure of 400 kPa, maintaining an effective confinement pressure of 100 kPa during the consolidation and shearing stages. Pore water pressures were monitored at the top and base of the samples during shearing to ensure fully drained conditions, with slow shearing rates that were determined as per the ASTM standards. Results from the pore pressure sensors indicated zero excess pore water pressures during the shearing stage of all tests, thus confirming fully drained conditions.

5.4 Results and Analysis

In this section, the results obtained from the three triaxial tests are presented and analyzed. For all reinforced specimens, the same area replacement ratio of 17% was adopted to highlight/isolate the effect of the column configuration on the results. The single column configuration had one central column of 60 mm diameter, with a spacing from the edge of the column to the sample edge of 42.5 mm. As for the triangular and square configurations, the columns had a center-to-center spacing of 76.2 mm and 62.5 mm, respectively.

5.4.1 Consolidation Phase

Consolidation curves for the three reinforced specimens are presented in Figure 53. All samples were consolidated at a 100 kPa effective confinement pressure. Results on Figure 53 yield two main observations. First, the volumetric strains that were measured at the end of primary consolidation were relatively similar in the three tests

(range of 5.5-6.2%). This is expected given that all specimens were reinforced at the same area replacement ratio, same sample preparation procedure, and same column densities. We can thus conclude that given the same replacement ratio, the ultimate degree of consolidation is neither affected by the number of columns nor the column configurations.

The second observation from Figure 53 relates to the measured rate of consolidation in the different specimens. Results indicate that the clay specimen that was reinforced with the triangular configuration exhibited a faster consolidation rate while the sample that was reinforced with the single column configuration exhibited the slowest consolidation rate. These observations are related to the respective radial drainage paths from the clay into the sand columns that governed the consolidation stage of the test. The observed consolidation rates correlated well with the maximum radial distances between the clay and the sand column edges. These maximum radial drainage lengths/paths were 27.0, 31.0 and 42.5 mm for the triangular, square and single column arrangements, respectively.
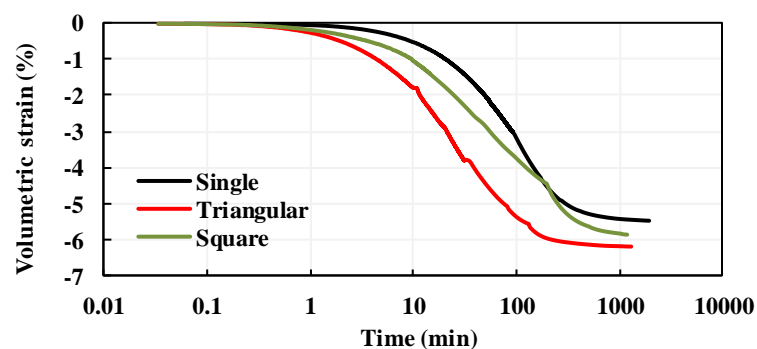
Figure 53: Consolidation graphs for the three performed tests

5.4.2 Stress-Strain Phase

Figure 54 shows the variation of the deviatoric stress and volumetric strain with axial strain during drained shear for the three reinforced clay specimens. The effect of the column configuration on the initial stiffness is clearly seen in the initial portions of the stress-strain curves. The sample with a central single column of 60 mm diameter had a stiffer response than the other two samples, while the sample with the triangular column configuration showed a stiffer response than that with the square configuration. A secant modulus of elasticity was calculated for the three tests at an axial strain of 1%, indicating values of $E_{1\%Single} = 9,900$ kPa, $E_{1\%Triangular} = 7,720$ kPa and $E_{1\%Square} = 5,870$ kPa.

This shows that although all three specimens had the same area replacement ratio, the drained stiffness at low axial strains which plays a key role in the serviceability-based design of the clay-sand column system, is highly dependent on the column configuration. Differences in the initial stiffness for specimens with different column configurations could be attributed to multiple factors, including (1) possible differences/variations in the confinement levels (radial stresses) that are provided by the surrounding clay to the sand columns and their dependency on the column configuration, and (2) differences in the slenderness ratio of the columns in the different configurations, whereby the central sand column exhibited a larger diameter to length ratio compared to the smaller diameter triangular and square column configurations. Sand columns with a larger diameter to length ratio could have a lower tendency for buckling/bulging leading to a stiffer stress-strain response (Wood et al. 2000; McKelvey et al. 2004). The results are in line with the work of Black et al. (2011) who stated that

columns with small diameter at the same area replacement ratio tend to be less effective than those with larger diameters.

At larger axial strains (around 10%), the stress-strain curves on Figure 54 indicate that the response of the reinforced clay specimens converge to an approximate deviatoric stress of about 128 kPa, irrespective of the column configuration. The peak deviatoric stresses on the other hand slightly differed (ranged between 130 and 135 kPa) and were mobilized at different axial strains depending on the column configuration. The specimen that was reinforced with the large diameter central sand column exhibited the largest peak deviatoric stress (135 kPa) at the smallest axial strain (~5%). The peak deviatoric stresses for the triangular and square column arrangements were relatively similar with the peak being mobilized at around 7% axial strain in the triangular arrangement and about 11% axial strain in the square arrangement. The variations of the volumetric strain with the axial strain are also shown on Figure 54 for the three column configurations. Results indicate that the volumetric tendency during shearing was compressive with all specimens contracting to a final volumetric strain of $\varepsilon_{v,final} \sim \cong$ 4.0%. These results indicate that for the area replacement ratio of 17%, the column configuration has minimal to no effect on the volumetric strain during shearing.
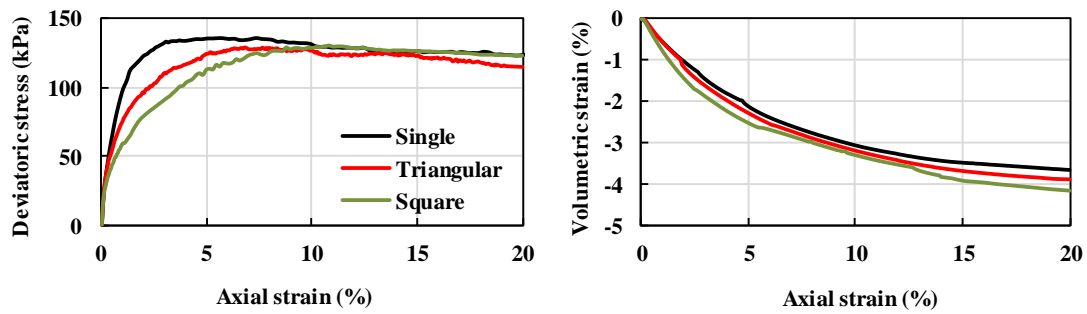
Figure 54: Variation of deviatoric stress and volumetric strain with axial strain for the three tests

The variation of the contact stresses that were measured using the miniature pressure sensors with axial strain is plotted on Figure 55 for the three column configurations. Also plotted on Figure 55 is the stress-strain curve of the control sand specimen. The stress-strain curve for the "sand" corresponds to a consolidated drained triaxial test performed on a sand sample with the same relative density to serve as a reference for strength mobilization when analyzing the results.

The measured contact stresses on the sand columns indicated a slightly higher strength and stiffness for the single central column as compared to the other configurations, an observation that is in line with the stress-strain graphs of the reinforced specimens shown in Figure 54. All columns reached the peak mobilized strength at axial strains between 4% and 8%, and continued to soften at higher axial strains. As for the reference sand graph, it should theoretically serve as an upper bound for the mobilized/measured contact sand stresses in the tests, and this is true for the triangular and square configurations. The contact stresses for the case of the central single large column followed closely the "sand" curve and slightly exceeded it at some strains. This response could be attributed to testing uncertainty and natural variability in

146

the testing protocol, sample preparation, placement of the pressure sensors, among others.
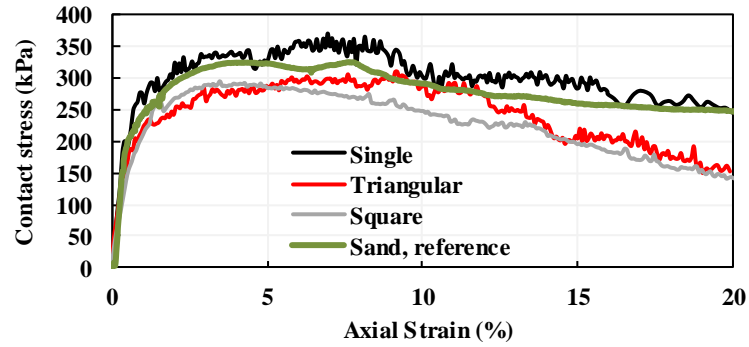
Figure 55: Contact sand stress for the different configurations and for the reference sand triaxial test at 100 kPa

5.4.3 Stress Concentration Ratio

The stress concentration ratio, a_r, defined as the ratio of the stress loading the sand column to that loading the clay matrix, was calculated from the contact stresses measured above the sand columns and the annulus clay, respectively. Figure 56 shows the mobilization of the stress concentration factor with axial strain for all three tests. It is interesting to see that the column configuration clearly played a role in determining the variation of the stress concentration factor with axial strain. It is clear that the stress concentration factor was higher in the case of the central sand column, followed by the triangular configuration and the square configuration.
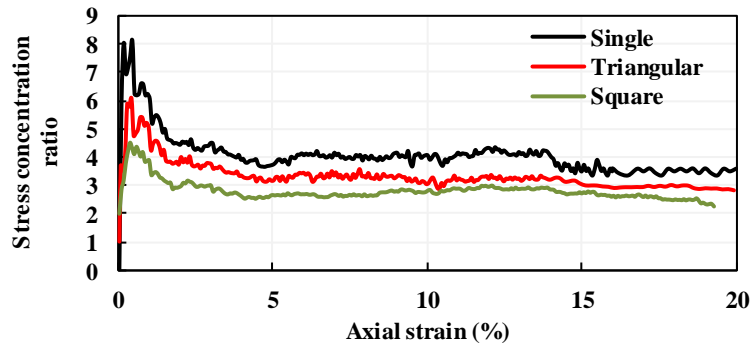
Figure 56: Stress concentration ratio for the single, triangular and square configurations from the measured stresses

All three curves reached a peak at early stages of the shearing phase, which is due to the softening/dilation of the sand columns and the hardening (compression) of the surrounding normally consolidated clay during shearing. The peak values of the stress concentration ratio were 8.1, 6.0 and 4.4 for the single, triangular and square configurations, respectively. The residual stress concentration ratios at large strains were between 2.3 and 3.6. The stress concentration factors at peak are partly in line with previous studies which reported values between 4.0 and 6.0 for similar area replacement ratios. This includes the work of Bachus and Barksdale (1984), Fattah et al. (2011) and Ghazavi and Afshar (2013). In recent studies, Black et al. (2006) performed triaxial tests and reported only residual stress concentration factors of 1.86 in drained tests.

The variations of the stress concentration factors with axial strain as observed from Figure 56 point to the importance of associating the stress concentration factors with a given level of axial strains. For example, for settlement calculations that involve relatively small strains, the stress concentration factors seem to be relatively large and dependent on the column configuration. At larger strains which may be more relevant to ultimate limit state and bearing capacity calculations, the stress concentration factors are

148

still affected by the column configuration but are reduced significantly compared to the peaks, with measured values that are more in line with values reported for stress concentration factors in the published literature.

5.5 Conclusions

This paper presented the results of drained triaxial tests performed on soft normally consolidated large diameter kaolin specimen that were reinforced with sand columns with different column arrangements at an area replacement ratio of 17%. Dense sand columns with diameters ranging from 30 (four columns), 35 (three columns) and 60 mm (single column) were used corresponding to columnar configurations of square, triangular and single-central. A fabricated upper cap with miniature pressure sensors allowed for the measurement of contact stresses above to the sand column and the surrounding clay.

The response during isotropic consolidation indicated that the time needed for samples to reach the end of the primary consolidation is highly dependent on the column configuration and the radial drainage path between the clay and the sand columns. The stress-strain results exhibited a stiffer response for the specimen reinforced with the large diameter central sand column. The 1% secant modulus varied between $E_{1\%Single} = 9,900$ kPa, $E_{1\%Triangular} = 7,720$ kPa and $E_{1\%Square} = 5,870$ kPa. The peak deviatoric stresses for all three tests was around 130-135 kPa and was reached at different axial strains depending on the column configuration. At large strains, the three stress-strain curves converged to the same residual stress. Results from contact stress measurements also indicated that the specimen with a single central

column mobilized more stresses than the triangular configuration, with the square configuration mobilizing the least stresses, particularly at lower strains. These stresses were used to calculate the stress concentration ratios for the three reinforced experiments, which showed peak values of 8.1, 6.0 and 4.4 for the single, triangular and square configurations, respectively.

It is of great importance to identify the strain range that is relevant to practical design, given the significant variations that the stress concentration ratios which are key parameters in the design of reinforced soft clays. For serviceability limit state applications (low axial strains), the stress concentration factors under drained conditions are different from those under ultimate limit state, at failure (higher axial strain); and under each of the two applications, the stress concentration factor is also dependent on the choice of the columnar configuration.

5.6 Appendix: Undrained Response

This appendix presents results of undrained tests that were conducted on composite clay-sand specimens using an area replacement ratio, a_r, of 17.1%. The aim is to supplement the drained tests that focused on the effect of varying column configuration with tests that were conducted under undrained conditions.

This section serves as a complementary part to the paper showing the results for consolidation and shearing for three additional tests using single, triangular and square configurations. The results were compared in a similar fashion to the ones presented in the paper.

5.6.1 Consolidation Phase

Consolidation curves for the three reinforced specimens that were tested under undrained conditions are presented in Figure 57. Similar to the case of drained tests, all samples were consolidated at a 100 kPa effective confinement pressure. Results on Figure 57 showed that the volumetric strains that were measured at the end of primary consolidation were relatively similar in the three tests (range of 4.8-5.5%). Moreover, the single column configuration also showed the slowest response to reach the end of primary consolidation, which, as mentioned earlier, is related to the radial distances between the clay and the sand column edges that is highest for the single column configuration.
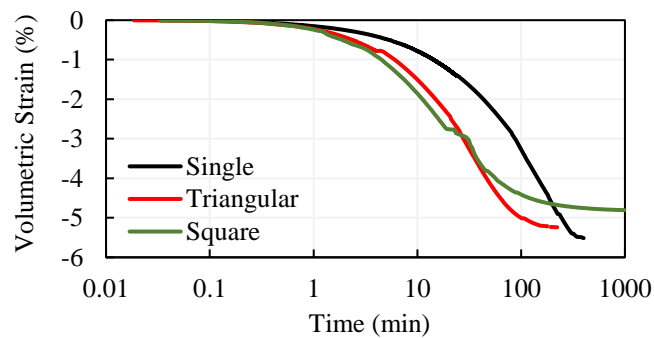
Figure 57: Consolidation graphs for the three different configurations

5.6.2 Stress-Strain Phase

The variation of deviatoric stress and excess pore water pressure with axial strain for the three undrained tests were plotted on Figure 58. Unlike their drained counterparts, the undrained tests show a more or less similar behavior that is not affected by column configuration, with the stress-strain curves of the square and single

151

column configurations plotting almost above each other. The deviatoric stress for the triangular configuration deviated slightly from the curves of the other two configurations at low axial strains. At an axial strain of 1%, the difference between the deviatoric stress for the triangular configuration (50 kPa) and the deviatoric stress of the single and square configurations (58 kPa) could be considered relatively minor.

The variation of the excess pore water pressure with axial strain indicated for the three column configurations showed similar trends with minor differences/variations with respect to the values measured at selected different axial strains. These minor differences in the generation of pore water pressure are expected given that the rate of shearing was selected based on ASTM standards to ensure the equalization of pore water pressure inside the samples.
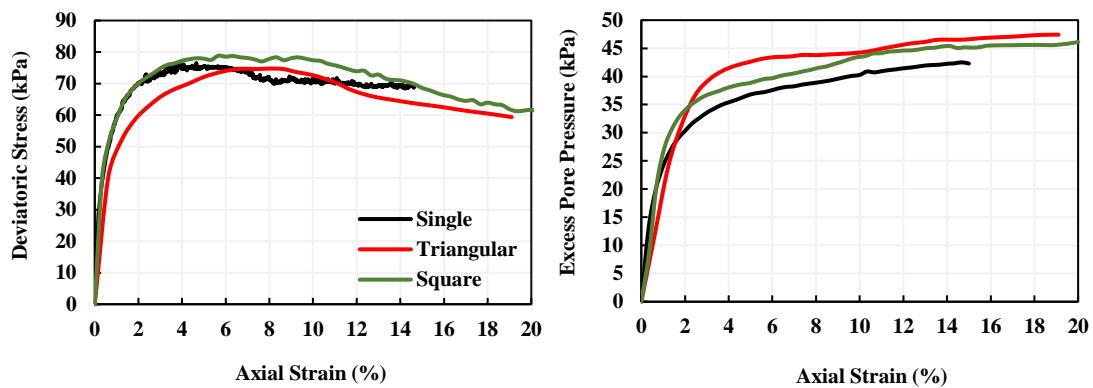
Figure 58: Variation of deviatoric stress and excess pore water pressure with axial strain for the three tests

5.6.3 Contact Stresses and Stress Concentration Ratio

Figure 59 shows the measured contact stresses above sand columns in all three tests. In addition, the curve representing the control sand specimen was included. The stress-strain curve for the "sand" corresponds to a consolidated undrained triaxial test

performed on a sand sample with the same relative density to serve as a reference for strength mobilization when analyzing the results.

The measured contact stresses indicate that up to 4% axial strain, almost all sand columns in the three different configurations mobilized similar stresses; however, after 4% axial strain, the contact stresses above sand columns for triangular and square configurations showed similar behavior, with the graph for the square configuration plotting above the other two graphs. The graph for single configuration exhibited the lowest stress concentration factors among the three configurations, with a mobilized contact stress of about 150 kPa for axial strains between 2% and 15%, when compared to the square and triangular configurations which showed contact stresses between 150 and 200 kPa.

The plotted "sand, reference" graph served as an indicator as to how high could mobilized stresses in a column reach if solely a sand column under similar conditions was sheared under undrained conditions. This undrained control sand specimen exhibited a maximum peak deviatoric stress of about 1800 kPa (not shown on Figure 59 so as not to distort the scale of the y-axis). Such high deviatoric stresses could not be mobilized in the sand columns due to the fact that the columns are surrounding by soft clay that is generating positive pore water pressure during undrained shearing. The large negative pore pressures that could be generated in a typical control sand specimen leading to extremely high deviatoric stresses in the control sand test were reduced to just around 150-200 kPa in all three configurations.
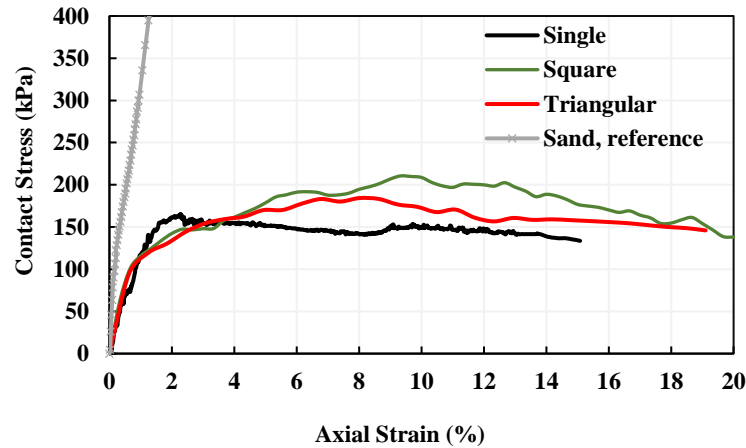
Figure 59: Contact sand stress for the different configurations and for the reference sand triaxial test at 100 kPa

The stress concentration ratio, n, was calculated from the contact stresses measured above the sand columns and the surrounding clay. Figure 60 shows the mobilization of the stress concentration factor with axial strain for all three tests. The three curves had a similar trend, increasing from around 2.0 to 3.0 at low axial strains, up to values between 4.0 and 5.0 when reaching high axial strains (above 15%). This shows that even when varying the column configuration under undrained conditions, the mobilized stresses above the columns were not higher for larger columns as in the case of the drained conditions, which showed clearly higher values of stress concentration factors for the single configuration, when compared to the triangular, which was in its turn higher than the square configuration.

The three curves in Figure 60 were consistent with regards to the trend followed. Between axial strains of 0% and 8%, all curves show an increase in the stress concentration ratio from around 2.0 to 4.0. At high axial strains, the stress concentration factor for all configurations continued to increase, with the square configuration deviating somehow above the other two curves reaching around 6.5 at axial strain of

154

13%, where the triangular and single configurations show values between 4.0 and 5.0, respectively.
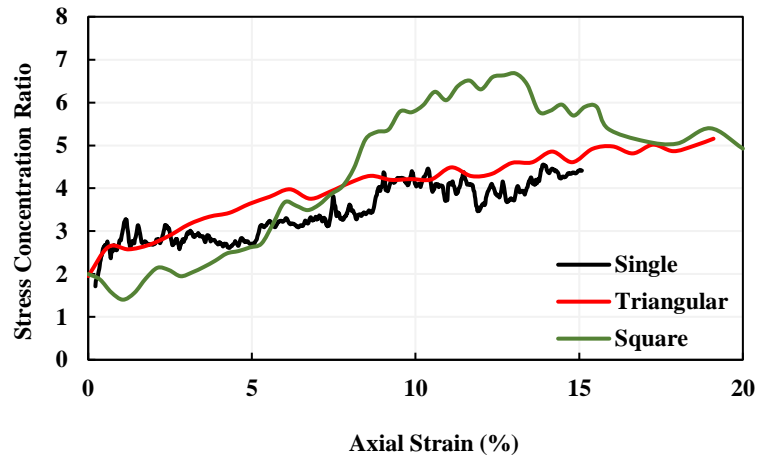
Figure 60: Stress concentration ratio for the single, triangular and square configurations from the measured stresses under undrained conditions

This shows that unlike the drained response, varying the column configuration for the same area replacement ratio under undrained conditions does not mean gaining additional stiffness/strength or reducing excess pore water pressures during shearing. It just indicates that during consolidation, and because of the drainage distance variation, there are benefits of reducing consolidation times obtained from closing the distances between granular columns, i.e. when using higher number of columns (smaller diameter).

CHAPTER 6

GEOTECHNICAL CHARACTERIZATION OF LAPONITE

6.1 Introduction

Transparent soils have been the subject of a number of geotechnical studies in recent years. Such materials are typically used to visualize variations in the internal structure of soils during loading as well as associated localized internal displacements. This is made possible by combining the transparency of these soils with the use of seeding particles and laser-based tracking tools and techniques.

Transparent soils have been produced by mixing granular fused quartz particles with specially sourced fluids that match their refractive index (RI), thereby decreasing the refraction of light within the medium (Iskander 2010). The level of transparency depends on the proportions of the solid particles and solution used.

Interest in, and efforts to, visualize, capture and/or measure internal deformations and/or changes in particle arrangements and structure or even fluid flow patterns within soil samples are not new. Early efforts included methods based on x-ray radiography (Bergfelt 1956; Robinsky and Morrison 1964; James and Bransby 1970), time-domain reflectometers (Orsi et al. 1992) and nuclear magnetic resonance (Ng et al. 1996). The concept of non-intrusive measurements of a transparent material behaving as a soil surrogate was first introduced by Wakabayashi (1950) by mixing glass beads with a liquid of the same RI. Similar studies were subsequently conducted using a similar approach but could only achieve similarly poor transparency (Chen and Wada 1986;

Brock and Orr 1991). Significant improvements and variations in materials and approaches have been proposed and tested since Iskander (2010). As of a few years ago transparent soil surrogates could be grouped into three categories: (1) amorphous silica powder behaving like clays (Iskander et al. 1994); (2) transparent silica gels behaving like sands (Ezzein and Bathurst 2011); and (3) Aquabeads used to model flow in a soil medium (Tabe 2015). Lately, a fourth group known as clay surrogates, such as Laponite RD, have emerged and have been used as a transparent synthetic clays (Wallace and Rutherford 2015).

When mixed with water, the Laponite white powder forms a transparent clay-like material. This material exhibits very low undrained shear strengths comparable to those of soft marine clays. Over the past five years a series of studies have reported on attempts to establish geotechnical properties of Laponite mixes (Wallace and Rutherford 2015), assess their transparency (Yi et al. 2018) and quantify their shear strengths using miniature ball penetrometer tests (Ads et al. 2020). Laponite was also used in physical laboratory-scale models of geotechnical systems using laser techniques and image processing to visualize failure surfaces upon after loading caisson foundations (Wallace and Rutherford 2017).

One of the characteristics of Laponite which was identified early on is that it exhibits a thixotropic behavior. Such behavior was defined by Mitchell (1960) as a time-dependent change in strength associated with a non-equilibrium state in inter-particle forces after mixing, remolding or compaction, and is common in highly sensitive clays. In the technical literature, thixotropy has been referred to as *aging*, *thixotropic hardening* and *structuration* (Mitchell 1960; Rodriguez and Santamarina 1999), and is a reversible, time-dependent strength gain. Mitchell and Soga (2005)

reported two sources of shear strength gain: A fixed remolded strength and a reversible aged strength. Laponite mixtures can respectively alternate between gel and liquid states when left to age or mixed. As such, both sources of shear strength gain may be anticipated. This particular aspect is discussed and addressed in detail in Pierozan et al. (2020), where the authors discuss the microstructural effects of the hydration and drying of Laponite mixtures.

One major practical limitation facing the use of Laponite is that mixtures cannot be prepared in high concentrations, partly because of the comparatively rapid gelation process. In order to address this issue, the use of additives was proposed during sample preparation to retard the time of gelation upon mixing the Laponite powder with water (Beemer et al. 2016). Sodium Pyrophosphate (SPP) has been used in recent studies in order to facilitate the preparation of Laponite mixtures at relatively high concentrations, producing mixtures of comparatively higher shear strength and stiffness. However, these studies only explored a limited number of mixtures, which does not allow an interested user to predict the geotechnical properties of mixes prepared at wider ranges of Laponite content, SPP dosage or aging time. An understanding of these effects is of great relevance because variables such as SPP dosage, which facilitates the preparation of mixtures at higher laponite content, may also result in a decreased thixotropic behavior. To date, our understanding and control of the impact of increasing SPP dosage on the geotechnical properties of Laponite remains limited.

This paper presents the results of a comprehensive geotechnical testing program designed and executed in an effort to establish relevant geotechnical properties of Laponite in representing clays in model tests. The experimental program included rheometer tests conducted to study the effect of thixotropy and hydration on the

viscosity and strength of the laponite mixtures. Consolidation tests were carried out on selected mixtures, in addition to consistency/Atterberg limit tests to investigate the effect of the Laponite content and aging time.

6.2 Materials and sample preparation

Laponite is a synthetic layered silicate known to have good transparency when mixed with water and has been used in a wide range of industrial applications (Thompson and Butterworth 1992). The specific product selected as the clay surrogate for this study is Laponite RD, produced by BYK Additives and Instruments. Laponite has a 2:1 layered silicate structure similar to that of the natural clay mineral Hectorite (Van Olphen and Fripiat, 1979). The Laponite particles are disk-shaped with a thickness of 0.92 nm and an average diameter of 25 nm (BYK Additives and Instruments 2014). When compared to typical Montmorillonite clay particles, the Laponite RD discs have a somewhat similar thickness but with an average diameter size forty times smaller (Mesri and Diaz, 1986). Various general properties and several strength parameters of Laponite as reported in the literature are summarized in Table 9.

Table 9: General Laponite properties and strength parameters.

Parameter	Value
Diameter[1]; nm	25
Thickness[1]; nm	0.92
Refractive index[1]; %	1.5
Specific gravity[1]; Gs	2.53
Plastic index[2]; %	1,100
Liquid limit[2]; %	1,280
$S_{u,C=4\%}$[3]; kPa	0.3
$S_{u,C=4.5\%}$[3]; kPa	0.4
$S_{u,C=9\%,SPP}$[4]; kPa	1
$S_{u,C=13.5\%, SPP}$[4]; kPa	1.6

[1] BYK Additives & Instruments (2014)

[2] El Howayek (2011)

[3] Wallace & Rutherford (2015)

[4] Ads et al. (2020)

The parameter, S_u, represents the undrained shear strength reported by different authors for different Laponite contents C. SPP indicates the presence of the rheological additive.

While Laponite could provide a suitable analog to natural soft clays, it presents a number of limitations and challenges: Long consolidation times; very low density/high void ratio (Beemer et al. 2016) and a very high plasticity index (1,100) making it even more plastic than bentonite. In order to allow for the preparation of denser mixes, i.e. increase the laponite powder content of the mixture, Sodium Pyrophosphate (SPP) has been used as an additive. It had previously been reported by Santagata et al. (2014) to decrease the viscosity of bentonite slurries. SPP works by delaying the gelation of the mixture, thus improving workability during sample preparation and generating mixes with up to 15% laponite content (Beemer et al. 2016). Without the addition of SPP, only

mixtures of relatively low laponite content (approximately 4.5% by mass) could be achieved. Increased Laponite concentrations and consequently, undrained shear strengths could be reached by initially adding SPP to the water prior to mixing in the Laponite. The following equations (Equation 8 and 9) represent the mass percentage of SPP and laponite for preparing samples at a certain laponite content and SPP dosage:

$$C_{SPP}(\%) = \frac{m_{SPP}}{m_w + m_{SPP} + m_{lap}} \times 100 \tag{8}$$

$$C_{lap}(\%) = \frac{m_{Lap}}{m_w + m_{SPP} + m_{lap}} \times 100 \tag{9}$$

Where C_{SPP} represents the rheological additive dosage (SPP), C_{lap} represents the laponite content, m_{SPP} represents the oven-dried mass of SPP, m_{lap} represents the oven-dried mass of laponite, and m_w represents the mass of distilled water.

As shown in Table 9, the undrained shear strengths of the various samples were reported to increase from 0.3 kPa for 4% Laponite content (by mass) to 1.6 kPa for 13.5% Laponite content, when a 1.99% SPP dosage was used. However, the maximum SPP concentration is limited by the solubility of the sodium additive in the water used (distilled, deionized, tap), which depends on the pH of the medium, as reported by Thompson and Butterworth (1992).

The Laponite mixtures in this study were prepared according to the mixture and timing methods proposed by BYK Additives and Instruments (2014) using the same mixer, duration and procedure throughout the Laponite sample preparation. Depending on the type of test conducted, mixtures were aged for 0, 1, 7, 14 or 28 days.

6.3 Undrained shear strength testing

A vane shear test setup was developed and used to determine the undrained shear strength of different Laponite mixtures. An experimental testing program was designed and executed to evaluate the effects of Laponite content, aging time, SPP dosage, storage temperature and remixing.

The vane blade adopted in the setup was selected based on the range of expected shear strengths and measured 25.4 mm in height, 12.52 mm in diameter and 0.762 mm in thickness. A stepper motor (Oriental Motors, model ARM46AC-T10) was used to rotate the vane and shear the Laponite mixtures at a constant speed of 1 rad/min (~60º/min), as recommended by ASTM D4648. A gauge (Mark-10, model MTT03-10Z) with a capacity of 0.07 N.m was used to control the torque during testing. The sensitivity of the measurements was on the order of 0.03 kPa when considering the apparatus capacity and vane blade dimensions. A leveling table was used to lift the sample to the required position, minimize sample disturbance. Readings were taken at a depth of 25 mm below the soil surface in accordance with the minimum depth of 1 blade diameter as specified in ASTM D4648. A minimum displacement of 1 radian was selected as reference for all tests. Figure 61 depicts the vane shear setup used in this evaluation.
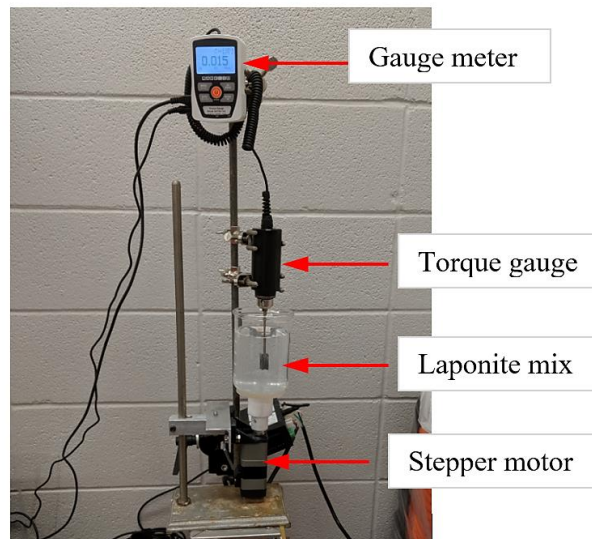
Figure 61: Vane shear setup used for undrained shear strength analysis

The Laponite content (by dry mass) adopted in this study ranged from 2% to 11%, while additive dosages ranged from 0.00% to 3.30%. The preparation of the various mixtures and samples followed the previously described mixing protocols. After mixing, each batch of laponite slurry was poured into 600 mL beakers with internal dimensions/diameter meeting the free border requirements specified in ASTM D4648 to eliminate boundary effects. The mixtures were then covered by thin layers of polyethylene sheets to prevent desiccation and were left to age for predetermined periods of time (1, 7, 14 or 28 days).

6.3.1 Effect of laponite content

A series of laboratory vane shear tests were conducted on 30 transparent clay surrogate mixtures with varying Laponite and SPP dosages, as detailed in Table 10. The dry laponite powder content ranged from 2 to 11%, which covers a range of mixture concentrations well beyond those reported in the technical literature. Moreover, the

percentage of dry SPP used ranged from 0 to 3.3%. Distilled water was used in all the mixtures and samples prepared in this study. It is worth noting that 3.3% SPP is the maximum soluble concentration in distilled water. For each mixture, four identical samples were prepared in separate molds for testing at 1, 7, 14 and 28 days, respectively. The temperature of the room in which the mixtures were stored was kept at $25°C$.

Table 10 includes a summary of the peak undrained shear strength values obtained for all 120 tests. In previous studies, such as Wallace and Rutherford (2015), the authors conducted experiments using mixtures containing Laponite contents of 4% and 4.5%, without the addition of SPP, which ultimately resulted in a peak strength of around 0.5 kPa. Results from the tests carried out in this study and summarized in Table 10 show peak undrained shear strengths exceeding 1 kPa and up to 2 kPa for mixtures with higher Laponite contents achieved using the SPP additive. These relatively high undrained shear strengths were obtained as early as seven days of aging for mixtures such as L9-S0.42, L11-S0.10, L11-S0.41 and L11-S1.58.

The effect of Laponite content can be "isolated"/quantified by comparing the undrained shear strength results at a constant temperature (i.e. 25℃), similar ranges of SPP dosage and at equal aging periods. Results presented in Figure 62 indicate that: All mixtures with fixed aging periods and SPP dosages have a positive slope when plotting the undrained shear strength with respect to Laponite content, indicating a clear increase in strength with increasing Laponite content. The rate of this increase is not constant and varies considerably for batches prepared with various concentrations of additive (Figure 62 a, b, c and d). The results presented in Figure 62 suggest that whereas adding SPP allow the creation of denser samples, there is price to be paid in terms of the shear

164

strength exhibited by these samples. As the SPP concentration at preparation increases and the suppression of thixotropic and other effects is more pronounced, the shear strengths exhibited at the same Laponite content appear to decrease as the SPP concentration increases.
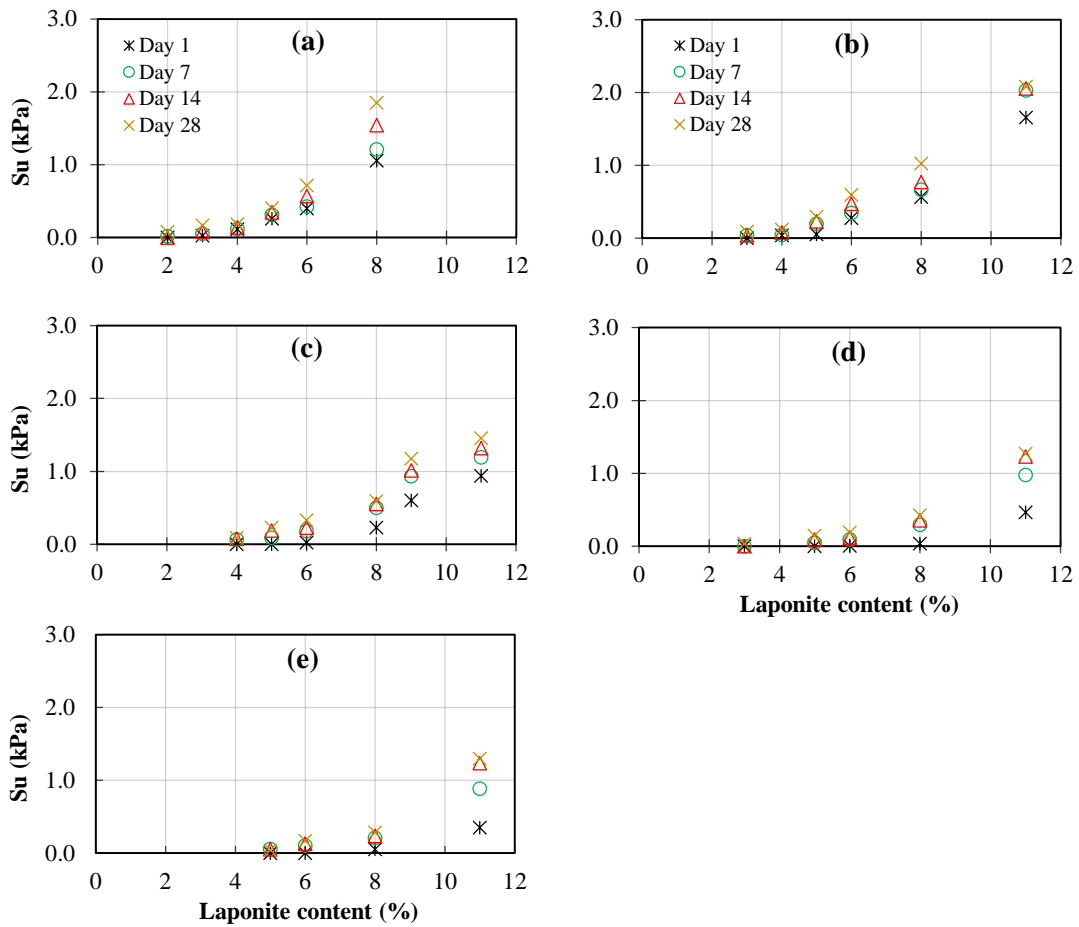
Figure 62: Undrained shear strength for increasing laponite content at different aging times for SPP dosages of: (a) 0%; (b) 0.05-0.10%; (c) 0.40-0.50%; (d) 1.6-1.8%.; and (e) 3.0-3.3%

Table 10: Undrained shear strength for 30 mixtures over time.

Mix Label	Lap (%)	SPP (%)	Su (kPa)				Mix Label	Lap (%)	SPP (%)	Su (kPa)			
			1 day	7 days	14 days	28 days				1 day	7 days	14 days	28 days
L2-S0.00	2	0.00	0.001	0.001	0.001	0.080	L6-S0.00	6	0	0.400	0.426	0.573	0.715
L3-S0.00	3	0.00	0.027	0.053	0.080	0.166	L6-S0.06	6	0.06	0.280	0.346	0.475	0.599
L3-S0.03	3	0.03	0.001	0.047	0.040	0.107	L6-S0.43	6	0.43	0.020	0.180	0.229	0.326
L3-S0.06	3	0.06	0.001	0.040	0.040	0.093	L6-S1.69	6	1.69	0.007	0.093	0.120	0.186
L3-S1.77	3	1.77	0.001	0.001	0.001	0.033	L6-S3.28	6	3.28	0.001	0.107	0.132	0.172
L4-S0.00	4	0.00	0.117	0.120	0.150	0.185	L8-S0.00	8	0	1.059	1.212	1.542	1.851
L4-S0.03	4	0.03	0.060	0.080	0.100	0.110	L8-S0.10	8	0.10	0.566	0.666	0.773	1.026
L4-S00.6	4	0.06	0.040	0.047	0.080	0.120	L8-S0.43	8	0.43	0.226	0.499	0.553	0.592
L4-S0.44	4	0.44	0.001	0.067	0.073	0.087	L8-S1.65	8	1.65	0.033	0.293	0.355	0.425
L4-S0.88	4	0.88	0.001	0.040	0.027	0.087	L8-S3.21	8	3.21	0.053	0.213	0.240	0.288
L5-S0.00	5	0.00	0.260	0.313	0.346	0.405	L9-S0.42	9	0.42	0.599	0.932	1.012	1.172
L5-S0.06	5	0.06	0.053	0.200	0.233	0.295	L11-S0.10	11	0.1	1.658	2.031	2.056	2.084
L5-S0.43	5	0.43	0.001	0.087	0.186	0.226	L11-S0.41	11	0.41	0.939	1.192	1.319	1.456
L5-S1.71	5	1.71	0.001	0.047	0.093	0.147	L11-S1.58	11	1.58	0.466	0.979	1.232	1.272
L5-S3.32	5	3.32	0.001	0.060	0.053	0.040	L11-S3.07	11	3.07	0.353	0.886	1.239	1.300

L: laponite content (%)

S: SPP dosage (%)

The results in Figure 62(a) correspond to the undrained shear strength S_u of laponite mixtures prepared without using SPP additive (i.e. 0% SPP content). They show a clear increase in S_u with increasing Laponite content. For example, the data points for an aging period of one day indicate an increase in S_u on average by a factor of 2.0 for every 1% increase in laponite content. The same is also true for aging times of 7, 14 and 28 days in Figure 62(a).

A similar increase in undrained shear strength with increasing Laponite content, for various values of SPP dosages, can be observed in Figures 62(b), 62(c), 62(d) and 62(e), where S_u increased on average by a factor of 2.0 per percent increase in Laponite. The increase in S_u with increasing Laponite contents is in agreement with the results reported by Mourchid and Levitz (1998) regarding the gelation and strength of soft clay surrogates. Furthermore, the rate of increase of S_u with laponite content cannot be described by a single exponent, as this parameter depends on other variables, such as SPP dosage and aging time.

6.3.2 Effect of SPP dosage

In order to isolate the effect of SPP dosage on the undrained shear strength of a Laponite mixture, variables, such as Laponite content, aging time and temperature, should be kept constant. The results presented in Table 10 clearly indicate that S_u decreases with increasing SPP dosage (e.g. for 5% laponite content after aging seven days), which is consistent with the objective of using this additive. SPP decreases the rate of gelation and is reflected as a decrease in the undrained shear strength at any given time.

167

An increasing SPP dosage for a given Laponite content renders the mixture less viscous and the undrained shear strength eventually decreases dramatically. This was observed for all Laponite contents and testing times evaluated in this study (one day through 28 days). Figure 63 shows the variation in S_u with increasing SPP dosages for select values of Laponite content and aging times. The results shown in Figure 63 clearly depict a decreasing trend in undrained shear strength with SPP dosage for the different values of Laponite content. The variation in S_u vs SSP for all the aging times and Laponite contents are best described as negative exponential functions.

In Figure 63(a) i.e. a Laponite content of 5%, the results for Day 1 show a steep decrease in S_u as SPP dosages are increased. The rate of decay is highest in the low range of SPP values, e.g. SPP< 0.5%. This rate of decay decreases with increasing aging time and shows the lowest rate of decrease in strength for Day 28. Similar trends can be observed in Figures 63(b), 63(c) and 63(d) for the different values of Laponite content considered in the study.

Specifically, as shown in Figure 63(a), the strength for Day 1 dropped about 99% for an increase in SPP dosage from 0% to about 1.7%. For aging times of seven, 14 and 28 days, the reduction in strength was about 75% for an SPP dosage increase from 0% to 1.7%. This reduction in strength is roughly 85% when SPP dosage increased from 0% to 3.3%.
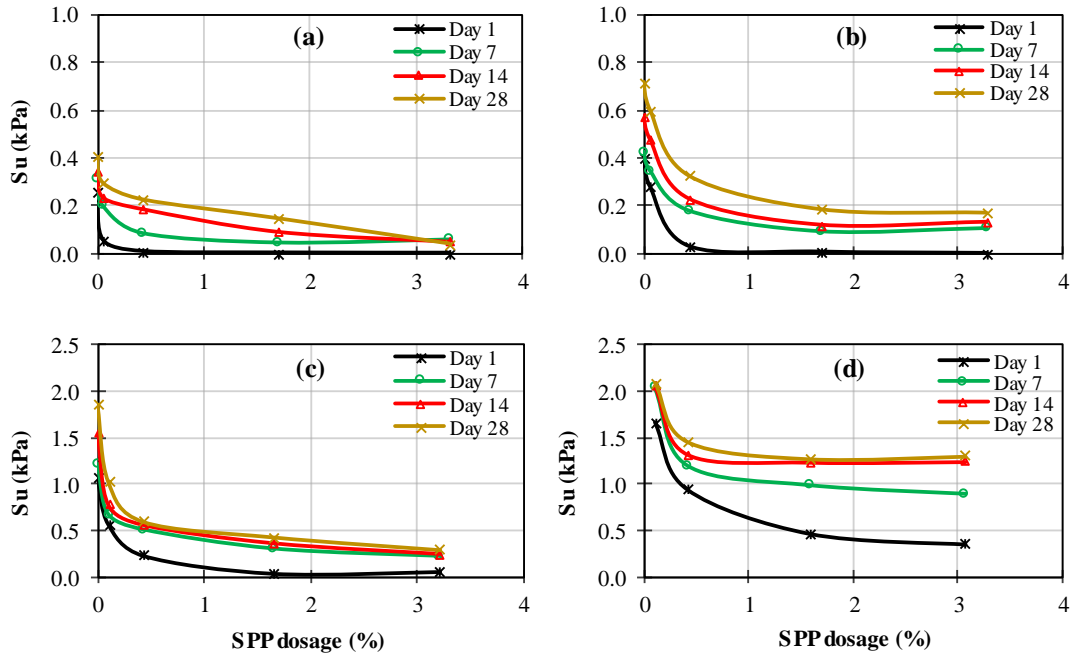
Figure 63: Undrained shear strength variation with SPP dosage at different aging times for Laponite contents of: (a) 5%; (b) 6%; (c) 8%; and (d) 11%.

The behavior observed in Figures 63(b) and 63(c) is similar to that discussed for Figure 63(a) for all aging times. The reductions in S_u were comparable in all three graphs, indicating similar behavior in undrained shear strength with SPP dosage variation for Laponite contents below 10%. The reductions were less evident for laponite contents of 11% in Figure 63(d).

In Figure 63(d), the results for Day 1 show reductions in undrained shear strength of 70% when SPP dosage increased from 0% to 1.7%. This reduction in strength is considerably lower than the minimum of 99% recorded for Day 1 at lower laponite concentrations seen in Figures 63(a), 63(b) and 63(c) for the same range of SPP dosage. Similarly, the results for Days 7, 14 and 28 displayed average reductions in strength of 35% and 40% for an increase in SPP dosage from 0% to 1.7% and 0% to

3.3%, respectively. This, too, is significantly lower than the minimum of 75% and 85% reductions noted earlier for lower Laponite contents.

6.3.3 Effect of Aging Time

In order to identify the effect of time on the undrained shear strength of Laponite mixtures, the variation in undrained shear strength was plotted as function of the aging time in Figure 64 for ten selected mixtures. These mixtures are representative of the behavior of the rest of the batches tested. These are not shown on the same figure for purpose of avoiding littler and maintain clarity.
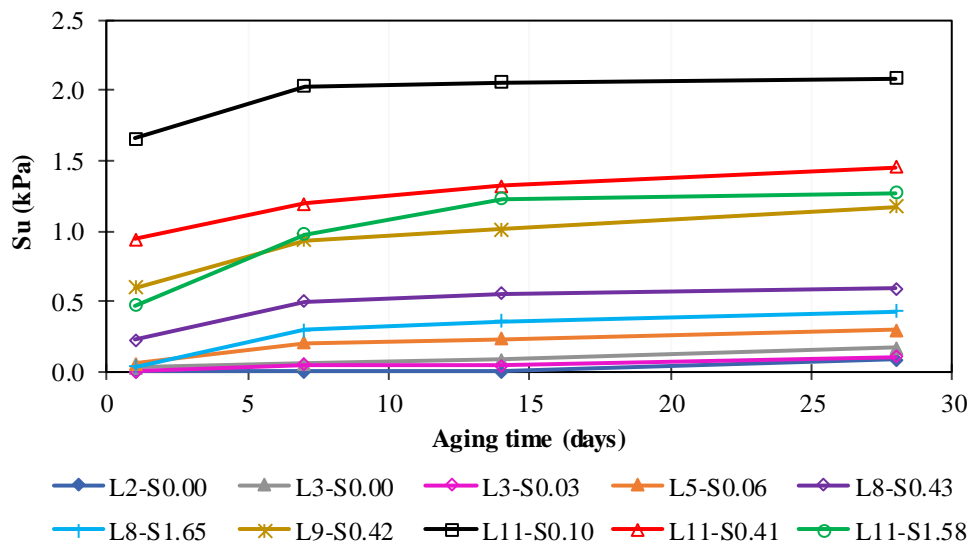
Figure 64: Undrained shear strength variation with time for ten selected mixtures.

All data points plotted in Figure 64 indicate that the undrained shear strength increased with time. However, the rate of increase in S_u decreased with time, reaching a

strength at Day 28 that, for all intents and purposes may be considered as the ultimate strength of the respective mixtures ($S_{u,t=28\ days} \cong S_{u,\infty}$).

The results show that for most mixtures, the undrained shear strength at Day 7 exceeded 70% of that at Day 28. As such a seven-day aging period may be taken as a reasonable indicator of the range/value of the ultimate strength of various Laponite mixtures.

6.3.4 Effect of Temperature and Remixing

An increase in temperature is expected to decrease the viscosity of materials and, accordingly, lead to a decrease in the undrained shear strength. However, Rodriguez and Santamarina (1999) reported that the rate of thixotropic strength gain increases with increasing temperature for clays that shows significant thixotropic behavior, leading to an increased rate of aging with increasing temperature. The impacts of temperature on viscosity and thixotropic behavior, which apply to highly sensitive clays, should therefore also be applicable to Laponite.

Considering this, an investigation was undertaken as part of this study on the effect of temperature on Laponite in order to determine whether viscosity or thixotropy dominate the effect of temperature on its undrained shear strength. The evaluation involved aging selected mixtures (L5-S0.00, L5-S0.06, L5-S1.71, and L8-S0.10) at 5° C and 40° C to study the effect of temperature at seven and 28 days.

The effect of remixing/remolding on the thixotropic behavior of the clay surrogate was also evaluated as part of this study to assess whether such remixing

would lead to a complete loss of undrained shear strength. The same mixtures selected to investigate temperature effects (L5-S0.00, L5-S0.06, L5-S1.71, and L8-S0.10) were tested to assess the effect of remixing. Table 11 shows a summary of the results obtained to quantify the peak undrained shear strengths of mixtures tested at: (1) one day, seven days, 14 days and 28 days at $25°C$; (2) seven days after initial preparation and subsequent remixing at $25°C$; and (3) seven days and 28 days at both 5° C and 40° C.

Table 11: Effects of remixing and temperature on the undrained shear strength.

Mix	Su (kPa)								
	25° C					5° C		40° C	
	1 Day	7 Days	14 Days	28 Days	7-R* Days	7 Days	28 Days	7 Days	28 Days
L5-S0.00	0.260	0.313	0.346	0.405	0.331	0.288	0.340	0.51	0.92
L5-S0.06	0.053	0.200	0.233	0.295	0.240	0.150	0.205	0.280	0.501
L5-S1.71	0.001	0.047	0.093	0.147	0.050	0.020	0.030	0.140	0.213
L8-S0.10	0.566	0.666	0.773	1.026	0.715	0.42	0.65	0.82	1.03

*Remixed sample

In the case of the remixed samples, they were initially prepared and allowed to age for seven days before remixing. The undrained shear strength was then measured after seven additional days had passed. The results in Table 11 reveal that the remolding did not lead to total strength loss. This is further discussed and explained in the next section reporting on the viscosity tests.

Comparison of the undrained shear strength values of the remixed samples with mixtures aged seven days and 14 days shows that almost all the S_u values for the

samples remolded after 7 days and allowed to reset were bounded between those at 7 days and 14 days. These observations suggest that some built in strength remained intact (thixotropy) regardless of the level of remixing, with some other source of strength destroyed upon remixing.

Regarding the effect of temperature, it is clear from the results presented in Table 11 that a decrease in temperature led to decreased rates of aging, which resulted in lower undrained shear strength values, in spite of the potential increase in viscosity that such lower temperatures would have caused. All peak undrained shear strength values for the selected mixtures at seven days and 28 days at 5° C were lower than the peak S_u for the control mixtures aged for the same duration.

In contrast, an increase in undrained shear strength was observed at a higher temperature of 40° C as compared to strength values at a temperature of 25°C, particularly for mixtures L5-S0.00, L5-S0.06 and L5-S1.71. The peak $S_{u,T=40°C}$ values at seven days largely matched the peak $S_{u,T=25°C}$ values at 28 days, whereas the peak $S_{u,T=40°C}$ values at 28 days exceeded the $S_{u,T=25°C}$ values at 28 days by a factor of 1.5 to 2.0.

An increase in temperature appears to have increased the rate of thixotropy strength gain, although Figure 64 shows that most mixtures have reached an almost constant strength at Day 28 and no volumetric changes were observed during samples aging. Based on the trend of shear strength results, it is conceivable that $S_{u,T=25°C}$ at Day 28 could continue to increase and reach the ultimate strength value $S_{u,T=40°C}$ after additional aging time.

In summary, the results discussed in this section indicate that the undrained shear strength increases with increasing Laponite content, decreasing SPP dosage and extended duration of aging. Also, an increase in temperature appears to generate an increase in the thixotropic behavior resulting in a comparatively shorter period of time to reach the ultimate shear strength of the mixtures. While the effect of remixing on shear strength deserves further investigation, preliminary results showed that remixing does not result in a complete loss of shear strength.

6.4 Viscosity

The progressive thixotropic strength gain was evaluated in this study by quantifying the rheology (viscosity) of Laponite for different mixtures directly after mixing and at different times. The use of Laponite as transparent clay surrogate is expected to exhibit a thixotropic behavior, resulting in time-dependent increases in stiffness and strength when at rest, while softening upon remixing. Such response was evidenced as part of the quantification of the undrained shear strength previously discussed in this paper.

The clay surrogate used in this testing program behaves either as a non-Newtonian fluid, for early aging times, such as couple of hours, or a non-Newtonian plastic fluid for longer aging times (Mannheimer et al. 1989; Yi et al. 2018). This can be better assessed by characterizing the viscosity of the various mixtures and samples. Furthermore, quantifying the viscosity of laponite should allow for a better understanding of the bond development with aging duration. Finally, remixing laponite samples and testing their viscosity thereafter also offers significant insight into the

difference between the various sources of strengths, which may be present in addition to the thixotropic shear strength gains.

6.4.1 Rheometer

A Physica MCR 301 rheometer (Anton Paar Company) that allows conducting tests under constant rate ramp as well as stress ramp, was used to quantify the viscosity of the Laponite samples. In order to obtain the variation in viscosity at different shear rates, testing was carried out using a controlled shear rate (CSR) mode of testing. While several methods can be adopted for the rheological measurements of fluids, the use of a vane spindle, rather than a plate spindle, is the most suitable for this soft material. This is because a vane spindle minimizes disturbances when penetrating the sample. Sample placement on the lower spindle when using a plate spindle would cause considerably more disturbance to the Laponite sample and thereby possibly destroy thixotropic strength gains developed prior to testing.

6.4.2 Time needed for CSR

As a prerequisite step to CSR testing, several stress-controlled tests (SCT) were conducted on transparent clay surrogate mixtures to determine the appropriate time for the ramped rates in the CSR tests. The time selected for each strain rate is critical to achieve adequate viscosity results based on the residual strength obtained from an applied strain rate. By plotting the variation of shear stress with time in a stress-controlled test, the time to be adopted in the CSR tests can be determined. This was done for different stresses in the stress-controlled tests and very similar plots were

obtained. The time history shown in Figure 65 and which is typical of all tests, indicates that a duration of 20 seconds was adequate to obtain the residual strength.

Accordingly, when performing the CSR tests, the shear stress obtained after 20 seconds was adopted/retained. The lowest shear rate used was $0.01\ 1/s$ and the highest was $500\ 1/s$. These rates covered large ranges and reached those exhibited during mass movements in slope failures.
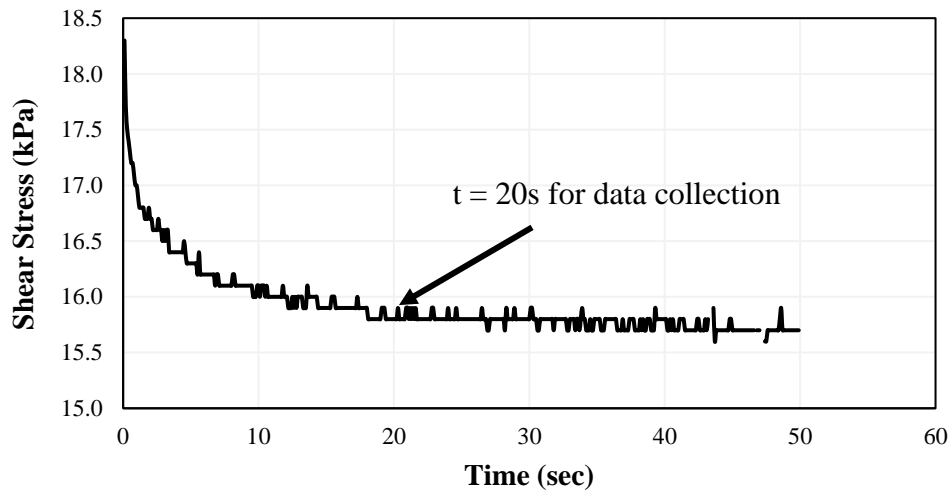
Figure 65: Rheometer variation of shear stress with time.

6.4.3 Shear stress variation with shear rate

Figure 66 shows the variation in shear stress with shear rate at different aging times for two mixtures, L4-S0.00 (no SPP) and L5-S0.06 (using 0.06% SPP). The data points plotted in Figure 66 represent the results of tests conducted at different times on three samples prepared for each mixture, i.e. (1) directly after mixing, (2) one day after mixing, (3) remixing the sample aged for one day and testing it immediately, and (4) the third sample tested after seven days of aging.

176
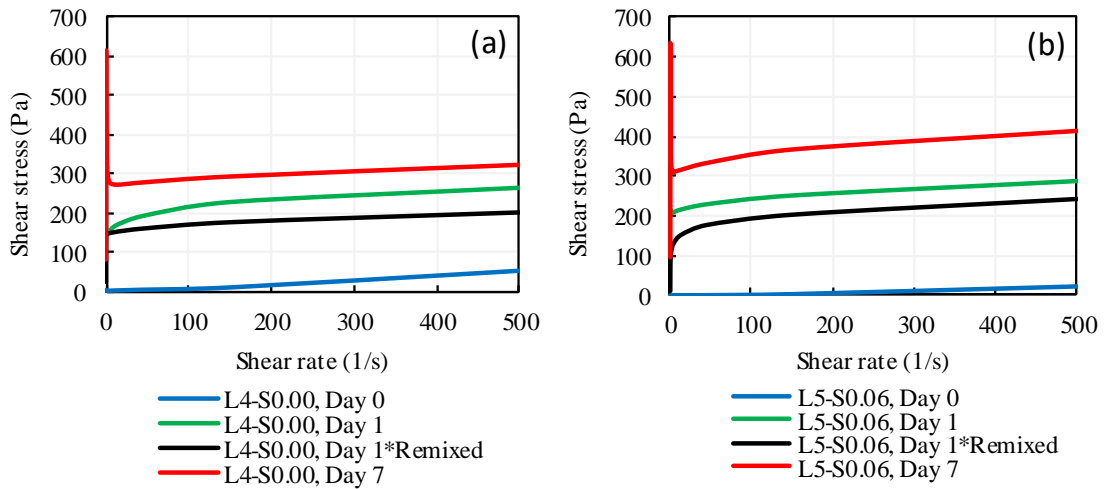
Figure 66: Variation in shear stress as a function of the shear rate for mixtures: (a) L4-S0.00; and (b) L5-S0.06.

As expected, the shear stresses measured at Day 7 for all mixtures exceeded those obtained at Day 1, which were in turn greater than the strengths measured at Day 0. The shear stress at Day 1 for the remixed sample was lower than that of the virgin samples (without remixing). These results are consistent with the vane shear test results presented earlier in this paper, where the various plots in Figure 66 show increasing strength with time.

A closer look at low shear rates of Figure 66, namely below $10 \ s^{-1}$, shows interesting behavior of shear stress for both samples L4-S0.00 and L5-S0.06. This is mainly for samples aging at least for 1 Day, since the fresh sample barely possessed any strength at very low shear rates. In Figure 67, variation of shear stress for both samples at low shear rates is plotted.
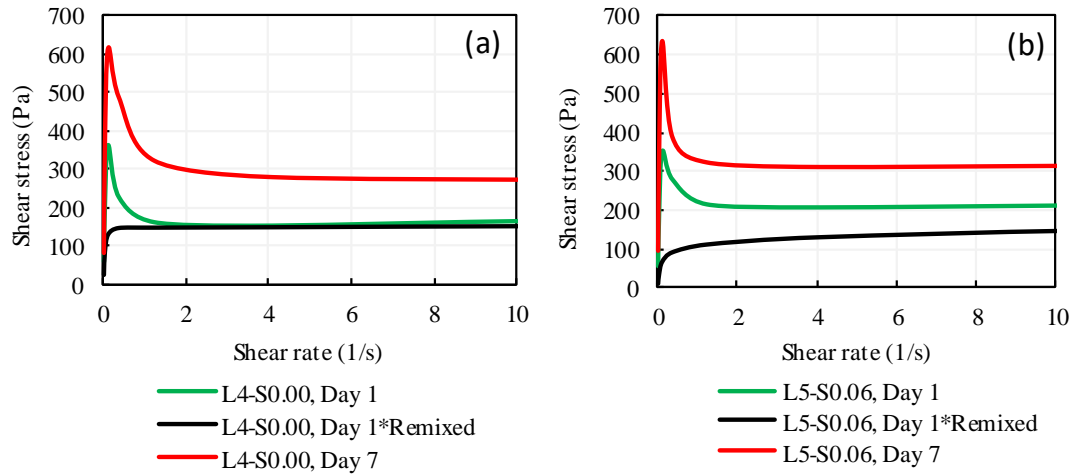
Figure 67: Variation in shear stress as function of the shear rate for mixtures: (a) L4-S0.00; and (b) L5-S0.06 at lower shear rates.

The results in Figures 67(a) and 67(b) show a different trend between the shear stress vs. shear rate curve for the remixed sample and those obtained for the virgin mixtures (Day 1 and Day 7 mixtures). This difference can be attributed to the thixotropic strength gain for aged mixtures, as reported by Mitchell (1960), who showed that sensitive clays present a well-defined peak strength and subsequent shear strength loss. This trend may be associated with the deterioration of the aged strength. No such peaks and post-peak degradation are observed in strength tests on remolded samples. A similar nonlinear trend in the shear stress vs. shear rate curve was also reported by El-Howayek (2011) for Low laponite content mixtures. The existence of multiple sources of shear strength is somewhat evident in these graphs, as the strength of the mixtures after remolding was greater than that at Day 0 but lower than that at Day 1, indicating a source of strength that is irreversible. It is also worth noting that results for Day 0 and Day 1 after remixing had a non-Newtonian behavior, since they were directly tested after sample mixing/remixing, while the results for Day 1 and Day 7 had a non-

Newtonian plastic behavior due to the thixotropic strength gain with aging time; and this is consistent with the findings of Yi et al. (2018).

Additional laponite mixtures (other than L4-S0.00 and L5-S0.06) were also tested, showing a behavior similar to the results previously displayed.

6.4.4 Apparent viscosity

The apparent viscosity, defined as the secant slope of the shear stress vs. shear rate curve, was calculated for both mixtures, as displayed in Figure 68 using a semi-log scale for shear rates ranging from $0.1 \ s^{-1}$ to $10 \ s^{-1}$.
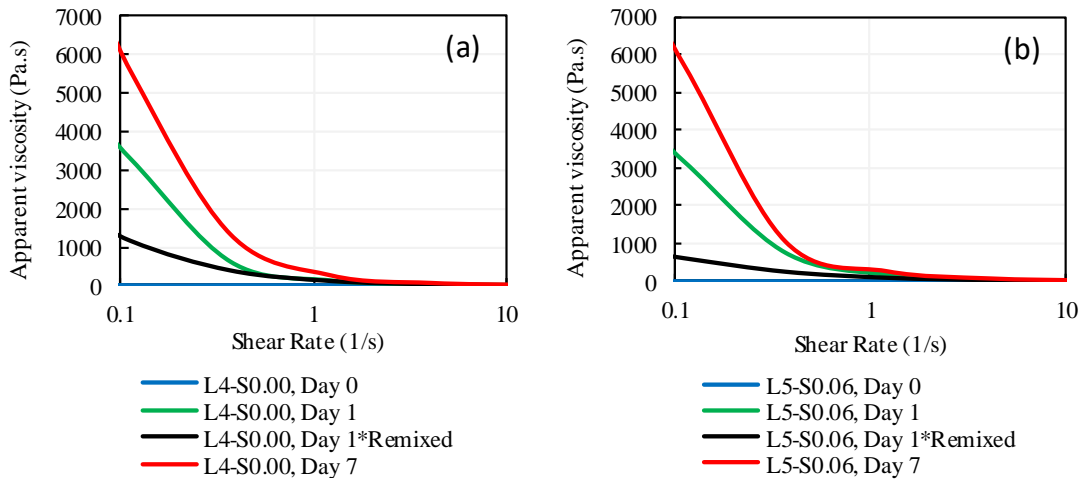
Figure 68: Viscosity variation with shear rate for mixtures: (a) L4-S0.00; and (b) L5-S0.06.

The values of apparent viscosity increased significantly with aging time between Day 0 and Day 7 for both mixtures, reaching values around $6000 \ Pa.s$. A comparatively stiff behavior is evident at low shear rates for aged mixtures and remixed

ones. Immediately after mixing, the apparent viscosity for both mixtures was negligible, as shown in Figures 68(a) and 68(b) along with the results for other aged mixtures.

The graphs also show that the apparent viscosity converged to very similar values for shear rates ranging from $2\ s^{-1}$ to $10\ s^{-1}$. The apparent viscosity values for strain rates ranging from 0.5 to 5 s^{-1} are comparable to those of very soft clays (Locat and Demers 1988).

6.4.5 Hydration and Thixotropy

An important aspect to evaluate when conducting viscosity tests is the source/s of the time-dependent strength gain. Specifically, the contribution to undrained shear strength due to the hydration and thixotropic behavior of the laponite. Also relevant is to assess the period of time over which shear strength gains occur and whether the different shear strength sources develop concurrently. To better explore such issues, the viscosity, which can be considered an indicator of the strength gain, is shown in Figure 69 as a function of two selected strain rates $\dot{\varepsilon} = 0.1\ s^{-1}$ and $\dot{\varepsilon} = 1\ s^{-1}$.
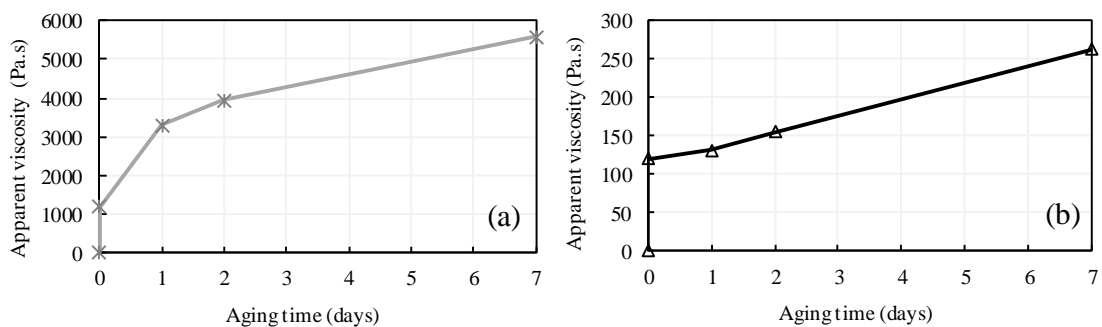
Figure 69: Viscosity variation with time at shear rates of: (a) 0.1 1/s; and (b) 1.0 1/s.

The results shown in Figure 69 correspond to six tests conducted on mixture L4-S0.00, with the data points showing the apparent viscosity values at: (1) Day 0, immediately after mixing shown as a point with coordinates (0,0); (2) Day 1 remixed and (3) Day 2 remixed, also plotted at time 0 (overlaying points) but with 1,200 y-intercept; (4) Day 1; (5) Day 2; and (6) Day 7. Samples with aging time of one and two days were tested after aging one and two days, respectively, and the corresponding apparent viscosity is plotted at aging times of 1 and 2 days on the x-axis in Figures 69(a) and 69(b). However, these samples were remixed directly after the test had finished and another rheology test was conducted directly. The apparent viscosity was reported to be the same, and thus was plotted at aging time of 0 days leading to overlaying points.

The results in the figures indicate that there is non-zero apparent viscosity related to an apparent strength for the remixed samples after 1 day of aging, which was set as time 0 in both Figures 69 (a) and 69(b). In addition, such non-zero value point at time 0 demonstrates that the reaction that occurred during the first day had ceased, since the two points overlaid each other. The results also show that the apparent viscosity results define an approximately linear trend with increasing time, particularly beyond Day 1. The results are consistent with the development of hydration-induced shear strength gains before Day 1, with only thixotropy-induced shear strength gains beyond that time. Such observation is consistent with results reported by Mitchell & Soga (2005): the irreversible nature of remolded strength and the reversible nature of thixotropic strength gain.

A linear trend was defined between the Day 1 and Day 7 data points in Figure 69. The linear trends defined for the two data sets in Figures 69(a) and 69(b) show a

181

particularly high R^2, exceeding 99% in both cases. The slope of the equations based on the prior analysis represents the rate of thixotropy-induced shear strength gains for these mixtures. However, the intercepts of the linear trends represent the hydration strength obtained before Day 1, assuming that the hydration-induced shear strength gain occur within the first day. Note that this interpretation was merely done to differentiate between two sources of strength for the laponite mixtures for a period of time of seven days.

6.5 Consolidation

Consolidation tests were conducted on selected mixtures with different laponite contents and SPP dosages to relate laponite mixtures to saturated clays in response to a change in pressure and possible seepage.

Consolidation tests were conducted on five different mixtures with and without the addition of SPP. Table 12 summarizes the initial state and properties of the different mixtures used in the consolidation tests. The tests were done on 7 days aged samples that were properly sealed to prevent possible evaporation in an attempt to maintain the initial water content. A special setup for the odometer was used to prevent leakage during the application of vertical stresses, especially that some mixtures did not have enough strength.

Table 12: Parameters for the 1-D consolidation mixtures used, including water content and initial void ratio.

Mix	Lap (%)	SPP (%)	w_0 (%)	e_0
L4-S0.00	4	0	2400	60.72
L5-S0.06	5	0.06	1900	48.07
L6-S0.06	6	0.06	1567	39.64
L8-S0.10	8	0.10	1150	29.10
L11-S0.41	11	0.41	733	18.55

e_0: initial void ratio

w_0: initial water content

The initial water content was measured after placing the mixtures in the oven prior to testing. Determination of the void ratio assumed that the clay surrogate was fully saturated after the seven-day period and adopted a laponite specific gravity of 2.53 as reported by Chini et al. (2015).

The initial void ratios for the mixtures were significantly higher than those of typical natural clays. The mixtures tested had a diameter of 62.5 mm and height of 25.4 mm. Figure 70 presents sample L4-S0.00 after placement in the odometer prior to the beginning of consolidation testing.

Figure 70: L4-S0.00 1-D consolidation sample in the odometer.

6.5.1 Consolidation curves

Figure 71 displays the loading and unloading curves for the five 1-D consolidation tests conducted as part of this study. The curves shown for both loading and unloading stages are consistent with those of natural clays. The average duration for every incremental load ranged from two to three days to reach the end of the primary consolidation phase. The total time for each test ranged from three to four weeks, including the unloading stages. The loading phase was done on six increments, with normal stresses of 6, 12, 24, 48, 72 and 96 kPa; while the unloading phase was conducted to normal stresses of 48 kPa and 12 kPa.

The final degree of consolidation reached for the tests ranged from 60 to 70%, independent of the initial laponite and SPP dosages used. The degree of deformation during the loading stage decreased as more stress was applied in all five tests. The application of the first loading increment of 6 kPa had a comparatively greater effect on the laponite mixtures with low laponite content [e.g. Figures 71(a) and 71(b)]. This is

184

evidenced by the decreasing degree of consolidations (red curve) observed with increasing laponite mixtures [Figures 71(c), 71(d) and 71(e)]. Mixtures shown in Figures 71(d) and 71(e), with 8% and 11% laponite, respectively, hardly responded to the 6 kPa loading increment, a response that was similar to that of a seating stage. This could be related to the increased stiffness of specimens with comparatively high laponite content. This observation highlights the importance of having used comparatively low load stresses for mixtures with low laponite content (e.g. 4%), consistent with recommendations by Wallace & Rutherford (2015). However, for the experiments to be comparable, similar load increments were adopted in all five tests carried out in this study.

The second loading increment resulted in a well-defined response for all mixtures, so as for the third and fourth loading increments, especially those that had minimal deformation during the first loading increment. For the last two loading increments, 72 and 96 kPa, all five mixtures deformed less and much slower compared to the four previous loading increments.

The first stage in the unloading phase involved decreasing the applied stresses from 96 kPa to 48 kPa. During this stage, swelling was on the order of 0.5-0.8 mm for all mixtures. A marked increase in height was observed when subsequently unloading to a stress of 12 kPa, during which swelling was more evident, resulting in displacements on the order of 1.0-2.3 mm.

It is important to note that these tests demonstrated an ability to reach degree of consolidations of 60%-70%. This corresponded to achieving final laponite mixtures of 10.3% and 21% after loading samples with initial laponite content of 4% and 11%,

respectively. It is worth noting that the maximum laponite content that could be mixed from slurry with maximum soluble SPP dosage is less than 15%. This proves that laponite mixtures with 21% laponite content could be achieved from consolidation tests.
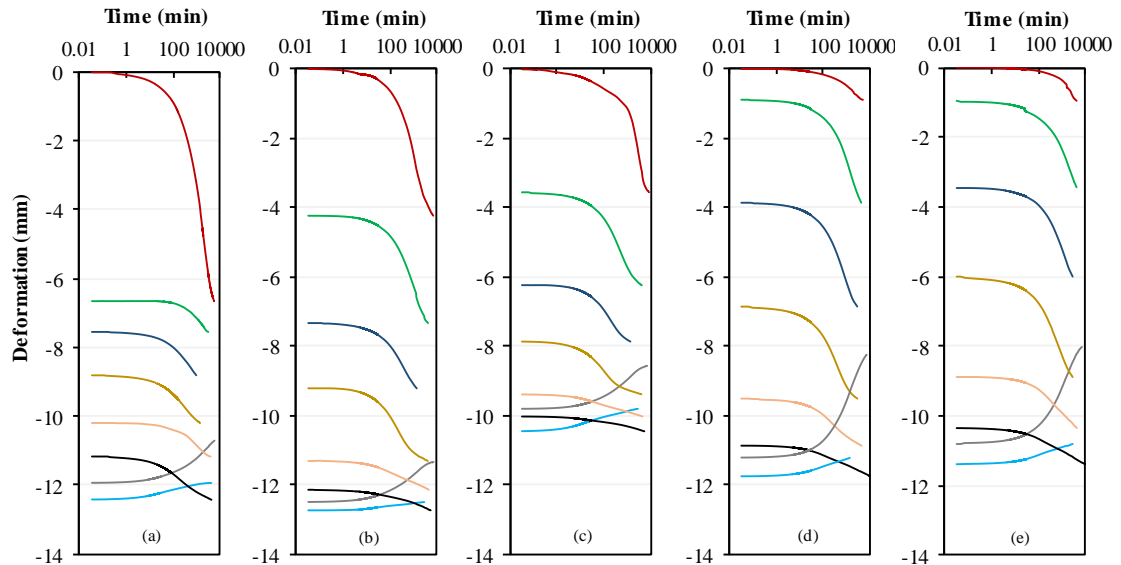
Figure 71: Loading and unloading consolidation graphs for mixtures: (a) L4-S0.00; (b) L5-S0.06; (c) L6-S0.06; (d) L8-S0.10; and (e) L11-S0.41.

6.5.2 Coefficient of consolidation

The coefficient of consolidation, c_v, was calculated for each compression stage corresponding to the different vertical stresses, and the variation of c_v with the vertical applied stress is shown in Figure 72. The results show an initial trend in which c_v either increases with increasing applied stress or remains constant, followed by a decreasing trend beyond approximately 48 kPa during which c_v, decreases with increasing effective vertical stresses. These trends are consistent with those reported by Wallace & Rutherford (2015).

186

The results also show a clear decrease in c_v with increasing laponite content (from 4% up to 11%). The decrease in coefficient of consolidation was particularly significant for laponite content values decreasing from 4% to 5%, beyond which c_v values decreased only slightly (for laponite contents ranging from 5% to 11%). Mix L4-S0.00 had the highest c_v, at 48 kPa with a value of 0.028 m^2/yr, which is comparable to that of bentonite at 50 kPa confinement and 20% bentonite content (Chenari et al. 2018). Thus, c_v values for a laponite content of 4% are comparable to those for 20% bentonite content.
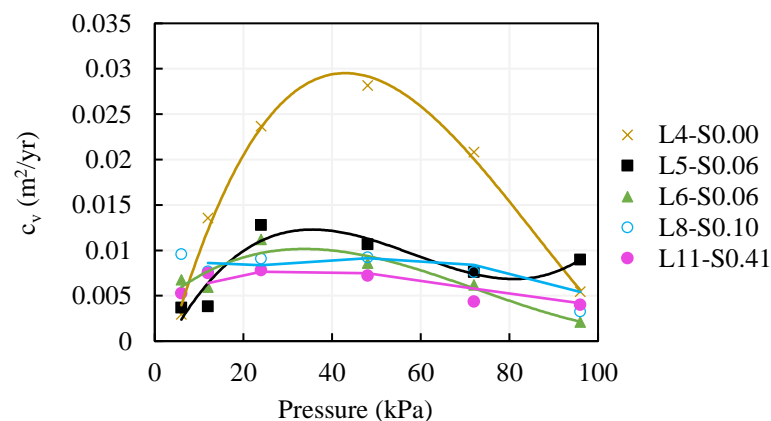
Figure 72: Variation in the coefficient of consolidation with effective vertical pressure for the five mixtures in the 1-D consolidation.

6.5.3 Void ratio and effective stress

Figure 73 shows the compressibility curves (in terms of void ratio vs effective vertical stresses) following both compression and swelling stages. The initial void ratio of the mixtures was considerably higher than that of typical clays due to the high water content used during sample preparation. After the end of primary consolidation, the

void ratio remained high, even for mixture L11-S0.41, which had an initial void ratio of 18.55 and a final void ratio of 6.67. This final void ratio is at least six to seven times higher than typical natural clays.

The compression and swelling indices decreased with increasing laponite content depicted by flatter curves in Figure 73, but the ratio between the initial and final void ratios in all tests was approximately 3 because the final degree of consolidation was similar in all tests. Starting with a void ratio of 60, the final void ratio after loading increments was roughly 22 for mixture L4-S0.00. In contrast, for mixture L11-S0.41, the void ratio decreased from 18.6 to 6.5 after the final loading increment. No evidence of pre-consolidation pressure was there for all tested mixtures. Table 13 summarizes the variation in the compression and swelling indices, C_c and C_s respectively, for all tests. Both indices show a decreasing trend with increasing laponite content. The value for the C_c and C_s for mixture L4-S0.00 are comparable to those reported in Wallace & Rutherford (2015).
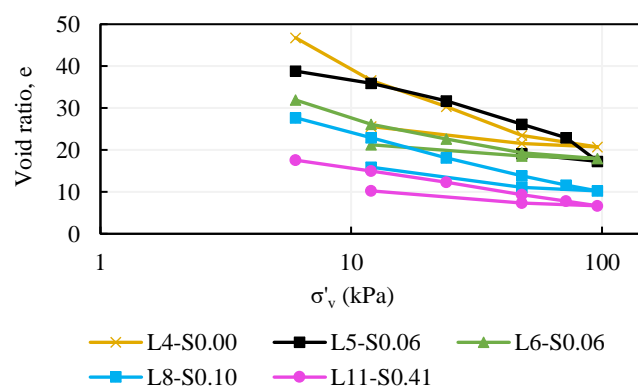
Figure 73: Compressibility curve for five mixtures after 1-D consolidation testing.

Table 13: Compression and swelling indices for the different 1-D consolidation tests conducted.

	Test					
	L4-S0.00*	L4-S0.00	L5-S0.06	L6-S0.06	L8-S0.10	L11-S0.41
Cc	16.60	16.63	13.95	9.10	9.65	9.34
Cs	6.30	6.05	5.27	4.49	4.61	3.91

*Wallace & Rutherford (2015)

A notable conclusion drawn from the consolidation tests conducted in this study is that no evidence was observed of SPP dosage affecting the compressibility parameters. Instead, the compressibility curves appear to be affected primarily by the changes in laponite content, at least for the mixtures considered in this study.

6.6 Atterberg Limits

Knowing that laponite mixtures respond differently when different laponite contents are used, when SPP additive is used and at different aging times, it is important also to determine any possible effect of these parameters on the Atterberg limits. In this section, the plastic limit of laponite was determined for different laponite contents and SPP dosages. Moreover, the 30 mixtures of laponite surrogate shown previously in Table 10 (with varying laponite and SPP dosages) were also tested to determine the liquid limit.

6.6.1 Plastic limit

The conventional method (hand rolling) was used to determine the plastic limit, according to ASTM D4318 (2010). The calculated plastic limit for laponite without the

addition of SPP was $PL = 200$. This is in line with the values of previous reported laponite plastic limit by Wallace & Rutherford (2015).

A value of $PL = 200$ is higher than typical PL for montmorillonite and bentonite clays. As for the plastic limit for mixtures with the addition of SPP, cycles of oven drying and wetting were followed to study its effect on plastic limit. The drying process was performed to stiffen the samples and allow for possible hand rolling, whereas wetting was done in the case of over drying. Surprisingly, the plastic limit ranged between 180 and 230 regardless of the SPP dosage, drying/wetting cycles with/without aging.

6.6.2 Liquid limit

The conventional Casagrande liquid limit method was used to determine the liquid limit, LL, of different mixtures. This type of test is expeditious and simple as compared to other soil testing setups. The reported liquid limit after an aging time of one hour after mixing and without the use of SPP was $LL = 1,200$, which reflects a plasticity index of 1,000 for a plastic limit of 200. This is also consistent with the values previously reported in the literature (Chini et al. 2015). On the plasticity index chart, laponite falls in the category of "high plastic inorganic clays" between the A-line and B-line. The liquid limit determined corresponds to around 8.0% laponite content. This measurement was obtained one hour after mixing to allow for some strength build up, considering that this test is unsuitable for completion immediately after mixing due to the high variability in the reported values of LL right after mixing. The variability decreases significantly after just an hour following mixing.

In the following analysis, the effect of laponite content and aging time were only considered when conducting the liquid limit tests. The effect of SPP additive wasn't studied, as the variation in the results were significantly high.

6.6.3 Effect of aging time on liquid limit

Mixtures L03-S0.00, L05-S0.00, L07-S0.00 and L08-S0.00 were prepared using the same sample preparation method discussed earlier in the paper and were left to age for a period of two weeks. It was not possible to create mixtures with laponite contents higher than 8% without the addition of SPP additive. Mixtures with laponite content lower than 8% were in the liquid state with an average blow count of 10 or less even after an aging time of 24 hrs.

The procedures followed to determine the liquid limit of the mixtures was as follows: the first batch of specimens from mixtures L03-S0.00, L05-S0.00, L07-S0.00 were left to age at room temperature of 25 ℃ in a well-sealed mold, but even after an aging time of 2 weeks, the blow count was lower than 25 for all of these mixtures. Therefore, some specimens from these mixtures were placed in the oven at a temperature of 110 ℃ to reduce the water content at different aging times during the 2 weeks period. The specimens were mixed thoroughly after being removed from the oven, and in many cases, water drops were added to ensure proper and easy mixing. This is because the oven dried specimens showed some cracks and crust formation, or even reaching the plastic state due to heavy loss in the water content. After several trials and dry-wet cycles, a blow count of 25 was attained for the different specimens. This was done at different aging times during the 2-week period. For example, specimens

with an aging time of 7 days were placed in the oven for an hour or so then removed to conduct the test, similarly for specimens aging for 14 days.

The second batch of specimens from mixtures L03-S0.00, L05-S0.00, L07-S0.00 were left to age, just after being freshly mixed, for different times inside the oven at a temperature of 110 ℃ after which they were taken out and tested to obtain the 25 blows. Also in many times, some water was added to facilitate the remixing procedure. This approach was followed to compare the results with the first method followed.

Finally, the specimens of mixture L08-S0.00 were left to age at room temperature of 25 ℃. The liquid limit was attained with 25 blows for aging times of one to 14 days after bare addition of water drops to the mix, after which it was properly mixed and tested afterwards.

The results showed that all the tested specimens with the various conditions and aging time gave comparable liquid limit results in the range of [1,150, 1,270]. Figure 74 below shows the variation of liquid limit for different mixes at different aging time. It was not possible to detect any positive trends in the liquid limit variation with aging time for any of the mixtures. The reported liquid limit values in Wallace and Rutherford (2015) is also in the range of 1,200, which states that the results obtained in this analysis are in the same range. This showed that regardless of the initial laponite content during mixing, and regardless of the aging time and dry-wet cycles performed, the liquid limit is anticipated to be an intrinsic property of the laponite material.

One important thing to note is that all liquid limit tests were conducted after disturbing the specimens by remixing just prior to its placement in the Casagrande cup. This is expected to destroy the thixotropic strength gain, and thus any effect of

thixotropy on the liquid limit results was not evident in this analysis. This is also in line with the rheology test results discussed earlier in the paper, which indicated that thorough mixing, after an aging time of one day or more, destroys the thixotropic strength gain.

It is quite not possible to determine the effect of thixotropy on the liquid limit, which might possibly result in variations of the liquid limit with aging time, since this means the mixtures should be left to age inside the Casagrande cup, but for samples with laponite content lower than 8%, the dry-wet cycles are inevitable, which leads to disturbing the samples and thus destroying again the thixotropic strength gain.
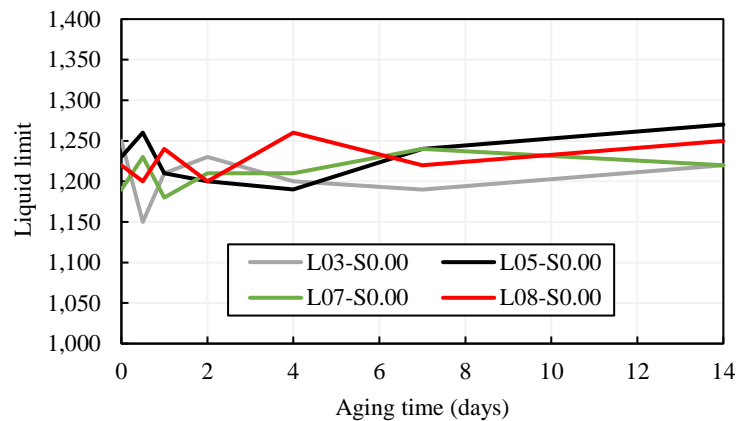
Figure 74: Liquid Limit for different mixes at different aging times

6.7 Conclusions

In this paper, a more comprehensive approach to the geotechnical characterization of laponite for use as clay surrogate was conducted. Different laponite contents as well as varying Sodium Pyrophosphate (SPP) additive contents were used to

study the behavior of laponite. Relevant geotechnical tests were conducted, including a vane shear test, rheometer, 1-D consolidation and Atterberg limits, the results of which led to a well-established understanding of the material under investigation from a geotechnical perspective. The main conclusions of this study are summarized as follows:

- An increase in undrained shear strength was found to occur with increasing laponite content, decreasing SPP dosage and increasing aging time after initial mixing (thixotropic behavior).

- The increase in undrained shear strength with increasing laponite content follows an exponential relationship.

- The undrained shear strength vs laponite content relationship showed that for 1% increase in laponite content, the undrained shear strength increased on average by a factor of 2.0.

- The decrease in undrained shear strength with increasing SPP dosage follows a negative exponential relationship.

- The undrained shear strength vs. SPP dosage relationship showed that, for laponite contents below 8%, an increase of SPP dosage from 0% to 1.7%, the average reduction in undrained shear strength was around 75%, whereas for increase in SPP dosage from 0% to 3.3%, the reduction in undrained shear strengths was around 85%. For higher laponite contents, the reductions in undrained shear strengths corresponding to SPP dosage increase from 0% to 1.7% and 3.3% were just 35% and 40%.

- The rate of undrained shear strength increase was particularly high for the initial aging period. For example, an aging time of seven days was sufficient to reach at least 70% of the undrained shear strengths achieved at 28 days aging time for most of the mixtures.

- The mixture temperature was found to affect the rate of strength gain. For example, an increase in temperature from 25℃ to 40℃ led to an increase in undrained shear strength after 7 days by factors ranging from 50% to 100%.

- Results from rheology tests revealed two sources that contribute to the increase in undrained shear strength after mixing: (1) thixotropy strength gain; and (2) hydration-induced strength gain. The relationship between apparent viscosity and shear rate showed a significant increase in viscosity at low shear rates, indicating the thixotropy strength gain. Remixing samples after one and two days reset the viscosity to one precise value, indicating a non-reversible strength source that is independent of the level of mixing, which is consistent with a hydration-induced strength gain.

- Results from 1D consolidation tests indicated that degree of consolidations as high as 60%-70% for laponite contents can be achieved. In fact, consolidation processes can lead to comparatively high laponite contents that are not achievable through initial mixing. For example, a laponite mixture with an initial laponite content of 11% could reach a final laponite content of 21% after applying a vertical stress of 96 kPa.

- The measured liquid limit ranged from 380% to 1,070% for combinations of laponite content and SPP dosage of (laponite=17.5%, SPP=3.30%) and (laponite=8.5%, SPP=0.00%), respectively.

CHAPTER 7

CONCLUSIONS AND RECOMMENDATIONS FOR FUTURE WORK

7.1 Conclusions

In this thesis, a comprehensive experimental program was designed and implemented to study the mechanics of load sharing in soft clays reinforced with sand column groups under varying loading and drainage conditions. This was approached at first by modifying an existing large-scale triaxial setup to include housings for multiple miniature pressure sensors, pore pressure sensors among other sensors/instrumentations. The distribution/location of the sensors facilitated the measurement of contact stresses above different materials and under different configurations. The scale of the samples were large enough to include reinforced samples with different configurations such as: square/hexagonal (four), triangular (three) and single (one-central column) arrangements. Drained and undrained responses under varying area replacement ratios ($a_r = 17.1\%; 30.4\%$) were studied. Moreover, the effect of partial drainage was studied, where four different shearing rates were considered to examine the effect of the loading rate on the response of the composite. In addition, the effect of column configuration on the response of the reinforced soft clays was investigated under drained and undrained conditions. The work also included a geotechnical characterization of a transparent material, Laponite, which behaves like clays, and could be a valuable replacement to soft clays when reinforced with columns to visualize internal deformations. The work was divided into four self-contained chapters. The main conclusions of the studies in all chapters are presented below:

1. The miniature pressure sensors were deemed reliable for the measurement of contact stresses above sand and clay materials under varying drainage conditions i.e. under drained, partially drained and undrained loading conditions.

2. The back-calculated stresses above sand, using the global deviatoric stress and the measured stresses above clay, constitute a realistic representation of the average stresses measured by the sensors above the sand columns. This means that if coarser material was used in future projects for reinforced samples, the mobilized stresses above this new material could be back-calculated from stresses measured above the clay matrix. This is true as the coarser material exhibits point loads on the sensor's active part and generates noises that distort the measured data. Thus, relying on the data from the load cell (global deviatoric stress) and the contact stress measured above the clay, one can easily and confidently back-calculate the stresses mobilized inside the second material.

3. The use of dense sand columns to reinforce soft kaolin clay at area replacement ratios of 17.1% and 30.4% could increase the drained ultimate strength of the specimen by 8% and 40%, and the undrained strength by 39% and 159%, respectively. This increased strength is attributed to the dense columns' ability to carry additional stresses. This was proved by the miniature pressure sensors' measurements placed above dense sand columns that showed mobilized stresses as high as 350 kPa. In comparison, the miniature pressure sensors above the clay annulus indicated stresses as low as 50 kPa to 60 kPa.

4. Local stress measurements indicated that the stress concentration ratios varied significantly with strain, drainage conditions, and area replacement ratio. At very low axial strains and under drained conditions, stress concentration ratios between

4 and 6 could be mobilized. These relatively high ratios decrease to about 1.5 at relatively large strains. For the case of undrained loading, the stress concentration factors are very low (1.5 to 2) at small strains and increase to values as high as 6.5 and 9.5 for cases involving area replacement ratios of 17.1% and 30.4%, respectively.

5. The results of the partially drained test series indicated that they were bracketed between the fully drained and the fully undrained tests that served as upper and lower bounds for the strength of the composite, respectively. During shearing, volumetric strains showed progressive consolidation and the excess pore water pressure decreased, both with decreased strain rate. Stress concentration ratio results showed response also bounded between the drained and undrained scenarios, with an average stress concentration factor in between 2.0 and 5.0.

6. The results of the partially drained tests included graphical representation of the normalized improvement index with the ratio of $t_{failure}/t_{50}$. The presented results showed that a ratio of $t_{failure}/t_{50}$ of around 15 seems to be a practical ratio at which the drained strength is mobilized in partially drained tests. Variation of the strength improvement index with the volumetric improvement index correlated well, meaning that one can predict the strength improvement of a partially drained test in a triaxial testing setup based on the ratio of the volumetric strain of the partially drained tests to the volumetric strain in the fully drained test. This was also verified with a finite difference analysis which showed a similar trend for the calculated degree of consolidation with volumetric improvement index.

7. The effect of column configuration for the same area replacement ratio of 17% under drained conditions seemed to be more pronounced on the response of the reinforced sample when compared to the undrained case. For the drained scenario, the stiffness at 1% axial strain was double for the single column configuration with respect to the square (four-column) configuration. This was related to the slenderness ratio (L/D) of the columns, which increased when moving from the single, to the triangular, then to the square configuration. However, the ultimate deviatoric stress for all configurations was the same (130 kPa). Also, the maximum volumetric strain during consolidation and shearing was the same between all three configurations, as the same material and same preparation method were adopted. The stress concentration ratio varied at low axial strains, and this is expected due to the stiffer response of the sand columns with lower slenderness ratio. For the undrained response, almost all three configurations responded in the same way during shearing, meaning that there is minimal effect of column configuration on the composite response under undrained conditions.

8. As for the geotechnical characterization of laponite material, various tests were done to come up with a better understanding of this material for use as a transparent material in replacement of natural/synthetic non-transparent clays. The results from various mixtures of the material at different concentrations with/without additive used – sodium pyrophosphate – allowed for the following observations: (a) the mini vane shear tests showed a maximum undrained shear strength of around 2.0 kPa achieved at an aging period of 28 days; (b) the rheology tests revealed two sources that contribute to the increase in undrained

shear strength after mixing (day 0), thixotropy strength gain and hydration-induced strength gain; (c) consolidation tests for different mixtures showed consolidation graphs similar to those of natural clays, and consolidation parameters were calculated for four different mixtures; and finally (d) the consistency tests showed that laponite is a very plastic material with a liquid limit of 1,200 and plasticity index of 1,000.

It is anticipated that the insights gained and reported in this thesis will facilitate the development of design methodologies for soft clays reinforced with sand column groups for applications involving both short and long-term stability of foundations.

7.2 Recommendations and Possible Future Work

While this dissertation considers many important aspects and topics that focused on the results of a large experimental program, there is a need to tie these findings and verify them numerically, using a finite element software. Although this was not part of this thesis as it is out of scope, yet it helps in understanding more certain aspects such as the progression of consolidation during shearing, the pore water pressure dissipation and the mode of failure. This is true for all the topics/themes covered during this dissertation which are: (1) the drained and undrained response of reinforced soft clays with sand column groups under different area replacement ratios, (2) the response of the composite under partially drained conditions (although a simple finite difference model was used in this study, finite element models are more effective at modeling the real problem rather than a simplified version of it) and (3) the effect of column configuration on the response of the composite that could verify the output, especially for the

undrained response which showed different results when compared to the drained response.

Moreover, characterizing Laponite from a geotechnical perspective was a first step towards using this material in geotechnical experimental programs to visualize internal deformations. Understanding the behavior of the material was a prerequisite for future works, yet, there are some aspects/limitations to think of before advancing more with this material. This includes: (1) the use of a transparent membrane in triaxial testing, i.e. in case Laponite is to be used for triaxial testing to visualize internal deformations of the reinforcement installed (particularly granular column), the membrane protecting the sample should be transparent to allow for capturing the displacements; membranes in the market at this point are all non-transparent; also, (2) a careful consideration should be adopted if a laser is to be used for visualizing internal deformations inside laponite. Lasers are use when only Laponite is being tested without the use of other soil/material. Using this laser during testing should be done in a special room, and not in open space, as it is very dangerous to someone's eye. Therefore, it is recommended to use seeding particles as discussed previously in the thesis, as it is better/safer, especially if there is not much room space for such experiments and the laboratory is accessed by a lot of researchers.

REFERENCES

Ads, A., Iskander, M., & Bless, S. (2020). Shear Strength of a Synthetic Transparent Soft Clay Using a Miniature Ball Penetrometer Test. *Geotechnical Testing Journal*, *43*(5).

AlMikati, A., Najjar, S., & Sadek, S. (2020). The Drained Response of Soft Clays Reinforced with Sand Column Groups. In *Geo-Congress 2020: Foundations, Soil Improvement, and Erosion* (pp. 411-420). Reston, VA: American Society of Civil Engineers.

AlMikati, A., Najjar, S., & Sadek, S. (2021). Forthcoming. Large-Scale Instrumented Triaxial Setup for Investigating the Response of Soft Clay Reinforced with Sand Column Groups. *International Journal of Geomechanics*. doi:10.1061/(ASCE)GM.1943-5622.0002148

Ambily, A. P., & Gandhi, S. R. (2007). Behavior of stone columns based on experimental and FEM analysis. *Journal of geotechnical and geoenvironmental engineering*, *133*(4), 405-415.

Andreou, P., Frikha, W., Frank, R., Canou, J., Papadopoulos, V., & Dupla, J. C. (2008). Experimental study on sand and gravel columns in clay. *Proceedings of the Institution of Civil Engineers-Ground Improvement*, *161*(4), 189-198.

Anton Paar Germany. (2006). Physica MCR Series Instruction Manual. Retrieved September, 2006, from www.anton-paar.com

Aslani, M., Nazariafshar, J., & Ganjian, N. (2019). Experimental Study on Shear Strength of Cohesive Soils Reinforced with Stone Columns. *Geotechnical and Geological Engineering*, *37*(3), 2165-2188.

ASTM D4318 (2010). Standard Test Methods for Liquid Limit, Plastic Limit, and Plasticity Index of Soils. *ASTM International, West Conshohocken, PA, USA*.

ASTM D4648 (2013). Standard test method for laboratory miniature vane shear test for saturated fine-grained clayey soil. *West Conshohocken, PA*

Atkinson, J.H., Evans, J.S. & Ho, E.W.L. (1985). Non-uniformity of triaxial samples due to consolidation with radial drainage. *Geotechnique*, *35*(3), pp.353-355.

Atterberg, A. (1911). Die Plastizitat der Tone. Int. Mitt. Bodenkd. 1, 10–43 (in German)

Bachus, R. C., & Barksdale, R. D. (1984). Vertical and lateral behavior of model stone columns. In *Renforcement en place des sols et des roches. Colloque international* (pp. 99-104).

Barron, R.A., (1948). Consolidation of fine-grained soils by drain wells.

Baumann, V., & Bauer, G. E. A. (1974). The performance of foundations on various soils stabilized by the vibro-compaction method. *Canadian Geotechnical Journal*, *11*(4), 509-530.

Beemer, R. D., Shaughnessy, E., Ewert, K. R., Boardman, N., Biscontin, G., Aubeny, C. P., & Grajales, F. J. (2016). The Use of Sodium Pyrophosphate to Improve a Translucent Clay Simulate. In *Geo-Chicago 2016*(pp. 83-93).

Bergado, D. T., Panichayatum, B., Sampaco, C. L., & Miura, N. (1988). Reinforcement of soft Bangkok clay using granular piles. In *International geotechnical symposium on theory and practice of earth reinforcement* (pp. 179-184).

Bergfelt, A. (1956). Loading tests on clay. *Géotechnique*, *6*(1), 15-31.

Black, J., Sivakumar, V., Madhav, M. R., & McCabe, B. (2006). An improved experimental test set-up to study the performance of granular columns. *Geotechnical testing journal*, *29*(3), 193-199.

Black, J., Sivakumar, V., & McKinley, J. D. (2007). Performance of clay samples reinforced with vertical granular columns. *Canadian geotechnical journal*, *44*(1), 89-95.

Black, J. A., Sivakumar, V., & Bell, A. (2011). The settlement performance of stone column foundations. *Géotechnique*, *61*(11), 909-922.

Black, J. A. (2015). Centrifuge modelling with transparent soil and laser aided imaging. *Geotechnical Testing Journal*, *38*(5), 631-644.

Bo, M.W., Wong, K.S., Choa, V., Arulrajah, A. & Horpibulsuk, S. (2016). Step loading compression of ultra-soft soil under radial drainage conditions. *Marine Georesources & Geotechnology*, *34*(7), pp.648-658.

Bou Lattouf, H.E. (2013). The effect of drainage conditions on the load response of soft clays reinforced with granular columns. (Masters dissertation). American University of Beirut

Brauns, J. (1978). Initial bearing capacity of stone columns and sand piles. In *Int. Symp. on Soil Reinforcing and Stabilizing Techniques in Engineering Practice* (Vol. 1, pp. 497-512).

Brock, D. C., & Orr Jr, F. M. (1991). Flow visualization of viscous fingering in heterogeneous porous media. In *SPE Annual Technical Conference and Exhibition*. Society of Petroleum Engineers.

BYK Additives and Instruments (2014). Technical Information B-RI 21–Laponite–
Performance Additive, BYK Additives and Instruments, Geretsried, Germany.

BYK Additives and Instruments (2020). Technical Information B-RI 21, Laponite –
Performance Additives. BYK Additives & Instruments, www.byk.com, Geretsried,
Germany, 24 p.

Casagrande, A. (1936). The determination of pre-consolidation load and it's practical
significance. In *Proc. Int. Conf. Soil Mech. Found. Eng. Cambridge, Mass.,
1936* (Vol. 3, p. 60).

Casagrande, A., & Fadum, R. E. (1940). Notes on soil testing for engineering purposes.

Castro, J., & Sagaseta, C. (2011). Deformation and consolidation around encased stone
columns. *Geotextiles and Geomembranes*, *29*(3), 268-276.

Charles, J. A., Watts, K.A. (1983). Compressibility of soft clay reinforced with granular
columns. In: Proceedings of the 8th European conference on soil mechanics and
foundation engineering, Helsinki, pp 347–352

Chassefiere, B., & Monaco, A. (1982). On the use of Attemberg limits on marine soils.
Marine Geotechnology 5, 153–179

Chen, J. D., & Wada, N. (1986). Visualization of immiscible displacement in a three-
dimensional transparent porous medium. *Experiments in fluids*, *4*(6), 336-338.

Chen, J. F., Han, J., Oztoprak, S., & Yang, X. M. (2009). Behavior of single rammed
aggregate piers considering installation effects. *Computers and Geotechnics*, *36*(7),
1191-1199.

Chenari, R. J., Taleb, A., Ghoreishi, M., & Payan, M. (2018). Physical modelling of cohesive soil inherent variability: consolidation problem. *International Journal of Geo-Engineering*, *9*(1), 25.

Chini, C. M., Wallace, J. F., Rutherford, C. J., & Peschel, J. M. (2015). Shearing failure visualization via particle tracking in soft clay using a transparent soil. *Geotechnical Testing Journal*, *38*(5), 708-724.

Cimentada, A., Da Costa, A., Cañizal, J., & Sagaseta, C. (2011). Laboratory study on radial consolidation and deformation in clay reinforced with stone columns. *Canadian Geotechnical Journal*, *48*(1), 36-52.

Das, B. M., & Sobhan, K. (2013). *Principles of geotechnical engineering*. Cengage learning.

El Howayek, A. (2011). Characterization, rheology and microstructure of laponite suspensions.

Elshazly, H., Elkasabgy, M., & Elleboudy, A. (2008). Effect of inter-column spacing on soil stresses due to vibro-installed stone columns: interesting findings. *Geotechnical and Geological Engineering*, *26*(2), 225.

Ezzein, F. M., & Bathurst, R. J. (2011). A transparent sand for geotechnical laboratory modeling. *Geotechnical Testing Journal*, *34*(6), 590-601.

Fattah, M. Y., Shlash, K. T., & Al-Waily, M. J. M. (2011). Stress concentration ratio of model stone columns in soft clays. *Geotechnical Testing Journal*, *34*(1), 50-60.

Ferreira, J. A., & Zornberg, J. G. (2015). A transparent pullout testing device for 3D evaluation of soil–geogrid interaction. *Geotechnical Testing Journal*, *38*(5), 686-707.

Ganiyu, A. A., Rashid, A. S. A., & Osman, M. H. (2016). Utilisation of transparent synthetic soil surrogates in geotechnical physical models: A review. *Journal of Rock Mechanics and Geotechnical Engineering*, *8*(4), 568-576.

Ghazavi, M., & Afshar, J. N. (2013). Bearing capacity of geosynthetic encased stone columns. *Geotextiles and Geomembranes*, *38*, 26-36.

Gniel, J., & Bouazza, A. (2009). Improvement of soft soils using geogrid encased stone columns. *Geotextiles and Geomembranes*, *27*(3), 167-175.

Greenwood, D. A. (1970). Mechanical improvement of soils below ground surface. In *Inst Civil Engineers Proc, London/UK/*.

Han, J., & Ye, S. (1991). Field tests of soft clay stabilized by stone columns in coastal areas in China. In *Proc., 4th Int. Deep Foundations Institute Conf* (Vol. 1, pp. 243-248).

Han, J. & Ye, S.L. (2001). Simplified method for consolidation rate of stone column reinforced foundations. *Journal of Geotechnical and Geoenvironmental Engineering*, *127*(7), pp.597-603.

Hansbo, S. (1980). Consolidation of fine-grained soils by prefabricated drains. In *Proc. of. the. 10th ICSMFE* (Vol. 3, pp. 677-682).

Hird, C.C., Pyrah, I.C. & Russel, D. (1992). Finite element modelling of vertical drains beneath embankments on soft ground. *Geotechnique*, *42*(3), pp.499-511.

Hu, W. (1995). Physical modelling of group behaviour of stone column foundations (Doctoral dissertation, University of Glasgow).

Hugher, J. M. O., & Withers, N. J. (1974). Reinforcing of soft cohesive soils with stone columns. *Ground engineering*, *7*(3).

Indraratna, B. & Redana, I.W. (2000). Numerical modeling of vertical drains with smear and well resistance installed in soft clay. *Canadian Geotechnical Journal*, 37(1), pp.132-145.

Indraratna, B., Ngo, N.T., Rujikiatkamjorn, C. & Sloan, S.W. (2015). Coupled discrete element–finite difference method for analysing the load-deformation behaviour of a single stone column in soft soil. *Computers and Geotechnics*, *63*, pp.267-278.

Iskander, M. G., Lai, J., Oswald, C. J., & Mannheimer, R. J. (1994). Development of a transparent material to model the geotechnical properties of soils. *Geotechnical Testing Journal*, *17*(4), 425-433.

Iskander, M. G., Sadek, S., & Liu, J. (2002). Optical measurement of deformation using transparent silica gel to model sand. *International Journal of Physical Modelling in Geotechnics*, *2*(4), 13-26.

Iskander, M. (2010). Modelling with transparent soils: Visualizing soil structure interaction and multi-phase flow, non-intrusively. Springer Science & Business Media.

Iskander, M., & Liu, J. (2010). Spatial deformation measurement using transparent soil. *Geotechnical Testing Journal*, *33*(4), 314-321.

James, R. G., & Bransby, P. (1970). Experimental and theoretical investigations of a passive earth pressure problem. *Geotechnique*, *20*(1), 17-37.

Juran, I. & Guermazi, A. (1988). Settlement response of soft soils reinforced by compacted sand columns. J Geotech Eng ASCE 114(8):930–943.

Kim, D., & Kim, J. R. (2007). Resilient behavior of compacted subgrade soils under the repeated triaxial test. *Construction and Building Materials*, *21*(7), 1470-1479.

Kumar, G., & Samanta, M. (2020). Experimental evaluation of stress concentration ratio of soft soil reinforced with stone column. Innovative Infrastructure Solutions, 5(1), 18.

Lai, J., Oswald, C. J., & Mannheimer, R. J. (1994). Development of a transparent material to model the geotechnical properties of soils. *Geotechnical Testing Journal*, *17*(4), 425-433.

Lei, G.H., Xu, L.D., Zheng, Q. & Ng, C.W.W. 2017. Role of equal-strain assumption in unit-cell theory for consolidation with vertical drains. *Journal of Central South University*, *24*(12), pp.2914-2923.

Leo, C.J. (2004). Equal strain consolidation by vertical drains. *Journal of Geotechnical and Geoenvironmental Engineering*, *130*(3), pp.316-327.

Lin, H., & Penumadu, D. (2005). Experimental investigation on principal stress rotation in Kaolin clay. *Journal of geotechnical and geoenvironmental engineering*, *131*(5), 633-642.

Liu, J., Iskander, M. G., & Sadek, S. (2003). Consolidation and permeability of transparent amorphous silica. *Geotechnical Testing Journal*, *26*(4), 390-401.

Liu, J., & Iskander, M. G. (2010). Modelling Capacity of Transparent Soil. *Canadian Geotechnical Journal*, *47*(4), 451-460.

Lo, S. R., Zhang, R., & Mak, J. (2010). Geosynthetic-encased stone columns in soft clay: a numerical study. *Geotextiles and Geomembranes*, *28*(3), 292-302.

Locat, J., & Bergeron, M. (1988). Étude à rebours de glissements sous-marins, fjord du Saguenay, Québec. In *Proceedings of the 41st Canadian Geotechnical Conference, Waterloo, Ont* (pp. 338-346).

Mannheimer, R. J., Park, J. T., Grimley, T. A., & Morrow, T. B. (1989). *Development and characterization of transparent slurries for basic and applied research in solids transport* (No. CONF-8909178-1). Southwest Research Inst., San Antonio, TX (USA).

McCabe, B. A., & Killeen, M. M. (2017). Small stone-column groups: mechanisms of deformation at serviceability limit state. *International Journal of Geomechanics*, *17*(5), 04016114.

McKelvey, D., Sivakumar, V., Bell, A., & Graham, J. (2004). Modelling vibrated stone columns in soft clay. *Proceedings of the Institution of Civil Engineers-Geotechnical Engineering*, *157*(3), 137-149.

Mesri, G., & Cepeda-Diaz, A. F. (1986). Residual shear strength of clays and shales. *Geotechnique*, *36*(2), 269-274.

Miranda, M., Da Costa, A., Castro, J., & Sagaseta, C. (2017). Influence of geotextile encasement on the behaviour of stone columns: Laboratory study. *Geotextiles and Geomembranes*, *45*(1), 14-22.

Mitchell, J. K. (1960). Fundamental aspects of thixotropy in soils. Transactions of the American Society of Civil Engineers, 126(1), 1586-1620.

Mitchell, R. J. (1970). On the yielding and mechanical strength of Leda clays. *Canadian geotechnical journal*, *7*(3), 297-312.

Mitchell, J. K., & Soga, K. (2005). *Fundamentals of soil behavior* (Vol. 3). New York: John Wiley & Sons.

Mourchid, A., & Levitz, P. (1998). Long-term gelation of laponite aqueous dispersions. *The American Physical Society,* 4887-4890.

Muir Wood, D., Hu, W., & Nash, D. F. (2000). Group effects in stone column foundations: model tests. *Geotechnique*, *50*(6), 689-698.

Murugesan, S., & Rajagopal, K. (2006). Geosynthetic-encased stone columns: numerical evaluation. *Geotextiles and Geomembranes*, *24*(6), 349-358.

Murugesan, S., & Rajagopal, K. (2008). Performance of encased stone columns and design guidelines for construction on soft clay soils. In *Geosynthetics in Civil and Environmental Engineering* (pp. 729-734). Springer, Berlin, Heidelberg.

Murugesan, S. & Rajagopal, K. (2010). Studies on the behavior of single and group of geosynthetic encased stone columns. J Geotech Geoenviron Eng ASCE 136(1):129–139.

Najjar, S. S., Sadek, S., & Maakaroun, T. (2010). Effect of sand columns on the undrained load response of soft clays. *Journal of Geotechnical and Geoenvironmental Engineering*, *136*(9), 1263-1277.

Najjar, S. S. (2013). A state-of-the-art review of stone/sand-column reinforced clay systems. *Geotechnical and Geological Engineering*, *31*(2), 355-386.

Najjar, S. S., Sadek, S., Bou Lattouf, H., & Maalouf, Y. (2020). Drained triaxial response of clay reinforced with sand columns. *Proceedings of the Institution of Civil Engineers-Ground Improvement*, *173*(3), 170-186. https://doi.org/10.1680/jgrim.18.00007

Nazariafshar, J., Mehrannia, N., Kalantary, F., & Ganjian, N. (2019). Bearing capacity of group of stone columns with granular blankets. *International Journal of Civil Engineering*, *17*(2), 253-263.

Ng, T. T., Kelley, M., & Sampson, J. (1996). MRI studies of direct shear tests on round particles. In *Engineering Mechanics* (pp. 572-575). ASCE.

Orsi, T. H., Anderson, A. L., Leonard, J. N., Bryant, W. R., & Edwards, C. M. (1992). Use of X-ray computed tomography in the study of marine sediments. In *Civil Engineering in the Oceans V* (pp. 968-982). ASCE.

Peng, X., & Zornberg, J. G. (2019). Evaluation of soil-geogrid interaction using transparent soil with laser illumination. *Geosynthetics International*, *26*(2), 206-221.

Peters, S. B., Siemens, G., & Take, W. A. (2011). Characterization of transparent soil for unsaturated applications. *Geotechnical Testing Journal*, *34*(5), 445-456.

Pulko, B., Majes, B., & Logar, J. (2011). Geosynthetic-encased stone columns: analytical calculation model. *Geotextiles and Geomembranes*, *29*(1), 29-39.

Raithel, M., & Kempfert, H. G. (2000). Calculation models for dam foundations with geotextile coated sand columns. In *ISRM International Symposium*. International Society for Rock Mechanics and Rock Engineering.

Rao, S., Prasad, Y. V. S., & Hanumanta Rao, V. (1992). Useof stone columns in soft marine clays. In *Proceedings of the 45th Canadian geotechnical conference, Toronto, Ont, October* (p. 9).

Rayess, A.Z. (2015). Triaxial response of natural clay reinforced with sand columns under partially drained conditions. Master's thesis, American University of Beirut, Beirut, Lebanon.

Robinsky, E. I., & Morrison, C. F. (1964). Sand displacement and compaction around model friction piles. *Canadian Geotechnical Journal*, *1*(2), 81-93.

Rodríguez, J.D. A., & Santamarina, J. C. (1999). Thixotropy: the case of Mexico City soils. In *XI Panamerican Conf. on Soil Mech. and Geotech. Eng* (pp. 441-448).

Sadek, S., Iskander, M. G., & Liu, J. (2002). Geotechnical properties of transparent silica. *Canadian Geotechnical Journal*, *39*(1), 111-124.

Santagata, M., Clarke, J. P., Bobet, A., Drnevich, V. P., El Mohtar, C. S., Huang, P. T., & Johnston, C. T. (2014). Rheology of concentrated bentonite dispersions treated with sodium pyrophosphate for application in mitigating earthquake-induced liquefaction. *Applied clay science*, *99*, 24-34.

Seah, T.H. & Juirnarongrit, T. (2003). Constant rate of strain consolidation with radial drainage. *Geotechnical Testing Journal*, *26*(4), pp.432-443.

Shahu, J. T., & Reddy, Y. R. (2011). Clayey soil reinforced with stone column group: model tests and analyses. *Journal of Geotechnical and Geoenvironmental Engineering*, *137*(12), 1265-1274.

Sivakumar, V., McKelvey, D., Hughes, D., & Graham, J. (2003). Clay reinforcement using sand columns: performance under triaxial loading. *Canadian Geotechnical Journal*, *41*(2), 299-312.

Sivakumar, V., McKelvey, D., Graham, J., & Hughes, D. (2004). Triaxial tests on model sand columns in clay. *Canadian Geotechnical Journal*, *41*(2), 299-312.

Sivakumar, V., Jeludine, D. K. N. M., Bell, A., Glynn, D. T., & Mackinnon, P. (2011). The pressure distribution along stone columns in soft clay under consolidation and foundation loading. *Géotechnique*, *61*(7), 613-620.

Skempton, A. W. (1954). The pore-pressure coefficients A and B. *Geotechnique*, *4*(4), 143-147.

STA. (2018). Vibroflotation vs. Sand Columns. https://www.sta-milano.com/en/vibroflotation /vibroflotation-stone-column

Stuedlein, A. W., & Holtz, R. D. (2012). Analysis of footing load tests on aggregate pier reinforced clay. *Journal of geotechnical and geoenvironmental engineering*, *138*(9), 1091-1103.

Tabe, K. (2015). Transparent aquabeads to model LNAPL ganglia migration through surfactant flushing. *Geotechnical Testing Journal*, *38*(5), 787-804.

Tan, S.A., Tjahyono, S. & Oo, K.K. (2008). Simplified plane-strain modeling of stone-column reinforced ground. *Journal of Geotechnical and Geoenvironmental Engineering*, *134*(2), pp.185-194.

Terzaghi, K. (1943). Theoretical soil mechanics, 235–344. New York: John Wiley & Sons, Inc.

Thompson, D. W., & Butterworth, J. T. (1992). The nature of laponite and its aqueous dispersions. *Journal of Colloid and Interface Science*, *151*(1), 236-243.

Van Olphen, H. & Fripiat, J. J. (1979). Data Handbook for Clay Minerals and Other Non-Metallic Minerals. Pergamon Press, Oxford and Elmsford, New York, NY, USA, 346 p.

Wakabayashi, T. (1950). Photo-elastic method for determination of stress in powdered mass. *Journal of the Physical Society of Japan*, *5*(5), 383-385.

Wallace, J. F., & Rutherford, C. J. (2015). Geotechnical properties of LAPONITE RD®. *Geotechnical Testing Journal*, *38*(5), 574-587.

Wallace, J. F. & Rutherford, C. J. (2017). Response of Vertically Loaded Centrifuge Suction Caisson Models in Soft Clay. Proc., Offshore Technology Conference 2017. 1-4 May 2017, Houston, Texas.

Watts, K. S., Johnson, D., Wood, L. A., & Saadi, A. (2000). An instrumented trial of vibro ground treatment supporting strip foundations in a variable fill. *Géotechnique*, *50*(6), 699-708.

White, D. J., Pham, H. T., & Hoevelkamp, K. K. (2007). Support mechanisms of rammed aggregate piers. I: Experimental results. *Journal of Geotechnical and Geoenvironmental Engineering*, *133*(12), 1503-1511.

Wu, C. S., & Hong, Y. S. (2009). Laboratory tests on geosynthetic-encapsulated sand columns. *Geotextiles and Geomembranes*, *27*(2), 107-120.

Yi, L. D., Lv, H. B., Ye, T., & Zhang, Y. P. (2018). Quantification of the transparency of the transparent soil in geotechnical modeling. *Advances in Civil Engineering*, *2018*.